Target patterns and pacemakers in reaction-diffusion systems

vorgelegt von
Diplom-Physiker
Michael Stich
Bayreuth

Von der Fakultät II - Mathematik- und Naturwissenschaften
der Technischen Universität Berlin
zur Erlangung des akademischen Grades
Doktor der Naturwissenschaft
– Dr. rer. nat. –
genehmigte Dissertation

Promotionsausschuss:

Vorsitzender: Prof. Dr. E. Sedlmayr

Gutachter: Prof. Dr. H. Engel

Gutachter: Prof. Dr. A. S. Mikhailov

Gutachter: Prof. Dr. E. Schöll, PhD

Tag der wissenschaftlichen Aussprache: 20.02.2003

Berlin 2003
D 83

Zusammenfassung

Die vorliegende Arbeit beschäftigt sich mit Musterbildung in Reaktions-Diffusions-Systemen. Ein typisches Muster ist das Kreiswellenmuster, welches aus konzentrischen Wellen besteht, die von einer Wellenquelle ausgesendet werden. In dieser Arbeit werden derartige Wellenquellen und durch sie entstehende Kreiswellenmuster mit analytischen und numerischen Methoden studiert. Bei der Modellierung wird zum einen berücksichtigt, dass das System oszillatorisch oder anregbar sein kann, und zum anderen, dass Wellenquellen aus Heterogenitäten des Mediums oder selbstorganisiert entstehen können.

Bei der Untersuchung heterogener Wellenquellen in oszillatorischen Systemen in der Nähe einer Hopf-Bifurkation werden zwei Schwerpunkte gesetzt. Erstens werden die Bedingungen zur Erzeugung von Wellenquellen und ausgedehnten Kreiswellenmustern sowie von Wellensenken und lokalisierten Wellenmustern systematisch abgeleitet. Insbesondere wird geklärt, unter welchen Umständen rein- bzw. rauslaufende Kreiswellen auftreten und welche Auswirkungen große Heterogenitäten haben. Zweitens werden hochfrequente Wellenquellen betrachtet. In diesem Fall treten Eckhaus-instabile Wellen auf, die ringförmige Amplitudendefekte und weiteres komplexes Verhalten hervorrufen. Für besonders hochfrequente Wellenquellen entstehen die Amplitudendefekte bereits an der Grenze der Wellenquelle, was als lokales Desynchronisationsphänomen erklärt wird. Auch Wellensenken können die raum-zeitliche Dynamik des ausgedehnten Systems entscheidend beeinflussen indem sie die Wellen anderer Muster unterbrechen.

Motiviert dadurch, dass ein oszillatorisches System in der Nähe einer Hopf-Bifurkation nicht in der Lage ist, stabile, selbstorganisierte Wellenquellen hervorzubringen, wird zur Modellierung selbstorganisierter Wellenquellen ein System vorgeschlagen, das sich in der Nähe einer Heugabel-Hopf-Bifurkation befindet. Dazu wird zunächst mit Hilfe der Normalformtheorie die Amplitudengleichungen für ein solches Medium hergeleitet und diskutiert. Ein wesentliches Merkmal des Systems ist, dass es birhythmisch ist, d.h., dass zwei verschiedene Grenzzyklen gleichzeitig stabil sein können. Es wird analytisch und numerisch gezeigt, dass das Modell stabile selbstorganisierte Wellenquellen hervorbringen kann und dass derartige Wellenquellen driften können, wenn Parameter einem räumlichen Gradienten unterliegen. Die Wechselwirkung von Wellenquellen wird numerisch untersucht. Neben koexistierenden Wellenquellen wird auch globale Inhibierung anderer Wellenquellen nach-

gewiesen. Wenn sich die Frequenzen der Grenzzyklen stark unterscheiden, sind Eckhaus-instabile Wellen möglich, die die Wellenquellen destabilisieren können. Weiterhin sind kinetische Instabilitäten der Wellenquellen möglich, bei denen die Begrenzungen der Wellenquellen oszillieren.

Selbstorganisierte Wellenquellen können auch in anregbaren Medien entstehen, sind jedoch in der Regel instabil. In dieser Arbeit wird auf der Basis des FitzHugh-Nagumo-Modells ein dreikomponentiges Aktivator-Inhibitor-System vorgestellt, in dessen anregbaren Regime stabile selbstorganisierte Wellenquellen entstehen können. Die Bildung von stabilen selbstorganisierten Wellenquellen ist möglich, wenn sich das System in der Nähe relaxationaler Oszillationen befindet, die zusätzliche Komponente stark diffundiert und wenn diese den Inhibitor ausreichend inhibiert. Für ein solches System gibt es auch die Möglichkeit der Bistabilität von Pulslösungen. Durch die Wechselwirkung verschiedener Pulslösungen miteinander können Wellenquellen entstehen und auch zu anderen Szenarien komplexer raum-zeitlicher Dynamik führen. Für den Fall verschwindender Aktivatordiffusion werden die Wellen, die von einer Wellenquelle ausgesendet werden, instabil und raum-zeitliches Chaos entsteht.

Diese Arbeit präsentiert somit neue Ergebnisse zur Dynamik großer und hochfrequenter heterogener Wellenquellen und weist erstmalig nach, dass selbstorganisierte Wellenquellen in birhythmischen und anregbaren Systemen stabil existieren können.

Abstract

Pattern formation in systems far from thermal equilibrium is a fascinating phenomenon. Reaction-diffusion systems are an important type of system where pattern formation is observed. The target pattern and the associated wave source called pacemaker are typical patterns in such systems. This thesis studies pacemakers and target patterns systematically by analytical and numerical means. The underlying dynamics of the system may be oscillatory or excitable and the pacemakers may either consist of spatial heterogeneities of the medium or be self-organized, i.e. result of intrinsic processes.

The investigation of heterogeneous pacemakers in oscillatory systems in the framework of the complex Ginzburg-Landau equation focuses on two aspects. First, the conditions of the creation of pacemakers and extended target patterns versus the creation of wave sinks and localized target patterns are derived systematically. In particular, inward traveling target patterns and large heterogeneities are discussed. Then, pacemakers which emit target waves with high frequencies are considered. In this case, the waves become Eckhaus unstable, causing ring-shaped amplitude defects or other complex patterns. For even larger frequencies, the amplitude defects already take place at the boundary of the heterogeneity, giving rise to a localized desynchronization phenomenon. Moreover, wave sinks can have a significant impact on the spatio-temporal dynamics of the system by breaking the waves arriving from other wave sources.

It is well known that oscillatory media close to a Hopf bifurcation are not able to give rise to stable self-organized pacemakers. Therefore, to model such pacemakers, a system close to a pitchfork-Hopf bifurcation is proposed. The normal form and amplitude equations of the pitchfork-Hopf bifurcation are derived. Such a system displays birhythmicity, i.e. bistability of limit cycles, and it is demonstrated analytically that stable self-organized pacemakers are possible. Simulations confirm the existence of stable self-organized pacemakers. In the presence of a parameter gradient, such patterns drift, as shown analytically and numerically. The interaction between pacemakers is studied numerically, giving rise either to coexisting pacemakers or to a new phenomenon called global inhibition: Established pacemakers suppress new cores or merge with them. When the frequencies of the limit cycles differ strongly, the waves may become Eckhaus unstable and the pacemaker may destabilize. Furthermore,

kinetic instabilities of the pacemakers are possible, creating breathing and swinging pacemakers.

Self-organized pacemakers in excitable media are usually unstable. In this thesis, a three-component activator-inhibitor system on the basis of the FitzHugh-Nagumo model is proposed that gives rise to stable self-organized pacemakers in the excitable regime. The formation of such patterns is demonstrated if several conditions are fulfilled: The system is close to relaxational oscillations, the additional component is strongly diffusive, and the additional component inhibits the inhibitor. Moreover, bistability of pulse solutions is observed in such a system. Different pulses can interact and may create pacemakers. Alternatively, other complex spatio-temporal dynamics is observed. If the diffusion of the activator vanishes, the waves emitted by the wave source are unstable and spatio-temporal chaos appears.

Thus, this thesis presents new results on the dynamics of pacemakers with large frequencies and demonstrates for the first time the possibility of stable self-organized pacemakers in birhythmic and excitable systems.

Contents

Chapter 1

Introduction

The spontaneous emergence of patterns is a fascinating phenomenon observed in many physical, chemical, and biological systems far from thermal equilibrium. Such patterns may show complex temporal or spatio-temporal dynamics, including chaotic behavior. Since these patterns are created by the internal dynamics of the system, this process is called *spatio-temporal self-organization* and is referred to as *pattern formation* in the following [1–3]. Typical examples are the patterns found in chemical reaction-diffusion systems [2,3], hydrodynamic and liquid crystal systems [3,4], electrochemical systems [5], semiconductors [6,7], gas-discharge systems [7], optical systems [8], granular matter [9], the heart [10,11], the central nervous system [12,13], and many other biological and ecological systems [14–19]. The complexity and diversity of self-organizing systems is mathematically reflected by nonlinear equations, which arise in a natural way when systems with many interacting elements, biological systems, or chemical reactions are considered. The framework to describe all these phenomena is provided by the research field called *nonlinear dynamics* [20].

This work is focused on pattern formation in *reaction-diffusion systems*, where the coupling of nonlinear reaction kinetics with a diffusive transport process leads to complex dynamical behavior. The most prominent example of a chemical pattern-forming reaction-diffusion system is the Belousov-Zhabotinsky reaction. It consists of the oxidation of malonic acid by bromate ions in an acidic medium, catalyzed by metal ions. Boris Belousov discovered self-sustained oscillations of this reaction under stirring conditions [21] and Anatol Zhabotinsky and Art Winfree later reported target, spiral, and scroll waves in the unstirred system [22–26]. Recently, major advances have been achieved with a modification of the Belousov-Zhabotinsky reaction using microemulsions, which shows inward traveling spiral and target waves, Turing structures, standing waves, oscillatory clusters, and other patterns [27,28]. Another example of a well-studied chemical reaction giving rise to complex

temporal and spatio-temporal behavior is the oxidation of carbon monoxide on platinum single crystal surfaces under low pressure conditions [29, 30]. A special feature of this reaction is the occurrence of spatio-temporal chaos and its control, which has been achieved recently [31].

The concept and mathematical structure of reaction-diffusion models are quite general, and therefore such models may also be applied to pattern-forming physical and biological systems. In the context of physical systems, reaction-diffusion models are for instance used to describe the dynamics of current filaments in semiconductor devices [6]. Other examples are the localized patterns found in gas-discharge systems [32, 33]. In the field of living systems which show oscillations or wave phenomena, reaction-diffusion models are successfully applied to explain excitation waves (and their breakdown) in the heart [10], the propagation of action potentials in neural tissue [12, 13], and aggregation patterns in slime mold colonies [34].

Every pattern-forming process is accompanied by the appearance of characteristic length and time scales. Typically, the extension of the pattern is much larger than the size of an individual element of the system. Therefore, to describe the dynamics of the pattern, it is often not necessary to take into account the individual dynamics of every single element together with their mutual interactions. Instead, it is possible to interpret the pattern dynamics as a collective phenomenon and describe it by a macroscopic mean-field variable or order parameter. Another important feature of self-organization is that, although there are often different time scales involved in the dynamics of a given system, its long-term behavior is typically governed by the slow processes. In this case, it is possible to strongly reduce the number of effective degrees of freedom by adiabatically eliminating the fast variables. These important properties of self-organizing processes have been stressed by Hermann Haken who established *synergetics* as a new field of research emphasizing the universal character of self-organization [35]. Thereafter, pattern formation essentially is a cooperative, synergetic effect of a distributed system which shows dynamic behavior on selected space and time scales.

A necessary condition for self-organization is that the system is far from thermal equilibrium. Therefore, the system should be *open*, i.e. continuously interchange matter and energy with its environment. If energy is constantly supplied to the open system, it is driven away from thermal equilibrium through the dissipation of energy into the environment. Then, the entropy may decrease inside the system and enable the spontaneous creation of *dissipative structures*. A characteristic feature of dissipative systems is the existence of *attractors*, stable states toward which the system evolves. The most fundamental attractors in dissipative sys-

tems represent stationary and time-periodic, i.e. oscillatory states. Important contributions in the study of dissipative systems and structures were made by Ilya Prigogine and co-workers in the 1960s and 1970s [36, 37].

From this point of view, the abundant examples for pattern formation in biological systems are not surprising. Biological systems continuously consume energy and use it to maintain the highly-ordered, complex state of life. This was already stressed by Erwin Schrödinger in 1944 when he explored the physical basis of biological processes [38]. In a seminal paper published in 1952, Alan Turing investigated the chemical basis of morphogenesis and showed that the coupling of nonlinear kinetics with diffusion may lead to spatial differentiation, i.e. to structures denoted later as Turing patterns [39]. Although such patterns have been found in chemical systems [40], there is no clearcut evidence for them in biological systems yet. Nevertheless, the relevance of basic physical and chemical processes for biological pattern formation is unquestionable and much progress in the understanding of living systems is expected from the studies on pattern formation in physical and chemical systems.

The investigation of pattern formation is an interdisciplinary task and important contributions were made by studying *dynamical systems* and *deterministic chaos* [41, 42]. These branches of applied mathematics can be traced back to Henri Poincaré, who first described complex dynamics in a system with three degrees of freedom [43]. Since then, the dynamics of such low-dimensional systems has been intensively investigated, in particular chaotic behavior and instabilities due to parameter changes, called *bifurcations* [44]. Two bifurcations of stationary states that become important in this thesis are the *pitchfork bifurcation*, which creates two stable stationary states, and the *Hopf bifurcation*, that gives rise to oscillatory behavior.

The large variety of systems and observed patterns demand an appropriate classification. For reaction-diffusion systems, it is possible and convenient to establish a connection between the observed patterns and the temporal dynamics of the system without diffusion. There are three main types of pattern-forming, or so-called *active media*: bistable, excitable, and oscillatory systems [45, 46].

Bistable media are characterized by two stable stationary states and the existence of front solutions. The fronts travel through the system and separate domains of different states from each other. Bistability is found in many reaction-diffusion systems and may appear via a pitchfork bifurcation of a stationary state. Excitable media have just one stable stationary

state, but a sufficiently strong perturbation of this state may lead to a large excitation which decays back to the initial state later. A neural system, for instance, may show excitable behavior. The neurons are quiescent until a super-threshold excitation, e.g. from a sensory cell, provokes its firing. The excitation moves along the ensemble of coupled neurons at a constant speed and without changing its shape. Such a wave is called a pulse and is the typical pattern of an excitable system although other patterns like wave trains or spiral waves may also occur. Often, excitable media are modeled by the FitzHugh-Nagumo equations. Oscillatory media show temporally periodic behavior and may give rise to wave trains, spirals, or concentric wave patterns. The simplest bifurcation which creates oscillations is the Hopf bifurcation. It is possible to derive a general model which holds for all systems undergoing such a bifurcation, regardless of their specific nature. This universal equation is the complex Ginzburg-Landau equation [47].

This thesis is focused on *target patterns* and *pacemakers* in reaction-diffusion systems. The target pattern is the first wave pattern that was found in the Belousov-Zhabotinsky reaction [22]. It consists of concentric waves that are periodically emitted from a small central region called the pacemaker. Since the work of Albert Zaikin and Anatol Zhabotinsky in 1970 [22], target patterns have been observed in many other chemical, physical, and biological systems (e.g. Refs. [19,29,48–52]) and are hence one of the generic patterns for nonequilibrium systems. So far, target waves have received much less attention than, for example, rotating spiral waves. This is to some extent explained by the fact that many target patterns are produced by local heterogeneities, which locally modify the properties of the medium, while stable spiral waves may exist in the uniform system and are therefore self-organized. Although heterogeneous pacemakers and their target wave patterns have been analyzed in a number of theoretical studies (e.g. Refs. [53–59]), aspects such as inward traveling or unstable wave patterns have not been systematically addressed.

Pacemakers are not necessarily formed by local impurities in the system. There is evidence that target patterns and pacemakers may also be found in uniform systems without heterogeneities [48,60]. Such self-organized target patterns may be stable and have been described in several models for oscillatory systems (e.g. Refs. [61–63]), although analytical solutions for self-organized pacemakers are rare (for an exception see e.g. Ref. [61]). Not much attention is usually paid to self-organized target patterns and pacemakers in uniform excitable media since at the moment there is no experimental evidence for the spontaneous appearance of target patterns in an excitable medium. However, there are studies which show that target patterns may be created in excitable media by noise [64] or by periodic forcing [65] even in

the absence of impurities.

Consequently, there is strong interest in the systematic study of heterogeneous and self-organized pacemakers in oscillatory and excitable media. This thesis presents new results obtained for such patterns: inward traveling waves, large cores, and desynchronization phenomena are investigated for heterogeneous pacemakers in oscillatory media, and stable self-organized pacemakers are shown to exist for the first time in birhythmic and excitable media.

This thesis is organized as follows. In Chapter 2, reaction-diffusion systems are introduced and the main mathematical tools to describe pattern formation in such systems are provided. The complex Ginzburg-Landau equation and the FitzHugh-Nagumo equations, which are the building blocks of the models discussed later, are of particular interest. A short overview of three-component models and both, target waves and pacemakers is given.

In Chapter 3, heterogeneous pacemakers in oscillatory media are investigated. The model is based on the complex Ginzburg-Landau equation where pacemakers are formed by a locally fixed frequency shift. Instabilities of the generated wave pattern, large cores, and inward traveling target patterns are of particular interest there.

Self-organized pacemakers in oscillatory media are investigated in Chapter 4. Since a system close to the Hopf bifurcation is not able to display stable self-organized pacemakers, a system where a Hopf and a pitchfork bifurcation occur simultaneously for the same set of parameters is considered. In this case, the uniform medium displays birhythmicity, i.e. bistability of two limit cycles, a regime described for many dynamical systems (e.g. Ref. [15]). For the present model, it is not only possible to investigate the system numerically and to systematically study self-organized pacemakers, but also to construct an analytic solution for such patterns.

Chapter 5 focuses on the results obtained for self-organized pacemakers in excitable media. As a model, a simple extension of the FitzHugh-Nagumo equations is proposed. There, it is possible to show that stable self-organized pacemakers may also exist in excitable media. Finally, this thesis is closes in Chapter 6 presenting conclusions and perspectives.

Chapter 2

Basic concepts of spatio-temporal pattern formation

This thesis focuses on target patterns and pacemakers in reaction-diffusion systems. Reaction-diffusion systems are spatially extended systems far from thermal equilibrium where the interplay of nonlinear reaction kinetics and diffusive coupling may give rise to the creation of spatio-temporal patterns. Although target patterns are typical for chemical systems, they are actually generic for pattern-forming media and are therefore also observed in physical and biological systems.

In this chapter, the reader is first acquainted with reaction-diffusion systems (Sec. 2.1) and with nonlinear dynamics, which is a powerful theoretical framework to describe pattern-forming processes (Sec. 2.2). It is convenient to classify such systems as bistable, oscillatory, and excitable. Since target patterns are found in oscillatory and excitable media, two paradigmatic models for such systems are discussed, the complex Ginzburg-Landau equation (Sec. 2.3) and the FitzHugh-Nagumo model (Sec. 2.4). The chapter closes with a discussion of the basic properties of three-component systems (Sec. 2.5) as well as target patterns and pacemakers (Sec. 2.6).

2.1   Reaction-diffusion systems

Typically, chemical reaction-diffusion systems consist of several species which react with each other and diffuse within the medium. The temporal behavior of a continuously stirred reaction system is governed by the rate equations for the chemical concentrations. Therefore, the spatio-temporal dynamics of a reaction-diffusion system is adequately described by adding diffusion terms to the rate equations. Although this section is devoted to chemical systems, similar mechanisms are present in physical and biological systems as well, justifying the general use of reaction-diffusion models.

Reaction kinetics

To introduce some basic concepts, a simple hypothetical chemical system in liquid phase is considered, consisting of three species U, V, and P. Two irreversible reactions

$$U + V \xrightarrow{k_1} 2U + P, \tag{2.1a}$$

$$3U \xrightarrow{k_2} P. \tag{2.1b}$$
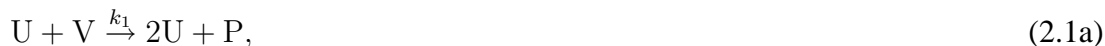
take place in the reactor, where k_1 and k_2 are the rate constants. First, the purely temporal dynamics of the system is discussed, i.e. the species are constantly stirred in the reactor to prevent diffusive transport processes. Even though any realistic system is spatially extended, no effective spatial degrees of freedom are present here. The impact of diffusion will be discussed later.

If the reactions (2.1) take place in an *open flow reactor*, the concentrations of V and P may be kept constant by a continuous influx of reactant V and by removing product P. A constant supply of free energy to the system which drives the system far from equilibrium is associated with the steady flow of chemical species. This energy is used in the reactions before it finally dissipates into the environment. As a result, the open system may continuously sustain irreversible processes, export entropy, and create dissipative structures.

According to the reaction scheme (2.1), the kinetics of species U is determined by the rate equation for its concentration u,

$$\dot{u} = f(u) = k_1 vu - k_2 u^3, \tag{2.2}$$

where the dot denotes the time derivative and v is the constant concentration of reactant V. Note that all rate constants and concentrations are positive. Although three chemical species are present, the dynamics of the system is described by only one variable and represents therefore a *one-component system*.

While the reaction scheme (2.1) is very simple and does not lead to complex dynamics, it already contains some typical features of the pattern-forming systems discussed later. For example, there is an autocatalytic reaction (2.1a) which is controlled by the decay reaction (2.1b): If the concentration u of U is low, the reaction with V leads to an increase of u and thus to an autocatalytic acceleration of reaction (2.1a), while for large concentrations of U, the reaction (2.1b) dominates and u decreases. As a result of the interplay between these processes, the concentration u approaches a constant positive value, representing the stable stationary state of the system. This state depends only on the constants k_1, k_2, and v, and not on the initial concentration of U.

Since stationary states fulfill the condition $\dot{u} = 0$, another stationary state, characterized by the trivial solution with vanishing u, is found for Eq. (2.2). This state, however, is unstable and therefore not realized. Hence, the medium is called monostable and its temporal behavior is characterized by relaxation into that state. A third solution of $f(u) = 0$, representing a state with a negative value of u, has no chemical significance. However, it is easy to imagine a different reaction scheme where all roots of $f(u)$ are positive. Then, two of the three stationary states are stable. Such a system is called bistable and exhibits temporal relaxation in one of the two stable states, depending on the initial condition.

Here, a two-component model is introduced that is already capable of exhibiting oscillatory behavior, the Gray-Scott model [66, 67]

$$A \rightarrow U, \tag{2.3a}$$

$$U \rightarrow V, \tag{2.3b}$$

$$U + 2V \rightarrow 3V, \tag{2.3c}$$

$$V \rightarrow P. \tag{2.3d}$$

Like the above example, it contains only one non-trivial reaction step (2.3c), corresponding to the autocatalytic production of v in the presence of u. The concentration of A is kept constant and the product P is not involved in the kinetics as the reactions are assumed to be irreversible. Thus, the rate equations for U and V are

$$\dot{u} = p_1 - p_2 u - uv^2, \tag{2.4a}$$

$$\dot{v} = -v + p_2 u + uv^2, \tag{2.4b}$$

where the concentrations and time are rescaled such that the system dynamics depends only on two parameters, p_1 and p_2. Both reaction schemes (2.1) and (2.3) lead to nonlinear rate equations. According to mass action kinetics, any reaction among two or more species leads to nonlinear coupling terms. Hence, nonlinear rate equations are imminent for many realistic systems. For pattern-forming systems, autocatalytic reactions like (2.1a) or (2.3c) are a typical source for nonlinear terms in rate equations.

The analysis of the Gray-Scott model shows that it has one stationary state which becomes unstable at a so-called supercritical Hopf bifurcation [67]. In this case the concentrations start to exhibit time-periodic behavior. At onset, such oscillations are characterized by vanishing amplitude and nonvanishing frequency.

The simple examples of nonlinear rate equations like Eqs. (2.2) and (2.4) which have been discussed, just serve as illustrations of chemical reaction kinetics and the concepts of

monostable, bistable, or oscillatory behavior, which are the building blocks of the complex dynamics encountered later in spatially extended reaction-diffusion systems.

A general system of reaction rate equations is given by

$$\dot{\mathbf{u}} = \mathbf{f}(\mathbf{u}; \mathbf{p}), \tag{2.5}$$

where $\mathbf{u}$ denotes the vector of n components u_i, $\mathbf{p}$ denotes the set of m parameters p_j, and $\mathbf{f}$ represents the vector containing the terms corresponding to the kinetics.

Diffusion

Now, a spatially extended chemical system is discussed where diffusion enables the transport of matter and represents the only kind of spatial coupling. This means that the medium is not stirred.

Any inhomogeneous distribution of concentration of a species U leads to a flux J which tries to balance the concentration differences. According to Fick's first law, the flux J is proportional to the concentration gradient,

$$J = -D\nabla u, \tag{2.6}$$

where D denotes the diffusion constant of U and ∇ is the vector of first spatial partial derivatives. Since diffusion leaves the total amount of substance U constant, the continuity equation

$$\partial_t u = -\nabla J \tag{2.7}$$

is valid, where ∂_t denotes the partial temporal derivative. Equations (2.6) and (2.7) give Fick's second law $\partial_t u = \nabla(D\nabla u)$. Assuming that D is not space-dependent, Fick's second law simplifies to the diffusion equation

$$\partial_t u = D\nabla^2 u. \tag{2.8}$$

For a system with n species the general form of the diffusion equation is therefore

$$\partial_t \mathbf{u} = \mathbf{D}\nabla^2 \mathbf{u}, \tag{2.9}$$

where $\mathbf{D}$ is the diffusion matrix.

Diffusion may alternatively be described by a microscopic hopping process. In the mean-field limit of that approach, the deterministic equations displayed above are recovered (for a good discussion, see Ref. [68]). In addition to chemical diffusion, diffusion-like terms in dynamical equations may correspond to heat conduction or optical diffraction.

Reaction and diffusion

The equations for reaction (2.5) and diffusion (2.9) can be combined to form a general n-component reaction-diffusion system

$$\partial_t \mathbf{u} = \mathbf{f}(\mathbf{u}; \mathbf{p}) + \mathbf{D}\nabla^2 \mathbf{u}, \tag{2.10}$$

where $\mathbf{f}$ denotes the reaction term and $\mathbf{D}\nabla^2\mathbf{u}$ the diffusion term.

Of course, Eq. (2.10) should be completed by appropriate initial and boundary conditions. Since in typical experimental systems, initial conditions may be varied to some degree, there are no restrictions on them at this general level. The appropriate boundary conditions to model the borders of a chemical reactor are no-flux boundary conditions. These are a special case of the Neumann boundary conditions, where the flux of the variable through the boundary is set to a constant, here to zero. In some simulations shown later, periodic boundary conditions are used. Periodic boundary conditions connect one point at the boundary of the medium with its opposite point and create a situation where moving patterns stay persistently in the medium.

The appearance of nonlinear terms in the evolution equations, or – more precisely – the fact that reaction-diffusion systems are described by a set of coupled nonlinear partial differential equations, has been explained in terms of chemical kinetics. However, such models are more general. For example, some models for pattern formation in semiconductor devices are also of reaction-diffusion type. The variables in this case may represent the electric current and field densities, and the nonlinearity responsible for the pattern formation may be caused by a negative differential conductivity [6]. Other examples where reaction-diffusion models are applied (at least as an approximation) are gas-discharge systems [7, 32, 33] or optical systems [8] where spot, hexagonal, and traveling wave patterns are found.

2.2 Mathematical modeling of pattern formation

In this section, some basic mathematical tools to describe and to analyze pattern formation in reaction-diffusion systems are introduced. First, diffusion is neglected and the temporal dynamics of uniform systems is studied. Such systems have been investigated in detail in the context of dynamical systems theory. The stationary states of the system are determined and linear stability analysis is applied to check their stability. The appearance of periodic solutions is often associated with stationary states that become unstable. The investigation of sys-

tems close to points in parameter space where the stability of states changes or new solutions appear is called bifurcation analysis. Close to bifurcations, the mathematical description of the system is simplified considerably with the help of normal form theory. With that background, it is then possible to consider the complete reaction-diffusion system including the diffusion effects. Additional information to this section can be found in Refs. [42,44,45,69] for example.

Attractors and linear stability

The first step in the analysis of the system dynamics is to investigate its temporal behavior, neglecting the spatial degrees of freedom. That is, an n-component reaction system of the kind (2.5)

$$\dot{\mathbf{u}} = \mathbf{f}(\mathbf{u}; \mathbf{p}),$$

which is matched by appropriate initial conditions has to be studied. Often, a reaction-diffusion system is interpreted as an ensemble of diffusively coupled active elements. From this point of view, the set of ordinary differential equations (2.5) describes the dynamics of an individual element of the system, sometimes also called *local dynamics*. The number n of components determines the dimension of the phase space in which the vector field $\mathbf{f}$ is defined. In this thesis, this dimension n is typically two or three. A *trajectory* of the system is given by the set of points in phase space that are visited by the system starting from the initial condition. Equation (2.5) is autonomous and therefore any solution of it is unique and the trajectories do not intersect in phase space.

Since the system is dissipative, conservation laws for quantities such as the energy do not exist. This means that trajectories coming from different initial conditions may asymptotically reach the same region in phase space. Mathematically, this is formulated with the help of the *limit sets*, denoting those regions in phase space to where almost all trajectories converge as time $t \to \pm\infty$. Of particular importance are the limit sets for $t \to +\infty$, which are called *attractors*. A system may have various attractors, each having its basin of attraction. All the initial conditions lying in a given basin of attraction will finally lead to the corresponding attractor. These basins of attraction are separated from each other by so-called separatrices. Limit sets for $t \to -\infty$ are called repellers.

Attractors may represent stationary, periodic, quasi-periodic, or chaotic states of the system. In the context of this work, stationary and periodic attractors are important. The station-

ary states or *fixed points* of system (2.5) are denoted as $\mathbf{u}_s$ and are found with the condition $\dot{\mathbf{u}} = 0$.

The next important step is to study the stability of such fixed points. Obviously, any asymptotic state of a dynamical system, i.e. any attractor, is stable because unstable states are never approached in a real or numerical experiment. A fixed point $\mathbf{u}_s$ is called *asymptotically stable* if small perturbations $\boldsymbol{\delta u}(t) := \mathbf{u}(t) - \mathbf{u}_s$ of that state are damped. Stability is checked by means of a *linear stability analysis*. The difference vector $\boldsymbol{\delta u}(t)$ is inserted into Eq. (2.5) and $\mathbf{f}$ is expanded around $\mathbf{u}_s$ in a Taylor series, where only the linear term is kept, yielding

$$\dot{\boldsymbol{\delta u}} = \mathbf{J}(\mathbf{u}_s)\boldsymbol{\delta u}, \quad \text{with } \mathrm{J}_{ij} = \frac{\partial f_i}{\partial u_j}. \tag{2.11}$$

The eigenvalues λ_i of the Jacobian $\mathbf{J}$ evaluated at the fixed point $\mathbf{u}_s$ determine the stability of the stationary state.

For an n-component system, the Jacobian possesses n complex eigenvalues $\lambda_1, ..., \lambda_n$. To each eigenvalue λ_i there exists an eigenvector $\mathbf{e}_i$. Then, the criterion of asymptotic stability reads

$$\text{For all } i = 1, 2, ..., n \quad \mathrm{Re}\lambda_i < 0 \quad \Leftrightarrow \quad \mathbf{u}_s \text{ asymptotically stable,} \tag{2.12}$$
$$\text{there exists an } i \in \{1, 2, ..., n\} \quad \mathrm{Re}\lambda_i > 0 \quad \Leftrightarrow \quad \mathbf{u}_s \text{ asymptotically unstable.} \tag{2.13}$$

Hence, for asymptotic instability it is sufficient that one eigenvalue is positive, even if there are $n - 1$ negative eigenvalues. If a fixed point has both positive and negative eigenvalues, it is said to be of saddle-type. The application of the linear stability analysis assumes that higher-order terms $\mathcal{O}(|\boldsymbol{\delta u}|^2)$ have no influence on the topology of the trajectories close to the fixed point. However, if at least one eigenvalue of the Jacobian is zero while the others are negative, a linear analysis is not sufficient. Later we shall see that this happens at bifurcations, requiring the use of the normal form theory to describe the dynamics there. The present discussion is restricted to *hyperbolic* fixed points, i.e. fixed points where no eigenvalue has a vanishing real part.

General linear stability analysis of fixed points in a two-dimensional phase space yields a quadratic equation for the eigenvalues $\lambda_{1,2}$,

$$\lambda_{1,2} = \frac{1}{2}\left(\mathrm{Tr}\mathbf{J} \pm \sqrt{(\mathrm{Tr}\mathbf{J})^2 - 4(\mathrm{Det}\mathbf{J})}\right), \tag{2.14}$$

where $\mathrm{Tr}\mathbf{J}$ denotes the trace, and $\mathrm{Det}\mathbf{J}$ the determinant of the Jacobian $\mathbf{J}$. It is convenient to classify the fixed points that can occur in such a system as either stable and unstable foci,

stable and unstable nodes, and saddles. A node possesses two real eigenvalues, a focus a pair of complex conjugated eigenvalues. Saddles have real eigenvalues with different signs. In Figure 2.1, an overview over the possible hyperbolic fixed points in a two-dimensional phase space is given.
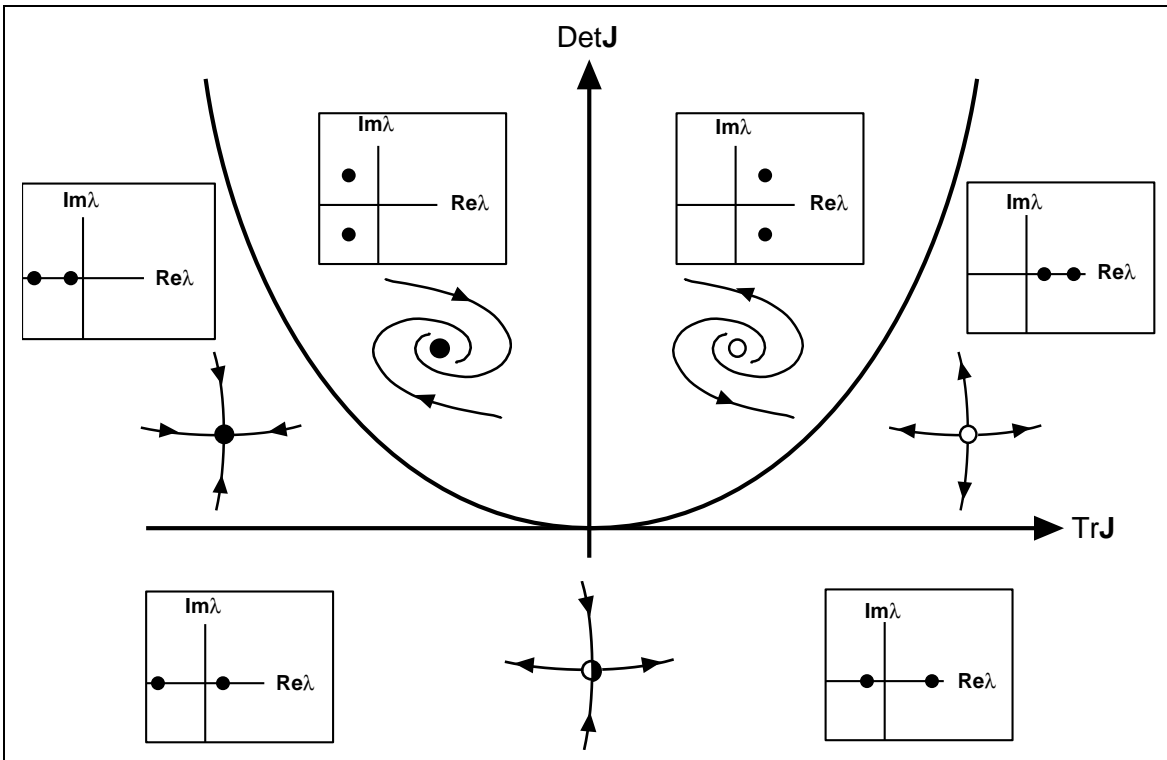

Figure 2.1: **Hyperbolic fixed points for a two-dimensional vector field.** *The trajectories are qualitatively shown for the five types of fixed points. The curve $\mathrm{Det}\mathbf{J} = (\mathrm{Tr}\mathbf{J}/2)^2$ separates the foci from the nodes, the curve $\mathrm{Det}\mathbf{J} = 0$ the nodes from the saddles. The insets schematically display the corresponding eigenvalues in the complex plane.*

While fixed points are the only possible attractor in one-dimensional phase spaces, another important type of attractor is possible in two-dimensional phase spaces, namely the *limit cycle*. The limit cycle is a closed trajectory in phase space that represents time-periodic behavior, i.e. oscillations. It is also possible to perform a linear stability analysis for limit cycles. This so-called *Floquet analysis* uses the Poincaré section, an $(n-1)$-dimensional plane in phase space which is transversally intersected by the limit cycle.

Bifurcations and normal forms

Up to now, the different stationary and periodic solutions of Eq. (2.5),

$$\dot{\mathbf{u}} = \mathbf{f}(\mathbf{u}; \mathbf{p}),$$

and their stability have been discussed. However, it is obvious that the dynamics also depends on the set of parameters **p**. Indeed, both quantitative and qualitative changes of the vector field are possible as the parameters are varied. Qualitative changes may consist of the appearance of a new attractor, or the conversion of an attractor into a repeller. If the topology of the vector field is modified as the result of a parameter change, a *bifurcation* or *instability* has taken place.

Bifurcations are usually classified according to the dimensionality n of the phase space which is required for the bifurcation to take place and to their *codimension*. In the mathematical literature there are rather technical definitions of this concept, but in this context it is sufficient to describe the codimension as the number of parameters that are necessary to be tuned in order to find the bifurcation point.

For simplicity, a stationary state $\mathbf{u}_s$ is considered which lies in the two-dimensional phase space and which depend on one parameter p only. Two cases are of interest here. Either one real eigenvalue of the Jacobian **J** changes sign from negative to positive or a pair of complex conjugate eigenvalues of **J** crosses the imaginary axis.

In the first case, the matrix **J** becomes singular ($\mathrm{Det}\mathbf{J} = 0$) at the parameter value $p = p_c$ and, according to the implicit function theorem (see, e.g. Ref. [42, 44]), the solution $\mathbf{u}_s(p)$ is no longer a smooth function of p. This implies a change of stability of the fixed point and the existence of new stationary solutions. The generic bifurcation for this situation is the *saddle-node* or *fold bifurcation* shown in Fig. 2.2(a). There, a stable node and a saddle appear at the bifurcation point. Therefore, a fold bifurcation creates a new stable stationary solution. Another bifurcation which may appear as one real eigenvalue becomes positive is the *pitchfork bifurcation* [Fig. 2.2(b)]. Here, a stable fixed point loses its stability and at the same time gives rise to two new stable fixed points. The system is then bistable.

In the second case, the matrix **J** is invertible at the parameter value $p = p_c$ and the stationary solution $\mathbf{u}_s(p)$ remains a smooth function at $p = p_c$. However, the trace $\mathrm{Tr}\mathbf{J}$ of the Jacobian vanishes at the parameter value $p = p_c$, and a so-called *Hopf bifurcation* occurs [Fig. 2.2(c)]. This is one of the most important and interesting bifurcations because it is the simplest bifurcation that leads to time-periodic behavior. As the bifurcation point is crossed, a focus loses its stability and gives rise to a harmonic limit cycle, whose amplitude is small and follows a square root dependence close to the bifurcation point. Far from the Hopf bifurcation, the amplitude may become large and the oscillations anharmonic. Already at onset, the oscillations have a nonvanishing frequency.
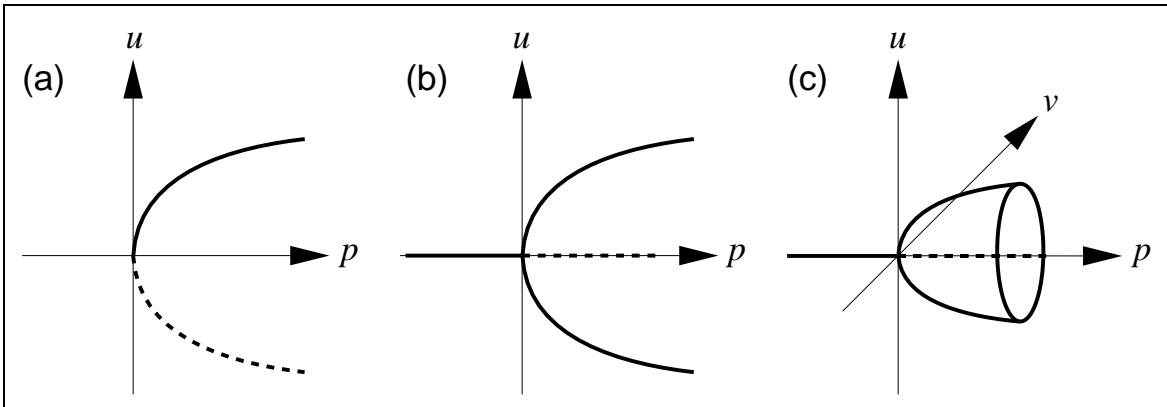
Figure 2.2: **Codimension-one bifurcations for one- and two-dimensional vector fields.** *(a) saddle-node or fold bifurcation, (b) pitchfork bifurcation, and (c) Hopf bifurcation. The variables are denoted by u and v, the control parameter by p, and the bifurcation point is located at the coordinate origin. Solid (dashed) lines denote stable (unstable) states.*

Some bifurcations like the Hopf or pitchfork bifurcation may appear in a super- or subcritical fashion. At a *supercritical* bifurcation, the new solution is stable while the old one becomes unstable. At a *subcritical* bifurcation, the new solution is unstable while the old one becomes stable. In Fig. 2.3(a-b), these different types of Hopf bifurcations are displayed. Figure 2.3(c) illustrates the situation when an unstable limit cycle born in a subcritical Hopf bifurcation is stabilized in a saddle-node bifurcation of limit cycles. Then, a phenomenon called *hysteresis* may be observed. The parameter value p_H, where the large-amplitude oscillations set in as p is decreased from large values, does not coincide with the parameter value p_F where they disappear as p is increased from small values. As a result, there is a region in
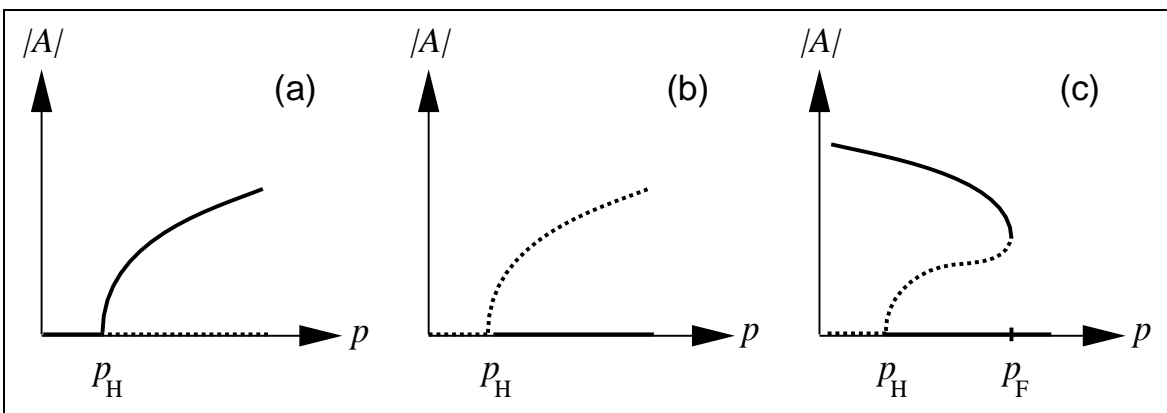

Figure 2.3: **Hopf bifurcations.** *The amplitude $|A|$ of the limit cycle is shown as a function of the control parameter p in a supercritical Hopf bifurcation (a), subcritical Hopf bifurcation (b), subcritical Hopf bifurcation with stabilized limit cycle (c). Solid (dashed) lines denote stable (unstable) states.*

parameter space where a stable limit cycle coexists with a stable fixed point.

The stable and unstable eigenvectors of a fixed point have been discussed above. The set of stable (unstable) eigenvectors spans the stable (unstable) subspace E^{s} (E^{u}) of a fixed point. Since a bifurcation is associated with at least one vanishing real part of an eigenvalue of the Jacobian, a center subspace E^{c} exists which is spanned by the eigenvectors associated with the bifurcating eigenvalues. By construction, the subspaces characterize the time evolution of the system only close to a given fixed point. The nonlinear generalizations of these subspaces are the stable, center, and unstable manifolds W^{s}, W^{c}, and W^{u}, which are defined in the whole phase space. Close to the fixed points, the manifolds are approximated by the linear subspaces.

The *center manifold theorem* plays an important role in the study of the dynamics close to bifurcations (see, e.g. Ref. [42]). It states that sufficiently close to the bifurcation and after a possible short transient, the dynamics of the system (2.5) takes place on the center manifold. Therefore, close to a bifurcation, it is sufficient to study the dynamics of the center manifold instead of the complete dynamics. Since the dimensionality of the center manifold is typically lower than the phase space dimension n, the reduced system usually is easier to solve. The specific differential equation that describes the dynamics on the center manifold is called a *normal form*. The normal form is universal in the sense that all dynamical systems undergoing the same bifurcation are described by the same normal form close to the bifurcation point. The validity of the center manifold theorem can be illustrated for a system where one real eigenvalue crosses the imaginary axis while all other eigenvalues remain negative. Close to the bifurcation point, the bifurcating eigenvalue has a real part close to zero. Therefore, its modulus is much smaller than the modulus of any other eigenvalue. This means that the eigenmode of the bifurcating eigenvalue has a much slower dynamics than any other eigenmode. As a result, after the decay of the transient, the temporal behavior of the system is characterized by the bifurcating eigenmode. In other words, the dynamics becomes very slow close to the bifurcation and the nonbifurcating eigenmodes may be *adiabatically eliminated*. The normal forms of the fold and the supercritical pitchfork bifurcation are given by

$$\dot{u} = p - u^2, \quad \text{fold bifurcation,} \tag{2.15a}$$

$$\dot{u} = pu - u^3, \quad \text{pitchfork bifurcation.} \tag{2.15b}$$

Since the normal form contains one variable only, such bifurcations can already be found in one-component systems. Furthermore, for any n-component system which exhibits a fold

or pitchfork bifurcation, the dynamics is restricted to a one-dimensional subspace of the n-dimensional phase space. The normal form of the Hopf bifurcation is given by

$$
\begin{aligned}
\dot{u} &= pu - v - u(u^2 + v^2), \\
\dot{v} &= u + pv - v(u^2 + v^2).
\end{aligned}
\tag{2.16}
$$

The method to adiabatically eliminate the fast modes can be applied not only close to bifurcations but also in more general situations when, for example, a system displays dynamics on very different time scales. Later, it will be shown that a field of weakly coupled oscillators described by an amplitude and a phase variable exhibits dynamics on different time scales, enabling an adiabatic elimination of the amplitude variable.

Distributed active media

The theory discussed so far has only been concerned with systems of ordinary differential equations (2.5). However, a reaction-diffusion system (2.10)

$$
\partial_t \mathbf{u} = \mathbf{f}(\mathbf{u}; \mathbf{p}) + \mathbf{D}\nabla^2 \mathbf{u}
$$

models a spatially extended (or *distributed*) medium and is represented by a set of partial differential equations. The phase space of such a system is effectively infinite-dimensional.

At this point it is convenient to translate some concepts of attractors and stability to spatially extended systems. Of course, the uniform solutions of Eq. (2.10) coincide with the solutions of the ordinary differential equation (2.5) studied above. In this way, uniform stationary states or homogeneous oscillations may be investigated. However, the asymptotic solution of Eq. (2.10) is, in general, space-dependent, representing, for example, spiral and target waves, Turing structures, or localized structures. In order to find an analytical solution of such patterns, a strong separation of length and time scales or the presence of very small terms in the equations often have to be assumed [14, 70].

The next concept that shall be extended to the dynamics of distributed systems is the concept of bifurcations. It is necessary to incorporate the spatial degrees of freedom into the description. While for a system (2.5) there is a discrete band of n eigenvalues, the spectrum of eigenvalues is continuous for a spatially extended system (2.10). For simplicity, a uniform system is considered which is situated in a stationary state denoted as $\mathbf{u}_{\mathrm{s}}$ and which resides in a one-dimensional infinitely-extended physical space. Then, it is possible to write near the bifurcation the unknown solution $\mathbf{u}(x, t)$ as an expansion of Fourier modes $\mathbf{u}_q(x, t)$ in the

following way

$$\mathbf{u}(x,t) = \mathbf{u}_\mathrm{s} + \int_0^\infty \mathbf{u}_q(x,t)\, dq, \tag{2.17a}$$

$$\mathbf{u_q}(x,t) = \mathbf{v}_q(x)A_q \mathrm{e}^{\lambda(q)t + \mathrm{i}qx} + \overline{\mathbf{v}}_q(x)B_q \mathrm{e}^{\overline{\lambda}(q)t + \mathrm{i}qx} + \text{h.o.t.}, \tag{2.17b}$$

where "h.o.t." denotes terms of higher order. The Fourier modes with a wavenumber q depend on the eigenvector $\mathbf{v}_q$, which is determined from the linearized problem, and on the complex amplitudes $A_q(x,t)$ and $B_q(x,t)$, which are discussed later. The superposition of the latter characterizes the pattern which is associated with the wavenumber q. The complex eigenvalue λ of the linearized problem can be decomposed into its real part σ and imaginary part ω in the following way

$$\lambda(q,p) = \sigma(q,p) + \mathrm{i}\omega(q,p), \tag{2.18}$$

where it is assumed for simplicity that the bifurcation only depends on one parameter p. For $p < p_\mathrm{c}$ all perturbations decay, i.e. $\sigma < 0$ for all q. The critical parameter value p_c is given by $\sigma(q_\mathrm{c}, p_\mathrm{c}) = 0$ for a critical q_c, while all other modes relax for $t \to \infty$, i.e. $\sigma(q, p_\mathrm{c}) < 0$ for all $q \neq q_\mathrm{c}$. Then, the critical Fourier mode $\mathbf{u}_{q_\mathrm{c}}(x,t)$ is given, after a short transient, by

$$\mathbf{u}_{q_\mathrm{c}}(x,t) = \mathbf{v}_{q_\mathrm{c}}(x)A_{q_\mathrm{c}} \mathrm{e}^{\mathrm{i}(q_\mathrm{c}x + \omega_\mathrm{c}t)} + \overline{\mathbf{v}}_{q_\mathrm{c}}(x)B_{q_\mathrm{c}} \mathrm{e}^{\mathrm{i}(q_\mathrm{c}x - \omega_\mathrm{c}t)}, \tag{2.19}$$

where $\omega_\mathrm{c} = \omega(q_\mathrm{c}, p_\mathrm{c})$. Therefore, the systems may be classified according to the mode with the eigenvalue that first crosses the imaginary axis. At the bifurcation point, the critical wavenumber q_c and critical frequency ω_c may be zero or nonzero, yielding three cases which are of interest here [1]. The case $q_\mathrm{c} = 0$, $\omega_\mathrm{c} \neq 0$ corresponds to the distributed Hopf bifurcation, the case $q_\mathrm{c} \neq 0$, $\omega_\mathrm{c} = 0$ to the Turing bifurcation, and the case $q_\mathrm{c} \neq 0$, $\omega_\mathrm{c} \neq 0$ to the wave bifurcation. The equations for the complex amplitudes A and B are determined by a multiple-scale or normal form analysis and are called *amplitude equations*. Such a derivation is performed in Appendix A.2 for the system investigated in Chapter 4.

2.3 The complex Ginzburg-Landau equation

Reaction-diffusion systems can display different types of oscillatory dynamics. However, in the vicinity of a supercritical Hopf bifurcation, where oscillations have small amplitude and are approximately harmonic, all such systems are described by the same model – the complex Ginzburg-Landau equation (CGLE). In this section, some general considerations

about this equation are presented before special features are discussed: uniform oscillations, plane waves, the Eckhaus instability of plane waves, spiral and target wave solutions, and the phase dynamics approximation.

General properties

The complex Ginzburg-Landau equation is given by

$$\partial_t A = (\lambda_1 \mu - \mathrm{i}\omega_\mathrm{H})A + g_1|A|^2A + d_A\nabla^2 A, \tag{2.20}$$

where A is the complex oscillation amplitude, μ the distance to the Hopf bifurcation point, ω_H the frequency of the system at the Hopf bifurcation, and λ_1, g_1, and d_A complex parameters which are determined by the underlying specific reaction-diffusion system. If the following rescalings for the amplitude $A \to \sqrt{(-g_1^r)/(\mu\lambda_1^r)}A$, time $t \to (\mu\lambda_1^r)t$, and spatial coordinates $x \to x\sqrt{(\mu\lambda_1^r)/d_A^r}$ are performed (the superscripts r and i denote the real and imaginary parts of the parameters respectively), the CGLE transforms to

$$\partial_t A = (1 - \mathrm{i}\omega)A - (1 + \mathrm{i}\alpha)|A|^2A + (1 + \mathrm{i}\beta)\nabla^2 A, \tag{2.21}$$

where $\omega = (\omega_\mathrm{H}/\mu - \lambda_1^i)/\lambda_1^r$, $\alpha = g_1^i/g_1^r$, and $\beta = d_A^i/d_A^r$. By going into a coordinate frame that rotates with the frequency ω, i.e. by performing the transformation $A \to A\exp(-\mathrm{i}\omega t)$, it is possible to scale out the frequency ω and the distance μ from the Hopf bifurcation point. Therefore, the dynamics of the CGLE effectively depends only on two parameters α and β, which are the nonlinear frequency and linear dispersion coefficients respectively. In this work, the parameter ω is kept to facilitate a qualitative comparison of the CGLE with an underlying reaction-diffusion system. In the context of the model considered in Chapter 3, this topic is discussed in Appendix A.1.

The CGLE exhibits a vast range of phenomena, ranging from plane and spiral waves to localized coherent structures and spatio-temporal chaos. The CGLE is not only the paradigmatic equation for oscillatory systems but also one of the most studied models in nonlinear science in general. It was derived by Newell and Whitehead in 1969 in the context of hydrodynamic systems [71, 72] and by Kuramoto and Tsuzuki in 1974 for chemical systems [73]. Furthermore, both the real Ginzburg-Landau equation describing phase transitions and the nonlinear Schrödinger equation displaying soliton solutions can be viewed as limit cases of the CGLE. For a recent review of the CGLE see Ref. [47]. The derivation of the CGLE from a specific reaction-diffusion model is explained in Refs. [53, 74]. The predictions based on this universal amplitude equation often remain qualitatively correct even further away

from the bifurcation point, where oscillation amplitudes are moderate and deviations from harmonicity are significant.

Uniform oscillations

Starting the discussion with the temporal dynamics of the uniform system, the diffusion term is dropped and the Stuart-Landau equation

$$\dot{A} = (1 - \mathrm{i}\omega)A - (1 + \mathrm{i}\alpha)|A|^2 A, \tag{2.22}$$

describing a limit cycle oscillator is obtained. Introducing the phase ϕ and the real amplitude ρ as

$$A = \rho \exp(-\mathrm{i}\phi), \tag{2.23}$$

and substituting this ansatz into Eq. (2.22), the two equations

$$\dot{\rho} = (1 - \rho^2)\rho, \tag{2.24a}$$
$$\dot{\phi} = \omega + \alpha\rho^2, \tag{2.24b}$$

are obtained. These illustrate a typical property of a nonlinear oscillator, namely, that a change in the phase, i.e. the frequency, depends on the amplitude. The stable limit cycle solution

$$A(t) = \rho_{\mathrm{SL}} \exp(-\mathrm{i}\omega_{\mathrm{SL}}t), \tag{2.25}$$

with constant frequency

$$\omega_{\mathrm{SL}} = \omega + \alpha \tag{2.26}$$

and amplitude

$$\rho_{\mathrm{SL}} = 1, \tag{2.27}$$

is the only attractor of the Stuart-Landau equation.

In the spatially extended system, the limit cycle solution (2.25) corresponds to uniform oscillations. A linear stability analysis for that state reveals that uniform oscillations are stable with respect to small phase perturbations if the Benjamin-Feir-Newell condition

$$1 + \alpha\beta > 0, \tag{2.28}$$

is satisfied. If this condition is violated, a chaotic spatio-temporal behavior denoted as phase turbulence sets in. This and other regimes displaying spatio-temporal chaos like amplitude and intermittent turbulence are not of interest in the context of this work and therefore not discussed further.

Plane waves

An important family of solutions of the CGLE are plane waves

$$A(x,t) = \rho_k \exp(\mathrm{i}kx - \mathrm{i}\omega_k t), \tag{2.29}$$

with frequency

$$\omega_k = \omega_{\mathrm{SL}} + (\beta - \alpha)k^2, \tag{2.30}$$

and amplitude

$$\rho_k = \sqrt{1 - k^2}, \tag{2.31}$$

where k denotes the constant wavenumber of the waves which according to Eq. (2.23) is equal to the phase gradient $k = -\nabla\phi$. The dependence of the wave frequency ω_k on the wavenumber k constitutes the dispersion relation. When $\beta - \alpha > 0$, the frequency increases with the wavenumber and the waves have *positive* dispersion. In the opposite case, the dispersion is *negative*. The *phase velocity* is defined as $v_{\mathrm{p}} = \omega_k/k$ and given by

$$v_{\mathrm{p}} = \omega_{\mathrm{SL}}/k + (\beta - \alpha)k. \tag{2.32}$$

It characterizes the speed at which the positions of wave maxima move. The *group velocity* is defined as $v_{\mathrm{g}} = \partial\omega_k/\partial k$, so that

$$v_{\mathrm{g}} = 2(\beta - \alpha)k. \tag{2.33}$$

It determines the velocity at which small perturbations (wave packets) propagate through the medium. It is the group velocity that determines the transport of matter and information in the system. Note that for $\alpha = \beta$ the group velocity is zero and the frequency of waves with arbitrary k is equal to that of uniform oscillations. This case, however, is not generic and not considered further.

Strictly speaking, the wavenumber k and the group and phase velocities are vector quantities, i.e. point into the direction of the propagating waves. In the context of this work, they may be treated as scalar quantities since their magnitude is of principal interest here. Whenever the direction of waves matters, it will be mentioned explicitly.

Uniform oscillations correspond to plane waves with $k = 0$. In the long-wavelength limit $k \to 0$, the phase velocity diverges, while the group velocity vanishes. In the long-wavelength limit, the amplitude of plane waves approaches that of uniform oscillations. On the other hand, the amplitude of plane waves vanishes as $k \to 1$, thus not admitting waves with wavelengths smaller than 2π (in renormalized units). At the same time, the frequency of the waves approaches $\omega_k \to \omega + \beta$.

Eckhaus instability

We have seen that plane waves exist only for wavenumbers $k < 1$. Actually, plane waves will become unstable before they reach this propagation failure boundary. It is possible to perform a stability analysis for the plane waves (see, e.g. Ref. [47]) which shows that waves with a wavenumber larger than

$$k_{\mathrm{EI}} = \sqrt{\frac{1 + \alpha\beta}{2(1 + \alpha^2) + 1 + \alpha\beta}}, \tag{2.34}$$

are unstable with respect to long-wavelength modulations. This instability is called *Eckhaus instability*. It can appear in two flavors and two different types of spatio-temporal behavior are possible. The Eckhaus instability can be supercritical and modulated amplitude waves are stable solutions [75]. Alternatively, this instability may be subcritical and the perturbation does not saturate. Then, the wave is compressed until the amplitude locally drops down to zero at some time moments corresponding to phase singularities. Such events are associated with a phase slip of 2π, the disappearance of a wave and a subsequent readjustment of the wavenumber on both sides of the defect [76].

In two spatial dimensions, spiral breakup into turbulence is then possible [77–80]. In this context, the distinction between convective and absolute Eckhaus instability is important [81]. If an infinitesimal perturbation of an unstable traveling wave state is advected away with the wave and asymptotically decays at any fixed position, the system is in the regime of convective Eckhaus instability. If this perturbation grows even at fixed positions, then the instability is called absolute. It has been demonstrated that wave breakup in a bounded domain reflects an absolute Eckhaus instability [77]. Recently, it has been shown that the eigenvalue spectrum of a reaction-diffusion system depends strongly on whether a bounded or an unbounded domain is considered, and that it is the so-called absolute spectrum which determines the breakup of spirals [79]. Furthermore, the boundary conditions and the size of the perturbation influence the onset of the instability.

Spiral and target waves

Spiral and target waves are typical two-dimensional wave patterns found in reaction-diffusion systems. Spiral waves are particularly well studied in the CGLE. The general form of a spiral wave is

$$A(r, t) = \rho_{\mathrm{sp}}(r) \exp(-\mathrm{i}\phi_{\mathrm{sp}}(r, \theta, t)), \tag{2.35}$$

where r and θ are the radial and angular coordinates of the two-dimensional spatial domain, ρ_{sp} the amplitude, and ϕ_{sp} the phase of the target waves. The phase can be written as

$$\phi_{\mathrm{sp}}(r, \theta, t) = \omega_{\mathrm{sp}} t - m\theta - \psi_{\mathrm{sp}}(r), \tag{2.36}$$

where ω_{sp} is the frequency of the spiral, m the topological charge, and $\psi_{\mathrm{sp}}(r)$ the radial contribution to the phase. For single-armed spirals, $m = \pm 1$ is fulfilled, where the sign of m determines the direction of rotation. A spiral wave of this kind has a phase singularity in its center where the amplitude $\rho_{\mathrm{sp}}(r)$ drops down to zero.

The general form of a target wave solution in the CGLE is given by

$$A(r, t) = \rho_{\mathrm{tp}}(r) \exp(-\mathrm{i}\phi_{\mathrm{tp}}(r, t)), \tag{2.37}$$

where ρ_{tp} is the amplitude and

$$\phi_{\mathrm{tp}}(r, t) = \omega_{\mathrm{tp}} t - \psi_{\mathrm{tp}}(r), \tag{2.38}$$

the phase of the target waves. In contrast to spiral waves, target waves do not have an angular dependence in the plane of the two-dimensional pattern and do not have a phase singularity in the center of the spiral.

Far from the center of the pattern, i.e. for $r \to \infty$, both the spiral and the target wave solutions approach the plane wave solution $\phi \to \omega_k t - kr$ with wavenumber k, amplitude $\rho \to \sqrt{1 - k^2}$, and frequency $\omega_k = \omega + \alpha + (\beta - \alpha)k^2$. However, while the spiral wave solution is stable and its frequency is determined by the parameters, the target wave solution is unstable and its frequency depends on the initial condition.

Phase dynamics approximation

Wave patterns can be described by phase dynamics equations if the wavelength is large and, more generally, phase perturbations are smooth [53]. Using the description in terms of phase ϕ and real amplitude ρ as introduced above as $A = \rho \exp(-\mathrm{i}\phi)$, the CGLE is equivalent to the equations

$$\partial_t \rho = (1 - \rho^2)\rho + \nabla^2 \rho - \rho(\nabla\phi)^2 + \beta\rho\nabla^2\phi + 2\beta\nabla\phi\nabla\rho, \tag{2.39a}$$

$$\partial_t \phi = \omega + \alpha\rho^2 + (2/\rho)\nabla\rho\nabla\phi + \nabla^2\phi - (\beta/\rho)\nabla^2\rho + \beta(\nabla\phi)^2. \tag{2.39b}$$

Now it is assumed that smooth phase perturbations with a large characteristic length L_p are present. Hence, it is expected that the amplitudes are close to $\rho_{\mathrm{SL}} = 1$. From the definition

of the amplitude deviation $\delta\rho$,

$$\delta\rho = \rho - 1, \tag{2.40}$$

follows

$$\rho^2 = 1 + 2\delta\rho + (\delta\rho)^2. \tag{2.41}$$

If the term $(1 - \rho^2)$ in Eq. (2.39a) is replaced by the expression for the amplitude deviation, the equation

$$\partial_t\rho = \rho\left[-2\delta\rho - (\delta\rho)^2 - (\nabla\phi)^2 + \beta\nabla^2\phi\right] + \nabla^2\rho + 2\beta\nabla\rho\nabla\phi \tag{2.42}$$

is obtained. Using the definition (2.40) and the abbreviations $f = \nabla^2\rho + 2\beta\nabla\rho\nabla\phi$ and $g = -(\nabla\phi)^2 + \beta\nabla^2\phi$, it follows

$$\partial_t\rho = \partial_t(\delta\rho) = g - (2 - g)\delta\rho - 3(\delta\rho)^2 - (\delta\rho)^3 + f. \tag{2.43}$$

Now it is used that the amplitude deviations are small $|\delta\rho| \ll 1$ and the amplitude is constant, i.e. $\partial_t(\delta\rho) = 0$. Then, the amplitude deviation is given by

$$\delta\rho \approx \frac{g + f}{2 - g}. \tag{2.44}$$

For $|f| \ll |g| \ll 1$, which reflects the fact that amplitude gradients are much smaller than phase gradients for the considered long-wavelength perturbation, the amplitude deviation $\delta\rho$ is given by

$$\delta\rho \approx \frac{g}{2} = \frac{1}{2}\left(-(\nabla\phi)^2 + \beta\nabla^2\phi\right), \tag{2.45}$$

which includes all terms which are proportional to L_p^{-2} and neglects all higher-order terms. With the help of Eq. (2.41), the following equation for ρ^2 is obtained

$$\rho^2 = 1 - (\nabla\phi)^2 + \beta\nabla^2\phi. \tag{2.46}$$

Since it has been required that $|\delta\rho| \ll 1$, this means that $|\nabla\phi| \ll 1$ is necessary. Above, a constant phase gradient has been associated with a plane wave with a constant wavenumber k and it follows

$$k \ll 1. \tag{2.47}$$

With help of Eq. (2.46), Eqs. (2.39) are finally reduced to a single dynamical equation for the local oscillation phase (see, e.g. Ref. [53]),

$$\partial_t\phi = \omega + \alpha + (\beta - \alpha)(\nabla\phi)^2 + (1 + \alpha\beta)\nabla^2\phi. \tag{2.48}$$

Note that the Benjamin-Feir-Newell condition for unstable uniform oscillations corresponds to a negative phase diffusion coefficient in the phase dynamics equation. In this thesis, it is assumed that $1 + \alpha\beta > 0$ is satisfied and uniform oscillations are modulationally stable. The phase equations (2.39b) and (2.48) do not depend explicitly on the phase ϕ. This reflects the fact that the complex Ginzburg-Landau equation is invariant with respect to global phase shifts $A \rightarrow A \exp(\mathrm{i}\phi_0)$, where ϕ_0 is a constant.

Quintic complex Ginzburg-Landau equation

The CGLE discussed above, is sometimes also called cubic Ginzburg-Landau equation because of the cubic term. The cubic CGLE describes a stable limit cycle coexisting with an unstable fixed point. This is reflected by the fact that the sign of the real coefficient of the linear term is positive and the sign of the real coefficient of the cubic term is negative.

If the Hopf bifurcation is subcritical, a stable fixed point coexists with an unstable limit cycle solution. If that limit cycle solution is stabilized in a saddle-node bifurcation of limit cycles [Fig. 2.3(c)], a stable fixed point coexists with a stable limit cycle. Such a situation can be modeled by the quintic complex Ginzburg-Landau equation given by

$$\partial_t A = \mu A + a|A|^2 A - g|A|^4 A + b\nabla^2 A, \tag{2.49}$$

where μ is the real bifurcation parameter and a, g, and b are complex coefficients [47]. The real parts of a and g are positive. This equation displays interesting dynamics, in particular moving fronts and stable localized pulse solutions.

2.4   The FitzHugh-Nagumo model

This section is devoted to the FitzHugh-Nagumo model which is a paradigmatic model for active media, in particular for the important class of activator-inhibitor systems. Such media may exhibit bistable, excitable, or oscillatory behavior.

In the year 1952, Hodgkin and Huxley published an article on the membrane potential and current of giant squid axons [82]. Their work quantitatively explained the excitability of neural cells and subsequently the propagation of action potentials. The Hodgkin-Huxley model contained 4 variables and more than 10 constants which made a qualitative understanding of the phenomena quite difficult. Later, FitzHugh [83] and Nagumo *et al.* [84] derived a simpler model which preserved the main findings qualitatively. The resulting equations nowadays are

called the FitzHugh-Nagumo model, which reads

$$\tau_u \partial_t u = u - u^3 - v + l_u^2 \nabla^2 u, \tag{2.50a}$$

$$\tau_v \partial_t v = \alpha u + \beta - v + l_v^2 \nabla^2 v. \tag{2.50b}$$

This model describes the evolution of two diffusive variables u and v in a spatially extended medium. The parameters l_u and l_v represent the diffusion lengths, and τ_u and τ_v the characteristic time constants of the system variables. It will be assumed that u has fast dynamics compared to v, i.e. $\tau_u \ll \tau_v$. The parameters α and β determine the local kinetics of the variable v. In particular, if $\alpha > 0$, the variable u is called activator, since it leads to an increase of u (at least for small u) and v. On the other hand, v is called inhibitor because it decreases u and v. Therefore, the FitzHugh-Nagumo model is an example of an *activator-inhibitor system*. It has already been pointed out in Sec. 2.1 that the presence of nonlinear terms (in this case the cubic term for u in Eq. (2.50a)) is necessary to observe pattern formation.

With the help of such a two-component activator-inhibitor system, it is possible to discuss many features of general pattern-forming active media. For each ordinary differential equation $\dot{u}_i = f_i(u_1, u_2, ..., u_n)$ there exists a curve in phase space called *nullcline* (or null-isocline) which obeys $\dot{u}_i = 0$. Consequently, the intersections of the nullclines determine the stationary states of the system. By means of the nullclines and the ratios of time and length scales, active media may be classified as *bistable*, *excitable*, or *oscillatory* (see, e.g. Ref. [45]). In Fig. 2.4, the nullclines of typical bistable, excitable, and oscillatory media, as present in the FitzHugh-Nagumo model (2.50), are shown.
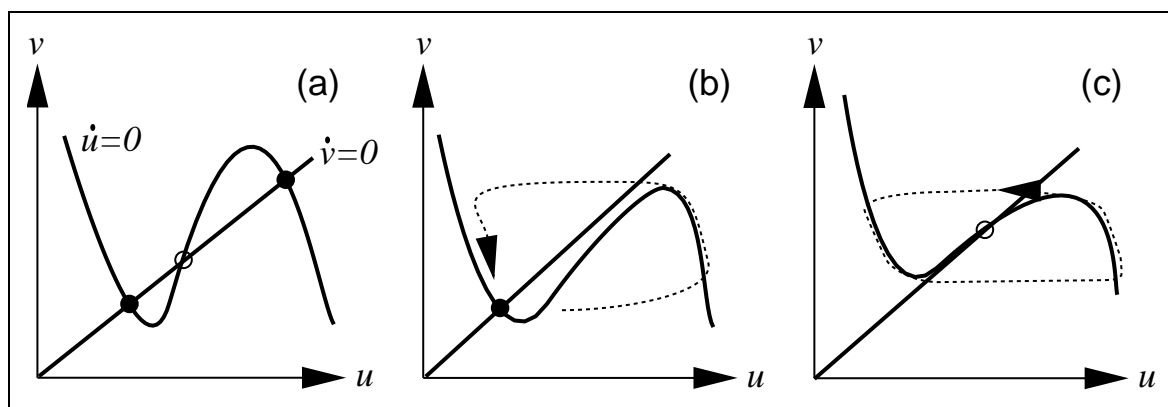

Figure 2.4: **Active media.** *Schematic drawings of a phase space with (a) bistable, (b) excitable, and (c) oscillatory dynamics. Solid lines denote the nullclines, black (white) dots denote stable (unstable) fixed points. The dotted line illustrates in (b) a typical excitable trajectory and in (c) the limit cycle.*

The nullclines of a typical bistable system [Fig. 2.4(a)] intersect three times, giving rise

to two stable and one unstable fixed points. The course of the separatrix between the basins of attraction of the two attractors depends on the characteristic times τ_u and τ_v. Therefore, the initial condition and the two time scales determine which stable state is chosen by the system.

In the spatially extended system, the typical pattern of a bistable medium is a *front*, i.e. an interface that separates two domains where the system resides in the two stable stationary states. The front velocity depends on the parameters and on the front curvature and generally does not vanish. Therefore, the domain where the metastable state is present shrinks and finally disappears. The diffusion lengths determine the width of the front. As seen in Sec. 2.1, one-component systems may already display bistability.

The local dynamics of an excitable medium [Fig. 2.4(b)] is characterized by a stable fixed point and the presence of a relatively fast activator. This indicates that an excitable element has to be described by at least two components. Since the characteristic time of the activator is much smaller than that of the inhibitor, the system quickly relaxes to the nullcline of u, starting from any initial condition. However, this nullcline is a non-monotonous curve in phase space and consists of two attracting branches for small and large values of u respectively, and one repelling branch for intermediate values of u. Since in the example shown in Fig. 2.4(b), the fixed point is located at the left part of the nullcline, small perturbations of that state decay immediately, while perturbations which overcome a certain threshold increase and decay only after the system has performed a large loop in phase space. In this case, the system first goes to the right branch of the nullcline of u, then moves along this nullcline, drops for large v from large to small values of u, and then relaxes to the fixed point on the left branch of the nullcline of u.

In the spatially extended system such a medium supports *pulses* if the diffusive coupling of the excitable elements is strong enough, in particular when the diffusion length of the activator is smaller than that of the inhibitor. Note that excitable behavior of a single element is not sufficient for the observation of pulses in the spatially extended system. In the leading part of the pulse, the activator increases strongly while the profile of the inhibitor concentration increases only very smoothly. In the center part of the pulse, the activator concentration reaches its maximum and starts to decrease slightly. In the tail of the pulse, the inhibitor reaches its maximum which is associated with a strong decrease in the activator concentration. While the inhibitor concentration returns slowly to its stationary value, the activator may relax quickly and with a non-monotonous profile. The shape and velocity of a pulse depend only on the parameters and not on the initial conditions. Roughly speaking, the

diffusion length of the activator determines the width of the leading part of the pulse, while the diffusion length of the inhibitor sets the overall width of the pulse. In two or three spatial dimensions, more complex patterns such as spirals or scroll waves are possible in excitable media.

Oscillatory media are characterized by a closed trajectory in phase space and are therefore necessarily described by at least two variables. In Fig. 2.4(c), an unstable fixed point surrounded by a limit cycle is present. The fixed point is unstable because it is assumed that u has much faster dynamics than v.[1] As a result, the oscillations are anharmonic and have large amplitudes. In a spatially extended medium governed by such *relaxational* oscillations, wave trains with an anharmonic profile are observed. If a limit cycle appears via a supercritical Hopf bifurcation, the oscillations are harmonic and have small amplitudes. In this case, the dynamics of the system is effectively described by the complex Ginzburg-Landau equation, which has been described in Sec. 2.3. The typical possible regular patterns in oscillatory systems are spiral waves and target patterns. The latter are discussed in Sec. 2.6.

Many variants of the FitzHugh-Nagumo model and closely related models exist like, for example, the Bonhoeffer-van der Pol model which goes back to fundamental work of van der Pol [85, 86] and Bonhoeffer [87]. The FitzHugh-Nagumo model has been investigated in detail in the recent decades and exhibits a rich variety of temporal [88] and spatio-temporal dynamics (for a review on excitable behavior, see Ref. [46]). Although not a normal form, the FitzHugh-Nagumo equations represent a fundamental model for pattern-forming systems.

2.5   Three- and four-component models

The complex Ginzburg-Landau equation and the FitzHugh-Nagumo model represent two-component systems. Such models are capable of displaying a wealth of phenomena, as explained in Sec. 2.3 and Sec. 2.4. In this section, a brief introduction into three- and four-component systems is given by presenting several typical examples.

Reaction-diffusion systems may consist of many reactants. For example, according to the Field-Körös-Noyes mechanism [89], the BZ reaction involves 14 species and 10 reactions (for a discussion see, e.g. Ref. [67]). In a mathematical analysis, the scheme can be reduced

---

[1]If the timescales of u and v are comparable, but the diffusion lengths very different, the appearance of Turing patterns is possible.

until the so-called three-component Oregonator model

$$\tau_u \partial_t u = qv - uv + u(1 - u) + D_u \nabla^2 u, \tag{2.51a}$$

$$\tau_v \partial_t v = -qv - uv + fw + D_v \nabla^2 v, \tag{2.51b}$$

$$\partial_t w = u - w + D_w \nabla^2 w \tag{2.51c}$$

is obtained, where u, v, and w stand for the concentrations of $HBrO_2$, Br^-, and the metal catalyst respectively [90]. The Oregonator model is the basic model for the BZ reaction which, however, is often modified to account for the multitude of variants of the BZ reaction. Since the parameter τ_v typically is two orders of magnitude smaller than τ_u, the variable v is often adiabatically eliminated, yielding a two-component model.

Another example of a three-component model is the Krischer-Eiswirth-Ertl model [91–94] for the CO oxidation reaction on platinum single crystal surfaces. In the distributed system it is given by the equations

$$\partial_t u = k_1 \, p_{\mathrm{co}} \, s_{\mathrm{co}} \, (1 - u^3) - k_2 \, u - k_3 \, uv + D \nabla^2 u, \tag{2.52a}$$

$$\partial_t v = k_4 \, p_{\mathrm{o_2}} \, [s_{1 \times 1} w + s_{1 \times 2}(1 - w)](1 - u - v)^2 - k_3 \, uv, \tag{2.52b}$$

$$\partial_t w = k_5 \left(\left[1 + \exp((u_0 - u)\delta u^{-1})\right]^{-1} - w \right). \tag{2.52c}$$

The components u and v denote the surface coverage of carbon monoxide and oxygen respectively. The variable w is related to the adsorbate driven phase transition in the top surface layer and represents the local fraction of the surface area found in the 1×1 surface structure (while the rest is in the 1×2 structure). Note that only carbon monoxide is able to diffuse on the platinum surface. For details, the reader is referred to Ref. [94]. The model can be further reduced by eliminating the oxygen variable. In this way, the Krischer-Eiswirth-Ertl model can be mapped [95] to the Barkley model [96] which itself can be viewed as a variant of the FitzHugh-Nagumo model. On the other hand, to explain experimental observations such as standing waves or the reflective collision of pulses, an additional variable representing subsurface oxygen must be taken into account [97], yielding a four-variable model.

It has already been mentioned that pattern formation in gas-discharge systems may be described by reaction-diffusion models. A striking experimental finding in such systems are spots that persistently move in a two-dimensional spatial domain. On collision, such objects may reflect, which is unknown behavior for two-component models. In the following, the extension of a two-component model to a three-component model for this system is sketched

according to Ref. [33]. The two-component model

$$\partial_t u = \lambda u - u^3 - v + \kappa_1 + D_u \nabla^2 u, \tag{2.53a}$$

$$\tau \partial_t v = u - v + D_v \nabla^2 v \tag{2.53b}$$

of an activator u and inhibitor v is able to produce moving spots in two-dimensional spatial domains which, however, are unstable. To stabilize the motion, a global feedback term can be added to Eq. (2.53a) in the following way

$$\kappa_1 = \kappa_1^{\text{new}} - \kappa_2 \frac{1}{S_\Omega} \int_\Omega u \, dx, \tag{2.54}$$

where κ_1^{new} and κ_2 are new parameters, and Ω the two-dimensional spatial domain with size S_Ω. The bifurcation to moving spots in nonlocally coupled media in a general context has been investigated by Krischer and Mikhailov [98]. As an alternative to global coupling, a three-component system

$$\partial_t u = \lambda u - u^3 - v - \kappa_3 w + \kappa_1 + D_u \nabla^2 u, \tag{2.55a}$$

$$\tau \partial_t v = u - v + D_v \nabla^2 v, \tag{2.55b}$$

$$\theta \partial_t w = u - w + D_w \nabla^2 w, \tag{2.55c}$$

can be used which gives rise to stable moving spots just by means of diffusion. The new variable w plays the role of an additional inhibitor and should have fast kinetics and strong diffusion. For $\theta \to 0$ and $D_w \to \infty$, the case of global coupling is recovered.

In Sections 2.2 and 2.3, it has been shown that a two-component model is not only necessary but also sufficient to describe the onset of oscillations at a Hopf bifurcation. Another important type of bifurcation, however, can only been found in a system with at least three species, namely the wave bifurcation (see, e.g. Refs. [1]).There, the uniform state becomes unstable and a pattern of traveling waves develops. Note the difference to the distributed Hopf bifurcation where uniform oscillations are the basic solution at threshold and traveling waves propagate on the background of uniform oscillations. The amplitude equations that govern a system undergoing a wave bifurcation in the one-dimensional spatial domain are given by

$$\partial_t A + v \partial_x A = \mu A - a|A|^2 A - b|B|^2 A + d \partial_{xx} A, \tag{2.56a}$$

$$\partial_t B - v \partial_x B = \mu A - a|B|^2 B - b|A|^2 B + d \partial_{xx} B, \tag{2.56b}$$

where A and B are complex amplitudes of counter-propagating waves, μ is the distance to the bifurcation point, v is the group velocity of the waves (and therefore a real number), and

a, b, and d are complex coefficients. The terms $v\partial_x A$ and $v\partial_x B$ are characteristic for systems where traveling patterns are found at the instability. The wave bifurcation has been observed in fluid systems but has also been investigated in the context of target patterns in reaction-diffusion systems by Zhabotinsky *et al.* [99] and Rovinsky *et al.* [63]. While Zhabotinsky *et al.* investigated a three-variable reaction-diffusion system, Rovinsky *et al.* worked with amplitude equations. Recently, Nicola studied the appearance of wave (and Turing) bifurcations in systems with nonlocal coupling, focusing on the dynamics of interfaces between Turing and wave domains [100].

It can be summarized that many relevant realistic models for reaction-diffusion systems have (at least) three components, while two-component models are usually reduced models which qualitatively explain many results (although not all) and which are typically easier to discuss mathematically. For patterns like stable moving spots or for bifurcations such as the wave instability, three-component models are essential. In the next section, it is shown that the description of self-organized target patterns also leads to three-component models.

2.6 Target patterns and pacemakers

Target patterns are one of the classical wave patterns observed in reaction-diffusion systems. The wave sources of these concentric waves are called pacemakers, which may be either created by heterogeneities of the medium or may arise as a direct consequence of the non-linearity of the system, i.e. are self-organized. Pacemakers may give rise to target patterns in oscillatory or excitable media. An overview of different theoretical approaches that have been put forward in the study of pacemakers is provided.

Target patterns

The first wave pattern described in the Belousov-Zhabotinsky (BZ) reaction consisted of concentric waves that were periodically emitted from a small central region [22]. First, these patterns were called *leading centers*, but nowadays *target (wave) patterns* seems to be the established term. The central region of the target patterns is called a *pacemaker* because it entrains the medium through the emission of waves. Note that some authors refer to the whole pattern as pacemaker or reserve this term for the heterogeneous pacemakers described below. Target patterns have also been observed in many other chemical, physical, and biological systems such as CO oxidation on platinum [29], liquid crystals [48, 101], semiconductor-gas

discharge systems [51], Rayleigh-Bénard convection [49, 102], *Dictyostelium discoideum* colonies [18, 50, 103–105], electrochemical systems [52, 106], combustion systems [107], and even ecological systems [19].

Target patterns for two typical chemical reaction-diffusion systems are presented here. Figure 2.5 displays an image of a part of a BZ medium containing four target patterns. Note that the pacemakers emit waves with different wavelengths. Figure 2.6 shows a time series
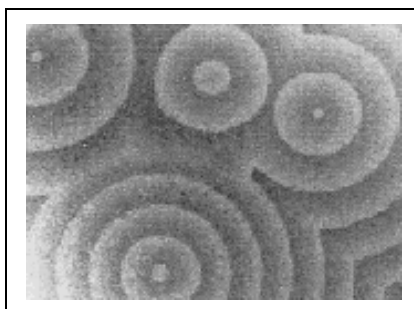

Figure 2.5: **Target patterns in the BZ reaction.** *Bright (dark) zones are blue (red) in reality and correspond to high (low) concentrations of Fe^{3+} in the ferroin-catalyzed version of the BZ reaction (from Ref. [108]).*

of images of the CO oxidation on a platinum single crystal surface during a single cycle of the background oscillations. Approximately ten target patterns can be identified. The frequencies of the pacemakers are higher than the background frequency, thus leading to slowly expanding wave patterns. Also in this case, the pacemakers exhibit a range of operating frequencies. Whenever pacemakers with different frequencies are present in a given medium,
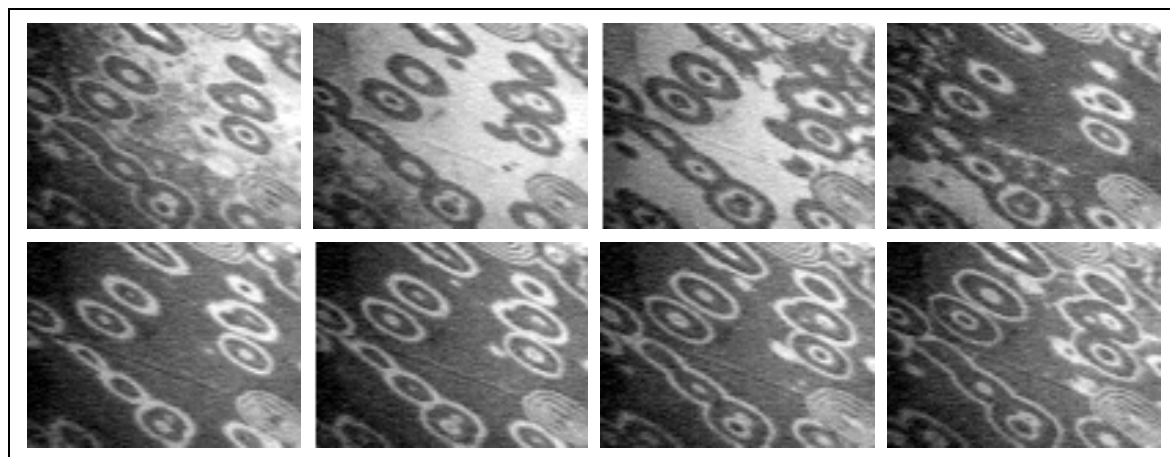

Figure 2.6: **Target patterns in the oscillatory CO oxidation on Pt(110).** *The target patterns have an elliptic shape due to diffusion anisotropy. Dark (bright) areas are oxygen (CO) covered. Time runs from top left to bottom right with an interval of $1s$. For details, see Ref. [109].*

they compete with each other, i.e. the pacemaker with the highest frequency will finally suppress all other pacemakers (at least in a medium with positive dispersion, as will be discussed in Sec. 3.1.2).

Although target patterns as observed in chemical reaction-diffusion systems motivate to large extent the studies presented in this thesis, it is instructive to keep in mind also other target pattern-forming media. In this context it is helpful to characterize the target patterns according to their dimensionality, their extension, the direction of waves, their stability, and the type of spatial coupling.

Target wave pattern are usually considered as two-dimensional patterns. However, sufficiently far from the wave source, target patterns are well approximated by one-dimensional plane waves (*cf.* Sec. 2.3). One-dimensional target patterns are also observed in experiments, for example in electrochemical experiments, where pattern formation takes place on a ring electrode [52, 106].

The classical target pattern consists of waves that emanate from its center. However, also inward traveling target waves are observed, e.g. in the modified BZ medium [27], the CO oxidation system, where the waves are induced by a laser [110], or in optical systems [111]. There, the interaction of a laser beam with sodium vapor via a so-called single mirror feedback scheme gives rise to inward traveling target and spiral waves (for details of the system, see the recent review Ref. [8]).

While typically target waves entrain the medium and therefore constitute *extended* patterns, *localized* target patterns are also possible. Then, the waves disappear in a certain distance from the core, giving rise to a pattern with an extension of at most a few wavelengths. Such localized target patterns are, for example, observed in nematic liquid crystals [48] or in the CO oxidation reaction under non-isothermal conditions, where they have been called raindrop patterns [30].

In many reaction-diffusion systems like the BZ reaction or the CO oxidation reaction, target patterns are asymptotically stable. However, target waves may be transient or undergo instabilities. For example, target patterns may develop and decay periodically as in nematic liquid crystals [48], or may be replaced by spiral waves like in *Dictyostelium Discoideum* colonies [105]. Target patterns in vibrated layers of granular matter are unstable and arise as a transient to stripe solutions [112]. Numerically, target patterns and their instabilities have been studied in a disc-shaped medium with global coupling [113] and long-range interaction [114]. Transient and localized target patterns have been found for a model for poly-

mers [115].

It should be mentioned that target patterns have also been discussed in the mathematical literature. In 1978, Greenberg demonstrated the existence of target pattern solutions for the $\lambda - \omega$ model, which can be viewed as a generalization of a CGLE [116]. In 1981 it was rigorously shown by Kopell [117] and by Hagan [118] that oscillatory reaction-diffusion systems give rise to stable target patterns in the presence of impurities. While the analysis of Kopell was also based on the $\lambda - \omega$ model, Hagan worked with a general reaction-diffusion model. Recently, Golubitsky *et al.* pointed out that boundary conditions may play an important role for the existence and stability of the target (and spiral) patterns (*cf.* Sec. 2.3) [80].

Within the field of chemical reaction-diffusion systems, and in particular in the context of the BZ reaction, a controversy on the nature of the pacemakers arose. While it was clearly demonstrated that the presence of impurities gives rise to target patterns in the excitable and oscillatory regime of the BZ reaction, the microscopic origin of spontaneous target patterns observed in well-filtered, oscillatory BZ solutions remains unclear. If it is assumed that the medium is uniform, pacemakers may form through the interplay of nonlinear kinetics and diffusion. Such self-organized pacemakers are indeed possible and are discussed further below. But actually, beside heterogeneities and deterministic self-organization, there are also other ways to explain target pattern formation media which are discussed in the following.

A mechanism based on thermal fluctuations has been proposed by Walgraef *et al.* in the context of the BZ reaction [119]: Thermal fluctuations should lead to spatial differences in the distribution of chemical concentrations and subsequently to the nucleation of pacemakers. However, according to Zhang *et al.*, fluctuations cannot explain the spontaneous emission of waves in oscillatory chemical systems [120]. Recently, Hastings argued that fluctuations should be able to trigger target patterns close enough to a Hopf bifurcation [121], as the system moves slowly from the excitable into the oscillatory regime.

For target patterns in the excitable regime of the BZ reaction, a fluctuation-nucleation mechanism is completely discarded [122]. However, if noise is applied to an excitable light-sensitive BZ medium, target patterns may be created and sustained, as shown experimentally and numerically by Alonso *et al.* [64]. It has been shown by Parmananda *et al.* [65] that subthreshold periodic forcing of a parameter in the excitable regime of the Oregonator model may also give rise to expanding target patterns.

In the completely different context of neural systems and with a different coupling scheme, qualitatively similar results were obtained by Lewis and Rinzel [123, 124]: If ex-

citable cells of a neural network were coupled in an appropriate way, the network started to show global oscillations which were triggered by target patterns that appeared at random locations.

Since stable self-organized spirals may exist in the BZ reaction, target patterns may be created by annihilating a pair of counterrotating spirals. The first target pattern created in this way was reported by Agladze *et al.* [125] who focused on the spiral dynamics prior to annihilation. Later, Müller *et al.* confirmed these findings and discussed the dynamics of the formed target pattern [126]. The main result is that the target pattern is unstable and decays to uniform oscillations.

Several target pattern solutions have been reported for the one-dimensional quintic complex Ginzburg-Landau equation. Here, a few are presented. Analytically, the formation of extended target patterns has been explained by Dewel and Borckmans [127, 128]. There, a bound state of two motionless localized structures called antipulses emits waves and gives rise to plane waves in the far field. This solution does not have axial symmetry, as usually assumed as pacemakers are modeled. Later, Deissler and Brand [129] found localized target patterns in the quintic CGLE, triggering much research for such solutions. Recently, Akhmediev *et al.* discussed stable breathing and moving oscillating localized structures in that equation [130].

Target patterns in semiconductor-gas discharge systems, fluid systems and granular media have, in general, other dynamic properties and arise in a different way than target patterns in chemical reaction-diffusion systems. Astrov *et al.* showed the existence of zigzag destabilized target patterns for a semiconductor-gas discharge system [51]. There, target patterns and spirals are observed after the system has undergone a sequence of hexagons, stripes and stripes with defects. Target patterns continuously evolve into spirals and back via the nucleation of defects. Target patterns in vibrated layers of granular matter are created at the boundary of the system, as reported by Umbanhowar *et al.* [112]. The target waves form at the metal container, proceed into the center, and finally form a stationary pattern. The experiments on smectic liquid crystals by Cladis *et al.* [101] also show target patterns that are initiated at the boundary. In experiments performed for the Rayleigh-Bénard convection by Assenheimer and Steinberg [49, 102], target patterns are stable or convert to spirals (and back) via the creation of defects. Boundary-induced stable target patterns in the CGLE have been described by Eguiluz *et al.* [131].

Heterogeneous pacemakers

Target waves have received much less attention than, for example, rotating spiral waves. This is partially explained by the fact that for years it was believed that pacemakers in chemical reaction-diffusion systems necessarily consist of *heterogeneities* which locally modify the properties of the medium [22]. Indeed, the majority of target patterns observed in the BZ reaction are associated with the presence of a local impurity like a dust particle or gas bubble which plays the role of a catalytic particle [54]. By carefully filtering the BZ solution, the number of evolving target patterns can be significantly reduced. The developing patterns have a range of operation frequencies, indicating that the frequency is not uniquely determined by the parameters of the system [132]. Furthermore, in the experiment described in Ref. [133], the activity of a pacemaker generating a target pattern in the BZ reaction was suppressed by application of another, high-frequency wave source. When this other source, however, was removed, the initial pacemaker reappeared at the same location with the same frequency.

Target patterns often appear on the background of oscillations and therefore general models for oscillatory systems like the complex Ginzburg-Landau equation or phase equations have been investigated in this context. A typical approach to model heterogeneous pacemakers in oscillatory systems is to modify the properties of the medium in such a way that the oscillation frequency is increased locally [22,54]. The properties of heterogeneous pacemakers in oscillatory systems and their target wave patterns have been analyzed in a number of theoretical studies (e.g. Refs. [53–59]). Chapter 3 presents new results for heterogeneous pacemakers.

Remarkably, it is not necessary for the medium to be oscillatory since an excitable medium also supports propagating waves. Heterogeneities may drive the system locally from the excitable into the oscillatory regime and hence may be able to trigger the emission of waves in an excitable medium.

Self-organized pacemakers

Stable target patterns and pacemakers may also be found in systems without external heterogeneities as a result of nonlinear kinetics and diffusion. Then, the frequency of the pacemaker is entirely determined by the medium. There are different kinds of models and systems which belong to this class.

For example, target pattern formation in liquid crystals [48] is due to the internal dynam-

ics of the system. Also for the BZ reaction, there are experimental observations by Vidal *et al.* where pacemakers could not be related to any impurities [60] (see also Ref. [134] on this topic). Such pacemakers have also been called intrinsic or homogeneous pacemakers.

It is striking, however, that stable self-organized pacemakers have not been found in basic models of oscillatory media such as the complex Ginzburg-Landau equation or phase dynamics equations. There, target patterns may be created by a suitable initial condition. However, such patterns are not stable and uniform oscillations are recovered by the system. In another approach, Ohta *et al.* [135–137] investigated a two-component activator-inhibitor model with coexistence of excitable kinetics and stable uniform oscillations, and reported several kinds of self-organized wave sources. These wave sources also turn out to be unstable.

Motivated by the examples mentioned above, models for self-organized pacemakers and target patterns have been developed for several specific systems. Target pattern formation in electro-hydrodynamic convection has been explained by a model introduced by Sakaguchi [62] and refined later [138]. This model is based on a Hopf bifurcation of a cellular spatial structure.

In the 1970s and 1980s Vasilev [139, 140], Kawczynski [141–143], Ortoleva [144, 145], Walgraef [119] and Mikhailov [146] proposed models for self-organized pacemakers. These pacemakers, however, were not always stable. An approximate analytical solution for stable self-organized pacemakers in a system where uniform oscillations were unstable, has been constructed [61]. Self-organized target patterns have been found near a Hopf bifurcation with a finite wavenumber where uniform oscillations of the medium are absolutely unstable [63]. Self-organized target patterns have also been reported for an Oregonator model displaying such a bifurcation [99].

Stable wave patterns resembling localized target patterns may also be found as a result of self-organization. Such a behavior, for example, is exhibited by the quintic complex Ginzburg-Landau equation [129], where stable breathing and moving oscillating localized structures have also been observed recently [130].

In the last decades, there has been a lot of effort to find a two-component reaction-diffusion model that gives rise to stable self-organized target patterns. However, all models known up to now, which are able to display stable self-organized pacemakers and extended target patterns, consist of at least three independent variables or alternatively provide other spatial coupling mechanisms than diffusion, such as global coupling. Although there is no proof that stable self-organized pacemakers are impossible in two-component reaction-

diffusion systems, there seem to be enough reasons to believe that such pacemakers are at least not generic for two-component models.

Chapter 4 demonstrates with analytical and numerical means that stable self-organized pacemakers are possible in birhythmic systems which are oscillatory media where two stable limit cycles coexist. Chapter 5 shows for the first time that stable self-organized pacemakers may also be found in excitable media.

Chapter 3

Heterogeneous pacemakers in oscillatory media

This chapter investigates heterogeneous pacemakers in oscillatory media. Such pacemakers have been studied since the discovery of target patterns in the Belousov-Zhabotinsky reaction [22]: Zaikin and Zhabotinsky already assumed the presence of several frequencies in the medium. On the one hand there is the background frequency of the oscillatory medium, which is determined by the system parameters, and on the other hand there are the frequencies which are introduced by the impurities present in the medium and which depend on the microscopic nature of each heterogeneity.

The complex Ginzburg-Landau equation is chosen as a theoretical model to study the effects that are possible in oscillatory systems where inhomogeneities are present. Though this equation is strictly applicable only close to a soft onset of oscillations where oscillations have small amplitudes and are approximately harmonic, its predictions are known to be qualitatively valid in a broader neighborhood of the supercritical Hopf bifurcation in many cases. Due to its general applicability, it is considered as a standard model for an oscillatory system.

To create a pacemaker in the complex Ginzburg-Landau equation, the medium should be nonuniform, i.e. it should possess a small localized region with modified parameters. Then, the local oscillation frequency inside this region is different from outside and this region may form a pacemaker which generates a spatially extended wave pattern. Such pacemakers and their wave patterns are focused on in this chapter. Additionally, localized patterns representing wave sink patterns will be considered. Some of the results presented in this chapter have been published in Ref. [147].

This chapter is organized as follows. First, the model is presented and the phase dynamics approximation for heterogeneous pacemakers is discussed (Sec. 3.1.1). Then, basic

properties of weak pacemakers and sinks and their wave patterns in the one-dimensional complex Ginzburg-Landau Equation are explored, including results on large heterogeneities (Sec. 3.1.2). In Sec. 3.2, the properties of strong pacemakers and sinks are investigated, which give rise to phase slips through Eckhaus unstable wave trains or localized desynchronization phenomena. Section 3.2.2 reports results of two-dimensional simulations carried out for heterogeneous pacemakers. The chapter is concluded with a discussion of the results in Sec. 3.3.

3.1   The model

This section describes the formation of target patterns in oscillatory systems with a heterogeneity in a systematic way. First, the pacemakers are distinguished from wave sinks. Then, the formation of target patterns in media with different dispersion is studied analytically and numerically. The derivation proceeds along the arguments presented by Kuramoto [53].

3.1.1   Pacemakers and wave sinks

This section discusses the phase dynamics approximation for oscillatory systems where a heterogeneity is present. The asymptotic phase distribution is subsequently derived and the condition for pacemakers is given. If the heterogeneity does not fulfill the pacemaker condition, it represents a wave sink.

Phase dynamics approximation

As introduced in Sec. 2.3, the complex Ginzburg-Landau equation (CGLE) is given by

$$\partial_t A = (1 - \mathrm{i}\omega)A - (1 + \mathrm{i}\alpha)|A|^2 A + (1 + \mathrm{i}\beta)\nabla^2 A. \qquad (3.1)$$

Suppose now that the oscillation frequency ω is changed by $\Delta\omega$ within a small region of radius R, so that

$$\omega(x) = \begin{cases} \omega & \text{for} \quad |x| > R, \\ \omega + \Delta\omega & \text{for} \quad |x| \leq R. \end{cases} \qquad (3.2)$$

Then, the region with the modified local oscillation frequency, the so-called *core*, becomes either a source or a sink of traveling waves depending on the parameters α, β, and $\Delta\omega$. To keep the notation simple, the origin is located at the center of the medium, which in this

section may have any spatial dimension. In the following discussion, an unbounded medium is considered, which is a good approximation for a sufficiently large realistic system.

Introducing the phase ϕ and the real amplitude ρ as $A = \rho \exp(-i\phi)$ and substituting this into Eq. (3.1), the two equations

$$\partial_t \rho = (1 - \rho^2)\rho + \nabla^2\rho - \rho(\nabla\phi)^2 + \beta\rho\nabla^2\phi + 2\beta\nabla\phi\nabla\rho, \tag{3.3a}$$

$$\partial_t \phi = \omega(x) + \alpha\rho^2 + (2/\rho)\nabla\rho\nabla\phi + \nabla^2\phi - (\beta/\rho)\nabla^2\rho + \beta(\nabla\phi)^2 \tag{3.3b}$$

are obtained. Like in the standard CGLE without heterogeneity, it is possible to reduce Eqs. (3.3) for smooth phase perturbations to the phase dynamics equation

$$\partial_t \phi = \omega(x) + \alpha + (\beta - \alpha)(\nabla\phi)^2 + (1 + \alpha\beta)\nabla^2\phi. \tag{3.4}$$

It is assumed that the Benjamin-Feir-Newell condition, $1 + \alpha\beta > 0$, is satisfied and the case of vanishing dispersion $\alpha = \beta$ is excluded.

After applying the nonlinear Cole-Hopf transformation

$$\phi = \frac{1 + \alpha\beta}{\beta - \alpha} \ln Q \tag{3.5}$$

to the phase equation (3.4), the new variable Q obeys the linear equation

$$\partial_t Q = \frac{\beta - \alpha}{1 + \alpha\beta}(\omega(x) + \alpha)Q + (1 + \alpha\beta)\nabla^2 Q, \tag{3.6}$$

which is formally equivalent to a Schrödinger equation for a quantum particle in a potential well. This well has a width $2R$ and a depth κ_{max}^2 given by

$$\kappa_{\text{max}}^2 = \frac{\beta - \alpha}{(1 + \alpha\beta)^2}\Delta\omega. \tag{3.7}$$

Note that the potential outside the well is not zero but has a constant value $(\beta - \alpha)(\omega + \alpha)/(1 + \alpha\beta)$. This term corresponds to the frequency of uniform oscillations $\omega + \alpha$. The aim of the following analysis is to derive expressions for the frequency Ω and the wavenumber k of the wave pattern. In terms of the variable Q, these quantities correspond to the largest eigenvalue of Eq. (3.6) denoted as λ_0 and to κ which characterizes the associated eigenfunction. Although Eq. (3.6) has been considered before in the context of target pattern formation [45, 53, 61, 148], it is presented here to explain both pacemakers and wave sinks, which are not discussed usually. For a detailed discussion of the analogy to the Schrödinger equation, see Refs. [45, 53].

A general solution of Eq. (3.6) is

$$Q(x,t) = \sum_n C_n \exp\left(\lambda_n t\right) Q_n(x),$$ (3.8)

where λ_n and $Q_n(x)$ are the eigenvalues and eigenfunctions of the linear differential operator

$$\widehat{L} = (1 + \alpha\beta)\nabla^2 + \frac{\beta - \alpha}{1 + \alpha\beta}(\omega(x) + \alpha).$$ (3.9)

All eigenvalues of this operator are real. Generally, the operator has both a discrete and a continuous spectrum. For long times, the solution with the largest eigenvalue λ_0 will dominate the expansion. In this case, we have $Q(x,t) \simeq C_0 \exp(\lambda_0 t) Q_0(x)$ and therefore

$$\phi(x,t) \simeq \frac{1 + \alpha\beta}{\beta - \alpha}(\lambda_0 t + \ln Q_0(x)).$$ (3.10)

It is convenient to discuss two special solutions for this equation. On one hand, for $R = 0$, the heterogeneity is absent and uniform oscillations with the frequency $\omega_{\mathrm{SL}} = \omega + \alpha$ are present [Eq. (2.26)]. On the other hand, as the heterogeneity becomes very large, $R \to \infty$, uniform oscillations with $\omega_{\mathrm{SL}} + \Delta\omega$ take place. Obviously, for any finite radius R, the frequency Ω of the waves lies between these two values. These frequencies correspond to the values λ_{SL} and $\lambda_{\max}$ respectively,

$$\lambda_{\mathrm{SL}} = \frac{\beta - \alpha}{1 + \alpha\beta}\omega_{\mathrm{SL}},$$ (3.11a)

$$\lambda_{\max} = \frac{\beta - \alpha}{1 + \alpha\beta}(\omega_{\mathrm{SL}} + \Delta\omega).$$ (3.11b)

Note that $\lambda_{\max}$ may be larger or smaller than λ_{SL}. The largest eigenvalue λ_0 of Eq. (3.6) is either identical to λ_{SL} or larger. This is discussed in detail below.

Pacemakers

Equation (3.10) represents the asymptotic phase distribution for large times which depends on the eigenvalue λ_0 and the corresponding eigenfunction.

If the largest eigenvalue λ_0 is larger than the eigenvalue of uniform oscillations λ_{SL}, it belongs to the discrete spectrum of the operator $\widehat{L}$. The corresponding eigenfunction $Q_0(x)$ is localized and $Q_0(x) \propto \exp(-\kappa|x|)$ for $|x| \to \infty$, where $\kappa = \sqrt{(\lambda_0 - \lambda_{\mathrm{SL}})/(1 + \alpha\beta)}$. Therefore, far from the center, the distribution of the phase is given by

$$\phi(x,t) \simeq \frac{1 + \alpha\beta}{\beta - \alpha}(\lambda_0 t - \kappa|x|).$$ (3.12)

This means that far from the central region where the local oscillation frequency is modified, propagation of approximately plane waves takes place and an extended target wave pattern is formed. Note that κ is related to the wavenumber k through $k = \kappa(1 + \alpha\beta)/(\beta - \alpha)$. The frequency Ω and the wavenumber k of the waves can be expressed in terms of the largest eigenvalue λ_0 in the following way:

$$\Omega = \frac{1 + \alpha\beta}{\beta - \alpha}\lambda_0, \tag{3.13a}$$

$$k = \sqrt{\frac{1 + \alpha\beta}{(\beta - \alpha)^2}(\lambda_0 - \lambda_{\mathrm{SL}})}. \tag{3.13b}$$

In the next section, the eigenvalue λ_0 is determined for a one-dimensional system.

A heterogeneity acts as a wave source or *pacemaker* if the condition

$$\lambda_0 > \lambda_{\mathrm{SL}} \tag{3.14}$$

is fulfilled. This can also be written as

$$(\beta - \alpha)(\Omega - \omega_{\mathrm{SL}}) > 0. \tag{3.15}$$

A necessary condition for this to hold is

$$(\beta - \alpha)\Delta\omega > 0, \tag{3.16}$$

which constitutes the basic criterion used later. In one- and two-dimensional systems, this condition is not only necessary but also sufficient to create a pacemaker. However, in three spatial dimensions, small and weak heterogeneities may have a ground state which belongs to the continuous spectrum and do not give rise to target patterns [53].

Wave sinks

If the largest eigenvalue λ_0 is equal to the eigenvalue λ_{SL} corresponding to uniform oscillations, it belongs to the continuous spectrum of the operator $\widehat{L}$. The respective eigenfunction $Q_0(x)$ has the asymptotics $Q_0(x) \to \mathrm{const}$ as $|x| \to \infty$. Therefore, far from the central region, the phase is approximately given by

$$\phi(x, t) \simeq \frac{1 + \alpha\beta}{\beta - \alpha}(\lambda_{\mathrm{SL}}t + \mathrm{const}), \tag{3.17}$$

which means that uniform oscillations with frequency ω_{SL} are taking place there. Hence, a heterogeneity cannot lead to an extended wave pattern and is thus called a *wave sink*. Note that close to the heterogeneity, localized wave patterns are possible.

To yield a condition for wave sinks, it is sufficient to require that the maximal eigenvalue λ_{max} is smaller than the eigenvalue for uniform oscillations, i.e. if the condition

$$(\beta - \alpha)\Delta\omega < 0 \tag{3.18}$$

is met.

In terms of the interpretation as a Schrödinger equation, a pacemaker corresponds to a potential well, while a wave sink corresponds to a potential barrier. Below, properties of pacemakers and wave sinks in media with positive and negative wave dispersion are discussed.

3.1.2   Target patterns and wave dispersion

Target patterns are typically formed by outgoing concentric waves. However, general models like the CGLE and the phase dynamics equation also admit solutions representing inward traveling target waves. Recently, wave patterns with such a behavior have been found experimentally in a modified version of the BZ reaction [27] and in the CO oxidation reaction [110]. In this section, the conditions for the appearance of inward and outward traveling target waves are formulated. Wave sinks are included into the discussion, rendering a broad view on the possible effects of heterogeneities in oscillatory media. Large heterogeneities are also considered.

It is convenient to discuss the different cases in terms of the wave dispersion and the sign of the frequency shift. The dispersion relation for plane waves in the CGLE has been discussed in Sec. 2.3: for $\beta - \alpha > 0$, the waves have positive dispersion, and for $\beta - \alpha < 0$, they have negative dispersion.

Positive wave dispersion

If $\beta - \alpha > 0$ and when the local oscillation frequency is *increased* ($\Delta\omega > 0$) inside a core region of radius R, this region becomes a source of waves and a classical target pattern of outward propagating waves is formed. In one-dimensional media, the wavenumber k of generated waves is determined by the equation

$$R = \frac{1 + \alpha\beta}{(\beta - \alpha)\sqrt{k_{\mathrm{max}}^2 - k^2}} \tan^{-1}\left(\frac{k}{\sqrt{k_{\mathrm{max}}^2 - k^2}}\right), \tag{3.19}$$

where

$$k_{\mathrm{max}} = \frac{1 + \alpha\beta}{\beta - \alpha}\kappa_{\mathrm{max}} = \sqrt{\frac{\Delta\omega}{\beta - \alpha}} \tag{3.20}$$

is the maximum wavenumber reached for very large cores. This equation is found by matching the solution valid far from the core where $Q_0(x) \propto \exp(-\kappa|x|)$ with the solution inside the core where $Q_0(x) \propto \cos(\sqrt{\kappa_{\mathrm{max}}^2 - \kappa^2}|x|)$. This derivation is described in standard textbooks for the case of a quantum particle in a potential well. The pacemaker frequency is given by

$$\Omega = \omega_{\mathrm{SL}} + (\beta - \alpha)k^2. \tag{3.21}$$

In Fig. 3.1, the wavenumber and frequency of a pacemaker are shown as a function of the radius of the heterogeneity. Note that the wavenumber is bounded by the maximal wavenum-
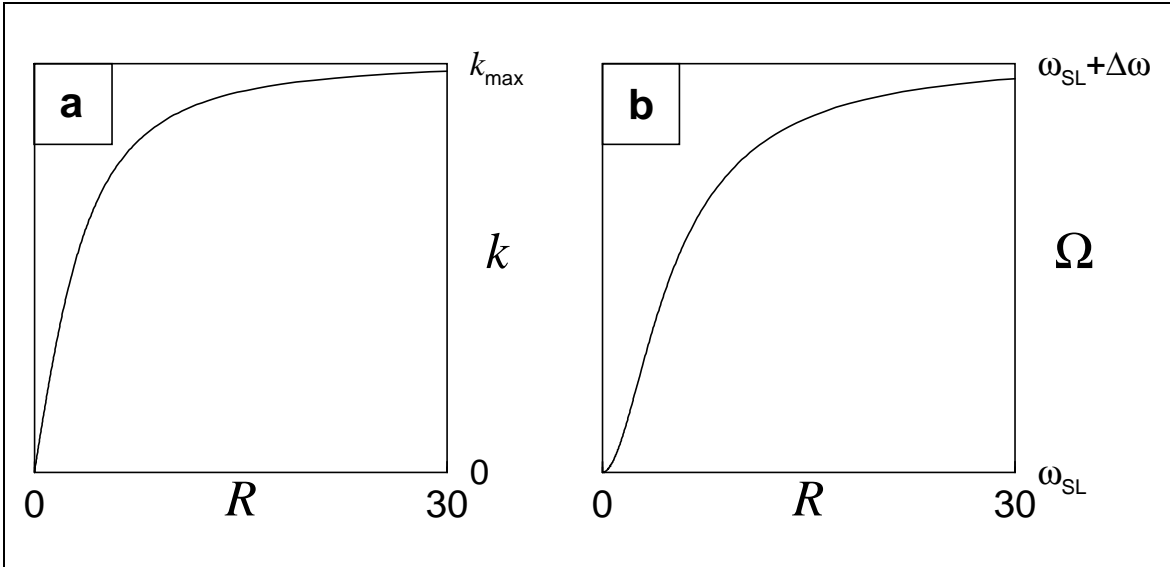
Figure 3.1: **Wavenumber (a) and frequency (b) of a pacemaker.** *The parameters are* $\alpha = 0.5$, $\beta = 1.0$, $\Delta\omega = 0.2$. *The maximum wavenumber is* $k_{\mathrm{max}} = \sqrt{0.4}$. *Note that the value of* ω *can be chosen arbitrarily.*

ber k_{max} and the frequency by $\omega_{\mathrm{SL}} + \Delta\omega$. As a result of the wave propagation, the medium becomes *entrained* by the wave source and the effective oscillation frequency approaches the same value everywhere in the system.

To investigate the CGLE with a heterogeneity, Eqs. (3.1) and (3.2) are integrated with an explicit Euler scheme where the Laplacian is discretized with a nearest-neighbor approximation (see Appendix A.4). No-flux boundary conditions are applied in all simulations

displayed in this chapter. Typically, initial conditions consist of uniform oscillations. The heterogeneity is usually located in the center of the medium but is not directly seen in the figures since the frequency is not displayed.

An example of a one-dimensional target wave pattern is shown in Fig. 3.2(a). The heterogeneity corresponds to a frequency *increase* ($\Delta\omega > 0$). For the chosen set of parameters, waves leave the core region and propagate outward. Since the waves are able to entrain the whole system, the core region indeed represents a pacemaker.

When the local oscillation frequency is *decreased* ($\Delta\omega < 0$) inside the core region, a localized wave sink pattern is produced [Fig. 3.2(b)]. Waves initiate near the core boundary and propagate inward. As a result, the frequency of the core oscillations is increased to the value of uniform oscillations ω_{SL}, giving rise to a pattern where a constant phase shift
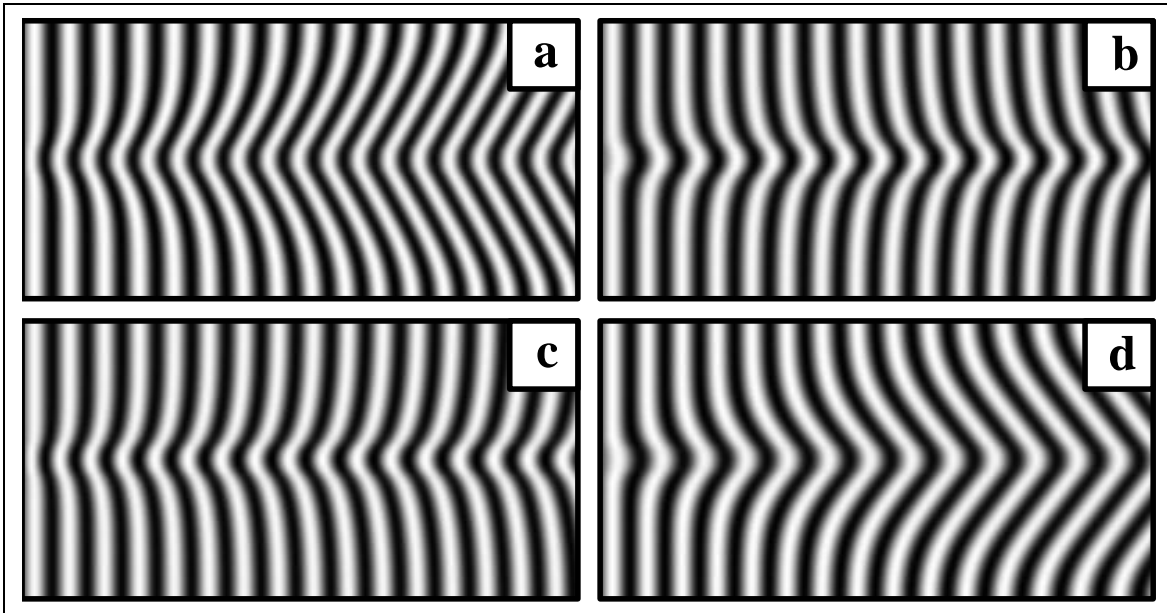
Figure 3.2: **Wave patterns for small heterogeneities.** *The heterogeneity with radius $R = 4$ is placed in the center of the medium with length $L = 80$. Space-time diagrams of ReA are shown in gray scale and the displayed time intervals are always $\Delta t = 200$. A linear gray scale color map is chosen where the minimum refers to black and the maximum to white. For ReA black approximately corresponds to -1.1, and white to $+1.1$. In all space-time diagrams in this thesis, space is displayed along the vertical axis and time along the horizontal axis. (a) Pacemaker in a medium with positive dispersion (outward propagating target pattern); $\Delta\omega = 0.2, \omega = 0, \alpha = 0.5, \beta = 1.0$. (b) Wave sink in a medium with positive dispersion; $\Delta\omega = -0.2, \omega = 0, \alpha = 0.5, \beta = 1.0$. (c) Wave sink in a medium with negative dispersion; $\Delta\omega = 0.2, \omega = 1, \alpha = -0.5, \beta = -1.0$. (d) Pacemaker in a medium with negative dispersion (inward propagating target pattern); $\Delta\omega = -0.2, \omega = 1, \alpha = -0.5, \beta = -1.0$. The initial conditions consist of uniform oscillations.*

between the center of the wave sink and the rest of the medium is established. The oscillation frequency is constant throughout the system. Hence, the heterogeneity is entrained by the uniform oscillations.

Negative wave dispersion

If the dispersion is negative, i.e. $\beta - \alpha < 0$, and if the local oscillation frequency is *increased* ($\Delta\omega > 0$) inside a core of radius R, such a heterogeneity leads to a localized wave pattern with frequency ω_{SL}. An example of this pattern is shown in Fig. 3.2(c). Waves are initiated inside the core and propagate outward, but then die at the core boundary. Hence, the heterogeneity actually represents a wave sink. For the chosen set of parameters, this case is similar to the wave sink for positive dispersion and negative frequency shift [Fig. 3.2(b)], because the asymptotic frequencies are the same and the sign of the phase shift is just inverted.

If the local oscillation frequency is *decreased* ($\Delta\omega < 0$) inside the core region, an extended wave pattern is formed. Outside the core of radius R, the medium is filled with propagating waves. The wavenumber k of these waves is given by Eq. (3.19) where, however, $(\beta - \alpha)$ is replaced by $(\alpha - \beta)$.[1] The frequency Ω of generated waves is given by Eq. (3.21). Note that Ω is smaller than the frequency ω_{SL} of uniform oscillations. The waves in this pattern propagate inward [Fig. 3.2(d)] since the frequency inside the heterogeneity is decreased. Despite the fact that waves are moving inward, the impurity entrains the medium and thus represents a pacemaker.

Note that to simplify the visualization in the above examples, relatively low values of ω are chosen to yield a common frequency $\omega_{\mathrm{SL}} = 0.5$ of uniform oscillations for all simulations in Fig. 3.2. For a discussion of the choice of ω in the simulations, see Appendix A.1.

Distributions of the local wavenumber

Figure 3.3 displays the spatial distributions of the local wavenumber, defined as $k = -\nabla\phi$ and evaluated numerically, for the four different wave patterns shown in Fig. 3.2. For pacemakers [Figs. 3.3(a,d)], the wavenumber is constant outside the core (except at the no-flux boundary, where it approaches zero). In the cases of wave sinks, the local wavenumber rapidly falls down to zero [Figs. 3.3(b,c)], showing that no plane waves are present.

---

[1]In the calculations presented in this thesis, the wavenumber k is assumed to be positive. However, if the vector character of k was taken into account, Eq. (3.19) for the one-dimensional system would remain valid also for the case of negative dispersion, since k would become negative for waves propagating toward the core.
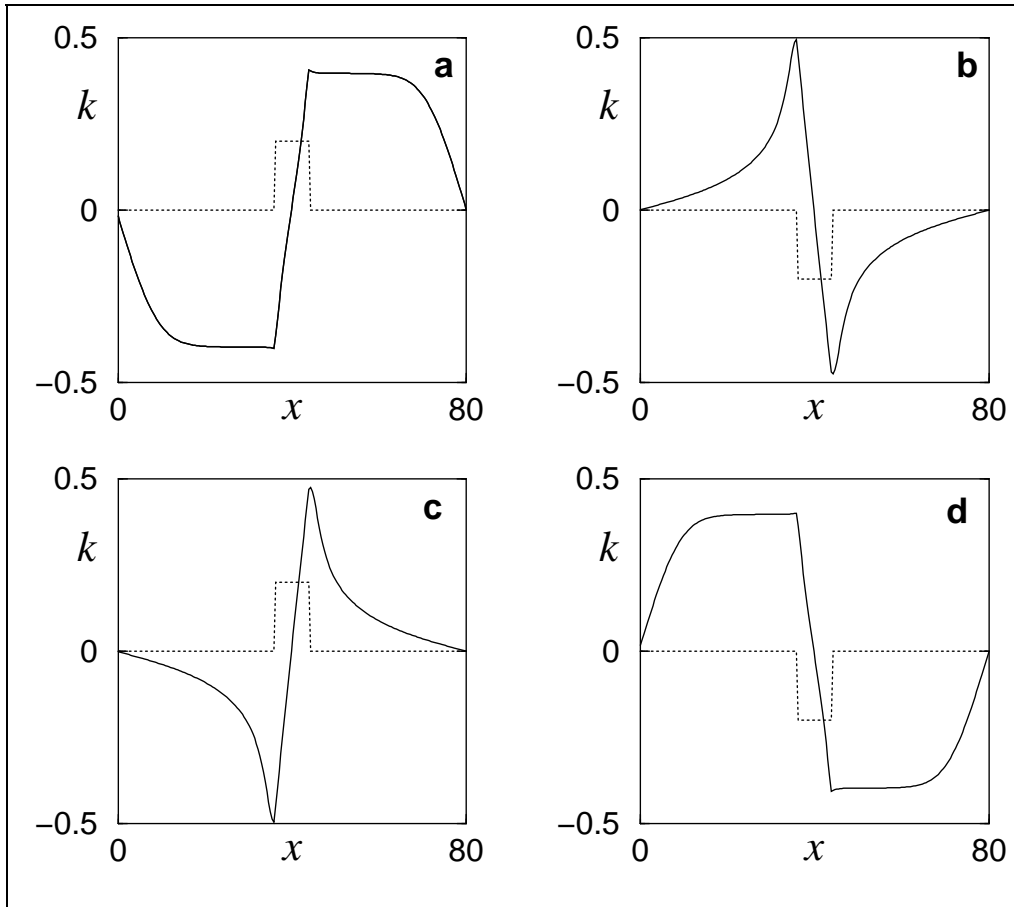
Figure 3.3: **Spatial distributions of the local wavenumber.** *The asymptotic distributions of k for the patterns displayed in Fig. 3.2(a,b,c,d) are shown. The local frequency shift $\Delta\omega$ is displayed as a dotted line.*

Since the value of k is determined numerically, it has different signs on both sides of the heterogeneity, and different signs for the different waves on a fixed side of the core: In one case the waves travel outward, in the other case they travel inward.

Group and phase velocities

The fact that a localized heterogeneity may produce a spatially extended pattern of *incoming* waves should be explained. The concepts of phase and group velocities are useful to characterize the four different patterns (see Sec. 2.3). The role of these velocities, and of sources and sinks have been discussed by van Hecke, van Saarloos, and co-authors [149, 150] in a different context.

The phase velocity describes the movement of the position of a certain phase value of a wave. Typically, the experimentally observed wave speed corresponds to the phase velocity.

If the frequency of a medium is locally increased, the phase changes faster there compared to the rest of the system. Therefore, a heterogeneity which increases the frequency is always associated with a phase velocity directed outward [Figs. 3.2(a,c)]. This can be formulated as

$$\Delta\omega > 0 \quad \Leftrightarrow \quad v_\mathrm{p} \quad \text{is directed outward.} \tag{3.22}$$

This definition not only applies for plane waves [Fig. 3.2(a)], but also for localized waves [Fig. 3.2(c)]. Accordingly, a local frequency decrease is always associated with a phase velocity pointing inward [Fig. 3.2(b,d)].

In this context, the group velocity determines whether the heterogeneity is able to give rise to a spatially extended pattern or not, i.e. whether this localized object constitutes a pacemaker or a wave sink. If the impurity entrains the system, then the group velocity is directed outward. The condition for a pacemaker in one- or two-dimensional spatial domains is given by Eq. (3.16), which can be written as

$$(\beta - \alpha)\Delta\omega > 0 \quad \Leftrightarrow \quad v_\mathrm{g} \quad \text{is directed outward.} \tag{3.23}$$

Consequently, the waves inside a wave sink have a group velocity pointing toward the center.

Expressed in terms of wave dispersion, the group and phase velocities are directed into the same direction for positive dispersion while the group velocity has the opposite sign with respect to the phase velocity in the case of negative dispersion.

Large cores

It has been stated above that for a wave sink a constant phase shift is present between the wave pattern in the center of the sink and the uniform oscillations outside. As the spatial extension of the heterogeneity increases, the phase shift becomes larger, and the propagation of waves *inside the core* should be possible for a large wave sink. This effect can be easily understood if the frequency of the wave sink is considered to be the reference frequency of the system. Then, the region around the wave sink has an *increased* frequency (in a medium with positive dispersion) and therefore acts as a pacemaker.

In Fig. 3.4, simulations for the four different wave patterns distinguished in context with Fig. 3.2 are displayed. While uniform oscillations take place in the cores of the pacemakers [Figs. 3.4(a,d)], wave propagation is observed inside the cores of the wave sinks [Figs. 3.4(b,c)]. In particular, this means that inward traveling target patterns may also be observed in systems with positive dispersion if large heterogeneities are present [Fig. 3.4(b)].
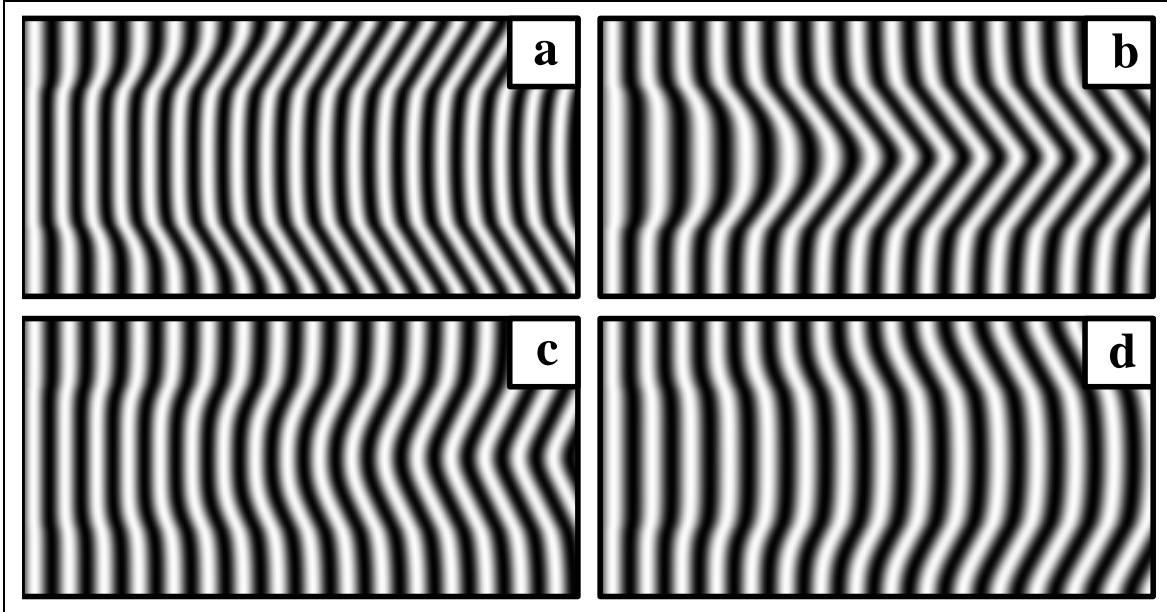
Figure 3.4: **Wave patterns inside large heterogeneities.** *The heterogeneity with radius $R = 20$ is placed in the center of the medium of length $L = 80$. Space-time diagrams of ReA are shown where the displayed time intervals are always $\Delta t = 100$. (a) Uniform oscillations inside the heterogeneity in a medium with positive dispersion; $\Delta\omega = 0.2$, $\omega = 2$, $\alpha = -1$, $\beta = 0$. (b) Inward traveling waves inside the heterogeneity in a medium with positive dispersion; $\Delta\omega = -0.2$, $\omega = 2$, $\alpha = -1$, $\beta = 0$. (c) Outward traveling waves inside the heterogeneity in a medium with negative dispersion; $\Delta\omega = 0.2$, $\omega = 0$, $\alpha = 1$, $\beta = 0$. (d) Uniform oscillations inside the heterogeneity in a medium with negative dispersion; $\Delta\omega = -0.2$, $\omega = 0$, $\alpha = 1$, $\beta = 0$.*

Accordingly, outward traveling waves may also be seen in systems with negative dispersion [Fig. 3.4(c)] if the impurities are sufficiently large. Another consequence is that while a pacemaker entrains its surrounding area, the dynamics inside the core is dominated by uniform oscillations.

3.2   Phase slips

Pacemakers may not only emit waves which propagate in a stable way through the medium. If the wavenumber of the waves becomes sufficiently large, the waves become Eckhaus unstable and phase slips occur in a certain distance from the core. Such patterns generally appear if the local frequency shift induced by the heterogeneity is very large. For very large frequency shifts phase slips take place at the border of the heterogeneity. Such desynchronization phenomena are studied in this section.

3.2.1 One-dimensional systems

The phase dynamics approximation is valid only when phase gradients (i.e. local wavenumbers) remain sufficiently small. Since the maximal possible wavenumber k_{max} is given by $k_{\mathrm{max}} = \sqrt{\Delta\omega/(\beta - \alpha)}$, the analytical results presented in the previous section hold only for weak pacemakers and sinks, which are found when the frequency difference $\Delta\omega$ in the core region is not too large, i.e. $|\Delta\omega| \ll |\beta - \alpha|$. If it is assumed that $|\beta - \alpha|$ is of order unity, the condition for the validity of the phase dynamics approximation is

$$|\Delta\omega| \ll 1. \tag{3.24}$$

The properties of strong pacemakers and sinks with large frequency difference $\Delta\omega$ are considered below.

As the frequency difference $\Delta\omega$ inside the core region is increased continuously in the simulation of the CGLE, the wavenumber of generated waves increases and pattern instabilities develop. These instabilities consist of the appearance of phase slips, i.e. changes of the phase of 2π, and the formation of amplitude defects. Therefore, these phenomena cannot be described in the framework of the phase dynamics approximation given by Eq. (3.4). Phase slips in the present context accompany desynchronization phenomena and are closely related to the Eckhaus instability of plane waves (see Sec. 2.3).

Eckhaus instability

An example for the formation of the phase slips as a result of the Eckhaus instability is shown in Fig. 3.5. There, an oscillatory medium with positive dispersion is considered. The initial condition consists of a target pattern emitting stable waves which have a wavenumber close to the Eckhaus instability given by Eq. (2.34),

$$k_{\mathrm{EI}} = \sqrt{\frac{1 + \alpha\beta}{2(1 + \alpha^2) + 1 + \alpha\beta}}. \tag{3.25}$$

Then, the frequency difference $\Delta\omega$ in the core region (which is displayed in the bottom part of Fig. 3.5) is increased from $\Delta\omega = 0.2069$ to $\Delta\omega = 0.2070$. The traveling wave is now unstable and the perturbation grows and modulates the traveling waves until the amplitude drops down to zero (seen as the first black dot in Fig. 3.5(b)). At this moment, a wave collapses and a phase slip occurs. Subsequently, a sequence of four phase slips occurs, with their respective locations moving with an approximately constant velocity toward the
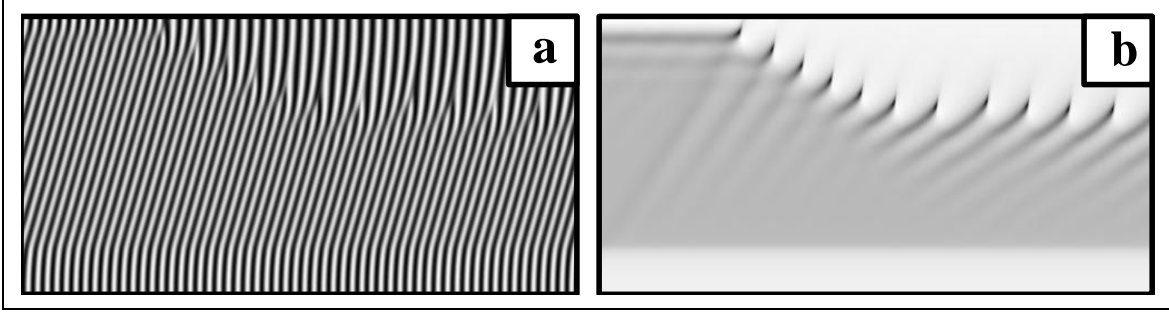
Figure 3.5: **Formation of phase slips through the Eckhaus instability.** *Space-time diagrams of (a) ReA and (b) |A| are shown. A linear gray scale color map is chosen where the minimum refers to black and the maximum to white. For |A|, black corresponds to zero, and white to |A| ≈ 1.1. The parameters are $\Delta\omega = 0.207$, $\omega = 0$, $\alpha = 0.55$, $\beta = 1.0$, $R = 14.8$, $\Delta t = 500$, and $L = 160$ (only half of the system is displayed, with the core located in the lower part of the figure).*

core. This motion is terminated at a certain distance from the core boundary. Eventually, a steady wave pattern with periodically generated phase slips is established. The wavenumber in the far region is reduced and lies below the Eckhaus threshold. Thus, the waves emitted by a pacemaker periodically undergo phase slips and a wave pattern characterized by a short wavelength near the core and a long wavelength in the far region is established. Simulations with larger systems (not shown here) do not reveal any significant dependence of the asymptotic pattern on the distance to the system boundary, as long as the system is not much smaller than the one shown in Fig. 3.5.

For each pacemaker with radius R and frequency shift $\Delta\omega$, it is possible to check whether a wave generated by a pacemaker is Eckhaus-unstable or not by comparing k as determined by Eq. (3.19) with the Eckhaus threshold (3.25). For a more general view, however, the Eckhaus threshold (3.25) is contrasted with the maximal wavenumber $k_{\max}$ given by Eq. (3.20)

$$k_{\max} = \sqrt{\frac{\Delta\omega}{\beta - \alpha}},$$

that a core with fixed $\Delta\omega$ may emit. The results are displayed in Figs. 3.6(A,B).

Figure 3.6(A) shows for the case $\Delta\omega > 0$ in which part of the parameter plane spanned by α and β outgoing target patterns (a) and in which part outgoing localized waves (c) are present. The regions (a) and (c) are separated by the solid line of vanishing dispersion $\beta = \alpha$. Recall that a frequency increase always gives rise to outgoing waves. The regions are labeled in correspondence to the patterns displayed in Figs. 3.2(a-d) and 3.3(a-d). The Benjamin-Feir-Newell (BFN) lines $\beta = -1/\alpha$ are drawn dashed and indicate where uniform oscillations become unstable. Hence, target waves exist in the region above the line of vanishing
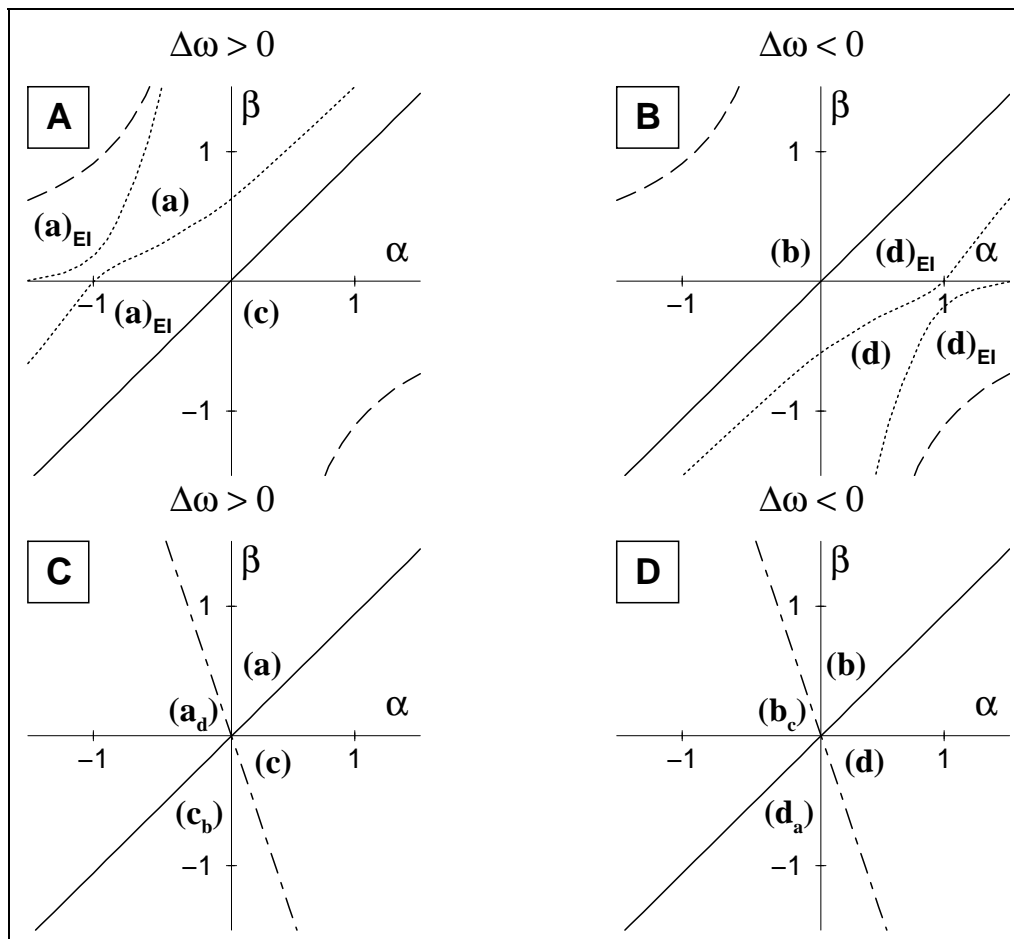
Figure 3.6: **Parameter space (α, β) for $\Delta\omega > 0$ (A,C) and $\Delta\omega < 0$ (B,D).** *The parameter regions where the four cases* (a-d) *from Fig. 3.2 are found, are denoted with* (a-d) *respectively. In (A) and (B), $\omega \gg 1$ is assumed. In (C) and (D), ω is scaled out (equivalent to $\omega = 0$). The following lines are plotted: dispersion line ($\beta = \alpha$, solid line), BFN line ($\beta = -1/\alpha$, dashed line), the lines where $k_{EI} = k_{max}$ (plotted for $\Delta\omega = 0.2$, dotted lines), and the line of vanishing phase velocity ($\beta = \alpha(1 - k^{-2})$, plotted for $k = 0.5$, dot-dashed line). In the regions denoted by* (a_d) *[(d_a)] pacemakers with ingoing (outgoing) plane waves for media with positive (negative) dispersion are found. In the regions denoted by* (c_b) *[(b_c)], sinks with ingoing (outgoing) localized waves for media with positive (negative) dispersion are found. The subscript* EI *indicates parameter regions where the waves may become unstable with respect to the Eckhaus instability.*

dispersion line and below the upper BFN line. However, the Eckhaus instability restricts the parameter region, where target waves are stable, to the area between the dotted lines. These lines embrace the region where the maximum wavenumber of a wave emitted by a pacemaker of arbitrary radius is still smaller than the Eckhaus wavenumber, i.e. $k_{EI} > k_{max}$. There, any wave emitted by a core with a fixed frequency shift (here $\Delta\omega = 0.2$) and arbitrary radius is stable with respect to the Eckhaus instability.

There are two parameter regions where Eckhaus unstable waves are possible. These regions are marked by (a)$_{\mathrm{EI}}$. First, between the upper BFN line and the upper dotted line, $k_{\mathrm{EI}} < k_{\mathrm{max}}$ is fulfilled because the Eckhaus wavenumber decreases strongly. At the BFN line $k_{\mathrm{EI}} = 0$ and any wave is unstable. Second, below the lower dotted line and the line of vanishing dispersion, the inequality $k_{\mathrm{max}} > k_{\mathrm{EI}}$ holds because k_{max} increases strongly as $\beta - \alpha$ becomes small. Recall that the phase dynamics approximation loses its validity for large wavenumbers.

For frequency shifts which are smaller than the frequency shift $\Delta\omega$ chosen here, the area within the two lines expands since k_{max} decreases. Then, the upper dotted line approaches the upper BFN line and the lower dotted line moves toward the line of vanishing dispersion. As the frequency shift increases, the parameter region where waves are stable for all pacemaker radii contracts and actually splits into two areas (at $\Delta\omega = 0.203$).

Note that in region (c), no extended waves are present, so that the Eckhaus instability criterion, which was derived for plane waves, is not applicable. However, other desynchronization phenomena are possible and actually observed, as discussed below.

In Fig. 3.6(B), the respective cases are displayed for $\Delta\omega < 0$, i.e. ingoing target patterns correspond to (d), ingoing localized waves to (b), and between the two dotted lines, target waves are stable with respect to the Eckhaus instability.

The main conclusion from Figs. 3.6(A,B) is that due to the Eckhaus instability, stable target patterns cannot be expected for arbitrary combinations of α and β, even if the pacemaker condition and the BFN condition are fulfilled. The parameter region where target patterns are stable with respect to the Eckhaus instability has been determined numerically. Furthermore, the figure displays a special symmetry of the system. If the signs of $\Delta\omega$, α, and β are inverted, the pacemaker condition and the BFN and EI criteria are invariant. The only difference is the frequency parameter ω, which is assumed to be much larger than unity in both, Fig. 3.6(A) and Fig. 3.6(B). Moreover, the results show that Eckhaus unstable target patterns are not only possible as the BFN line is reached but also as the line of vanishing dispersion is approached. There, however, the use of the phase dynamics approximation may be not justified since the phase gradients become large.

Figures 3.6(C,D) show how the appearance of target patterns and wave sinks takes place if the parameter ω is scaled out of the CGLE (*cf.* Appendix A.1). In this coordinate frame, inward traveling target waves are possible even for positive dispersion and positive frequency shift. This effect is not observed in reaction-diffusion systems close to the Hopf bifurcation

where ω is large. Nevertheless, since much work is devoted to the rescaled CGLE in general, this case is presented here.

Figure 3.6(C) shows for the case $\Delta\omega > 0$ in which part of the parameter space target patterns (a,a_d) and in which part wave sinks (c,c_b) are expected. The label (a) denotes the usual outgoing target patterns for positive dispersion, and the label (a_d) ingoing target waves for positive dispersion. The subscript stands for the pattern that is actually resembled, i.e. in this case ingoing target waves for negative dispersion, which are denoted as (d). The regions (a) and (a_d) are separated by the line of vanishing phase velocity, here drawn for waves with wavenumber $k = 0.5$. As this line is crossed, the direction of waves is changed. For $k \to 1$, this line approaches $\beta = 0$, for $k \to 0$, its asymptotics is $\alpha = 0$. Although the line of vanishing phase velocity has been derived for plane waves, it also describes well the change of wave direction for a wave sink. Corresponding simulations are not shown here.

Phase slip patterns in a medium with positive dispersion

If the frequency shift $\Delta\omega$ in the core is further increased, the location where phase slips occur moves closer to the core boundary and complex wave patterns become possible (Fig. 3.7).

For example, phase slips may appear in a period-2 fashion, as shown in Figs. 3.7(a,b). The frequencies of phase slips and waves need not to be commensurable. It is also possible that the phase slips on the two sides of the core do not occur simultaneously, giving rise to an asymmetric breakdown of waves [Figs. 3.7(c,d)]. At very large values of the frequency difference $\Delta\omega$ [Figs. 3.7(e,f)], phase slips typically occur symmetrically, but very close to the core boundary. Note that since the local wavenumber strongly changes already near the core boundary, the formation of phase slips in this case cannot be interpreted as a result of an Eckhaus instability for plane waves, but rather as a local desynchronization phenomenon. Generally, for increasing $\Delta\omega$, the location where phase slips occur moves closer to the core until the core boundary is reached. A further increase of the frequency shift leads to an increase in frequency of the phase slips.

The simulations displayed in Fig. 3.7 are examples where phase slips occur for a pacemaker. When the local oscillation frequency is decreased inside the core in a medium with positive dispersion, a wave sink is present instead [see Fig. 3.2(b)]. If the local decrease $\Delta\omega$ of the oscillation frequency is strong, phase slips can develop at the boundary of the heterogeneity. This is shown in Fig. 3.8. The effective oscillation frequency of the pattern inside the core is different from the frequency of uniform oscillation outside the core. Some oscillations
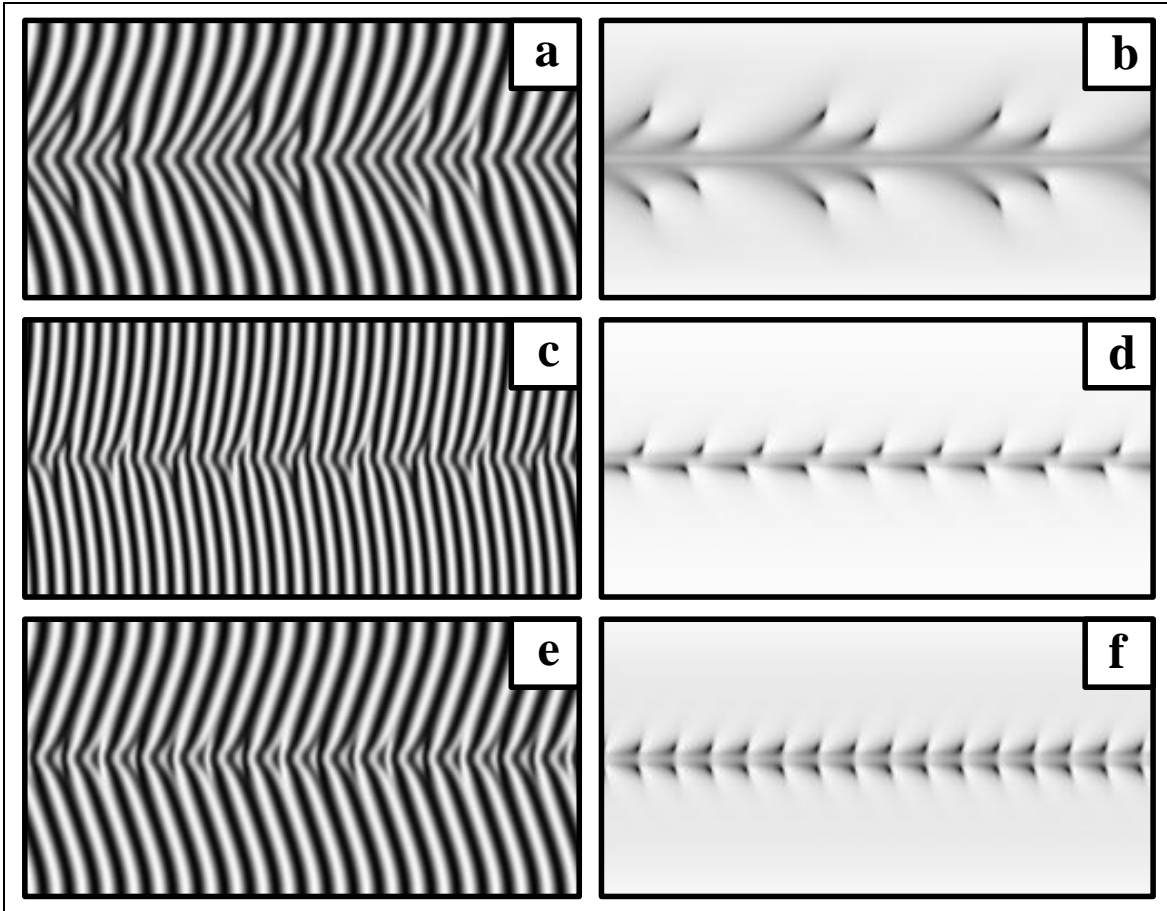
Figure 3.7: **Phase slip patterns in a medium with positive dispersion.** *Space-time diagrams of different asymptotic wave patterns exhibiting phase slips. The left row displays ReA, the right row shows $|A|$. The parameters are $\omega = 0$, $\Delta\omega = 0.6$, $\alpha = 0.5$ (a,b); $\omega = 0.3$, $\Delta\omega = 0.7$, $\alpha = 0.8$ (c,d); $\omega = 0$, $\Delta\omega = 0.8$, $\alpha = 0.5$ (e,f). The other parameters are $\beta = 1.0$, $R = 2.0$, $\Delta t = 250$, and $L = 80$.*
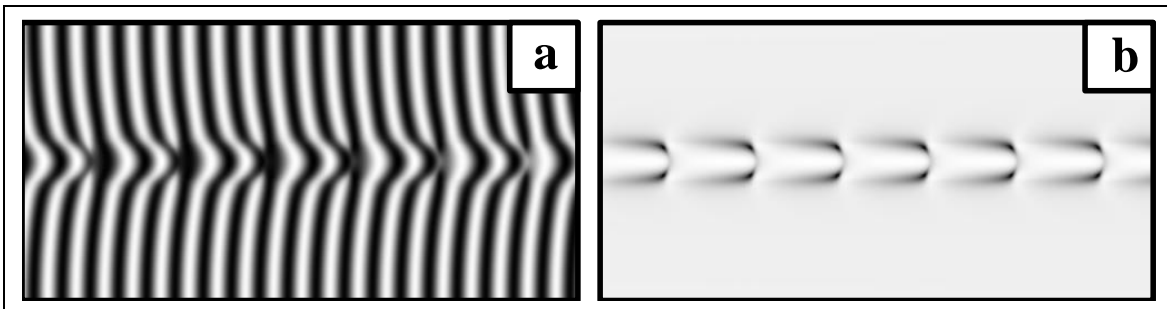

Figure 3.8: **Phase slips at a wave sink in a medium with positive dispersion.** *Shown are the space-time diagrams for the asymptotic behavior of ReA (a) and $|A|$ (b). The parameters are $\Delta\omega = 0.3$, $\omega = 0$, $\alpha = 0.5$, $\beta = 1.0$, $R = 5.2$, $\Delta t = 250$, and $L = 80$.*

in the outside region are unable to induce waves propagating inside the core. It is clearly seen that the modulations that finally lead to the phase slips are bound to the border of the core. In this case, the phase slips clearly represent a local desynchronization phenomenon.

Phase slip patterns in a medium with negative dispersion

Phase slips are also possible in media with negative dispersion. In Fig. 3.9, a target pattern with inward propagating, Eckhaus-unstable waves ($\Delta\omega < 0$) is shown. Also for negative dispersion, phase slips occur at a finite distance from the core boundary. While the wavenumber k is smaller in the far field than near the pacemaker, the frequency Ω is smaller close to the pacemaker than in the far field. This reflects the fact that in a medium with negative dispersion, the frequency decreases for increasing wavenumbers. Since group and phase velocities have different directions for negative dispersion (if ω is sufficiently large, as discussed above), the difference of these two velocities can be nicely illustrated: The waves move inward [Fig. 3.9(a)], while the modulations of the amplitude, which finally lead to the phase slips, are directed outward [Fig. 3.9(b)]. The waves seen in the diagram for ReA correspond to the phase velocity, while the amplitude modulations reflect the group velocity.
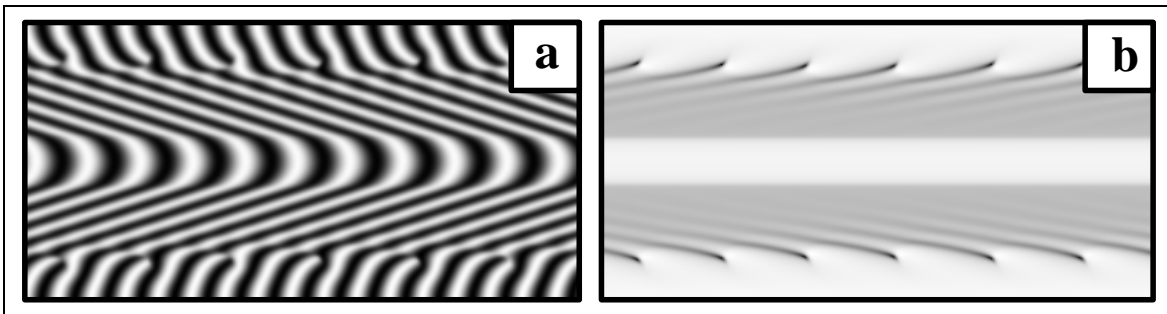

Figure 3.9: **Eckhaus instability in a medium with negative dispersion.** *Shown are the space-time diagrams for the asymptotic behavior of ReA (a) and $|A|$ (b). The parameters are $\Delta\omega = -0.2072$, $R = 14.8$, $\omega = 1$, $\alpha = -0.55$, $\beta = -1.0$, $\Delta t = 250$, and $L = 160$.*

Figure 3.10 displays other examples of inward propagating target patterns where the decrease $\Delta\omega$ of the local frequency inside the core is stronger and the phase slips already appear closer to the core boundary. The simulation shown in Figs. 3.10(a,b) corresponds to the simulation of Figs. 3.7(a,b), where the signs of $\Delta\omega$, α, and β are simply inverted. Due to this symmetric change, the space-time diagrams for the amplitude $|A|$ display the same behavior (but not the diagrams of ReA, of course). In the simulation shown in Figs. 3.10(c,d), the phase slips occur with a period-1 behavior close to the core and resemble the simulation shown in Fig. 3.7(e,f). Finally, Fig. 3.11 shows phase slips in the wave pattern of a wave sink
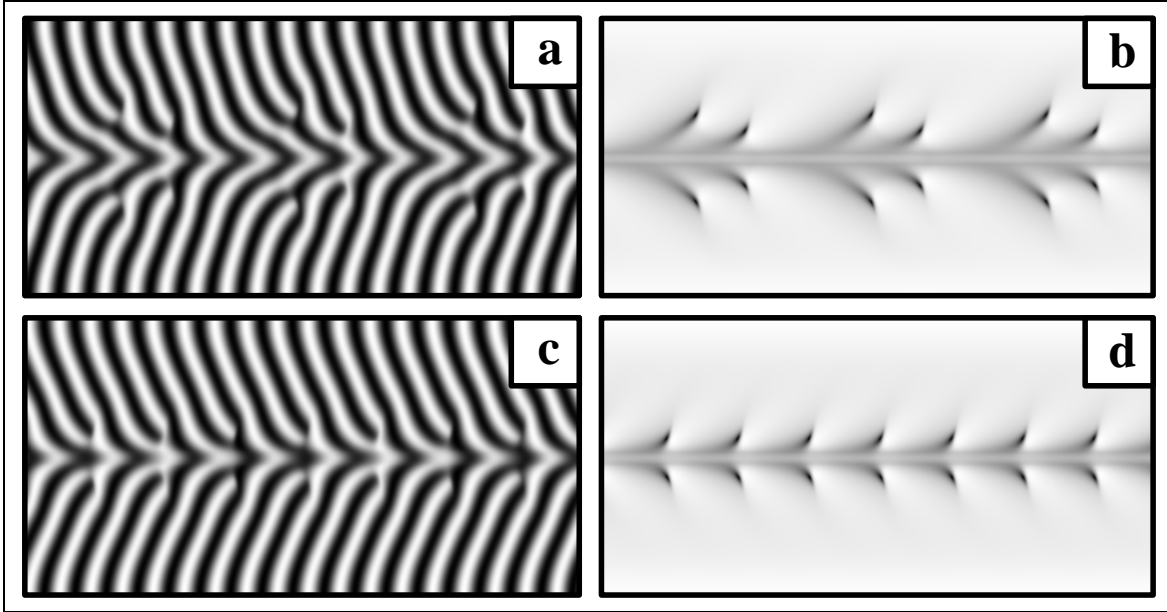
Figure 3.10: **Phase slips in a medium with negative dispersion.** *Shown are the space-time diagrams for the asymptotic behavior of ReA (a,c) and $|A|$ (b,d). The parameters are $\Delta\omega = -0.6$, $\alpha = -0.5$ (a,b); $\Delta\omega = -0.65$, $\alpha = -0.55$ (c,d). The other parameters are $\omega = 1$, $R = 2.0$, $\beta = -1.0$, $\Delta t = 250$, and $L = 80$.*
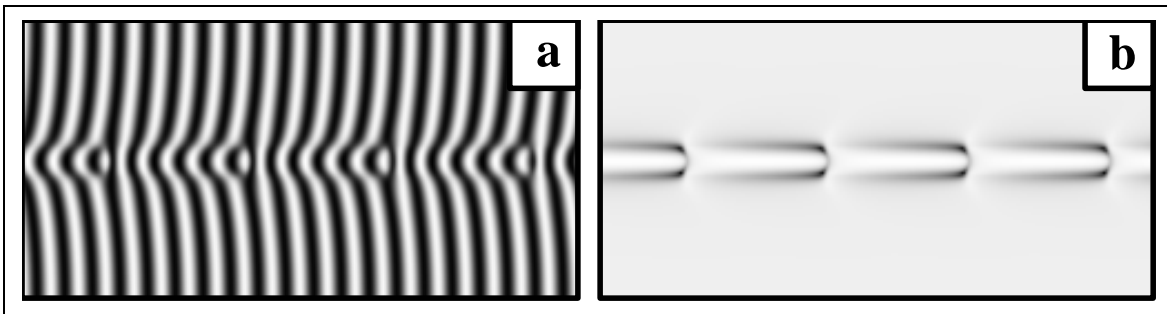

Figure 3.11: **Phase slips at a wave sink in a medium with negative dispersion.** *Shown are the space-time diagrams for the asymptotic behavior of ReA (a) and $|A|$ (b). The parameters are $\Delta\omega = 0.3$, $R = 4$, $\omega = 1$, $\alpha = -0.55$, $\beta = -1.0$, $\Delta t = 250$, and $L = 80$.*

with $\Delta\omega > 0$. Outside the core region, uniform low frequency oscillations are present. The heterogeneity with its large frequency cannot entrain the system with negative dispersion, but the uniform oscillations are also unable to entrain the wave sink. Instead, periodic phase slips appear at the boundary of the core, similar to the case of positive dispersion (Fig. 3.8). Again, the phase slips and the amplitude defects result from a local desynchronization process.

3.2.2 Two-dimensional systems

In two spatial dimensions, simulations have been carried out to confirm the existence of stable pacemakers and wave sinks, and to investigate the behavior of unstable target patterns. Since the basic effects are present in both one- and two-dimensional systems, only selected examples are shown for two-dimensional media. The initial conditions always correspond to uniform oscillations.

In Figure 3.12, a two-dimensional target pattern in a medium with negative dispersion is shown. For such parameters, the target waves run toward the pacemaker. To simultaneously study the effects of a pacemaker and a wave sink in two spatial dimensions, two small heterogeneities are present in this system, one corresponding to a pacemaker and the other to a wave sink. The pacemaker is located in the center of the target pattern (clearly seen in Fig. 3.12(a)), while the sink is close to the right lower corner. The wave sink locally compresses the waves and the amplitude decreases which can be seen in Fig. 3.12(b) as a dark spot. Note that the wave field remains continuous, i.e. no phase slips occur here.
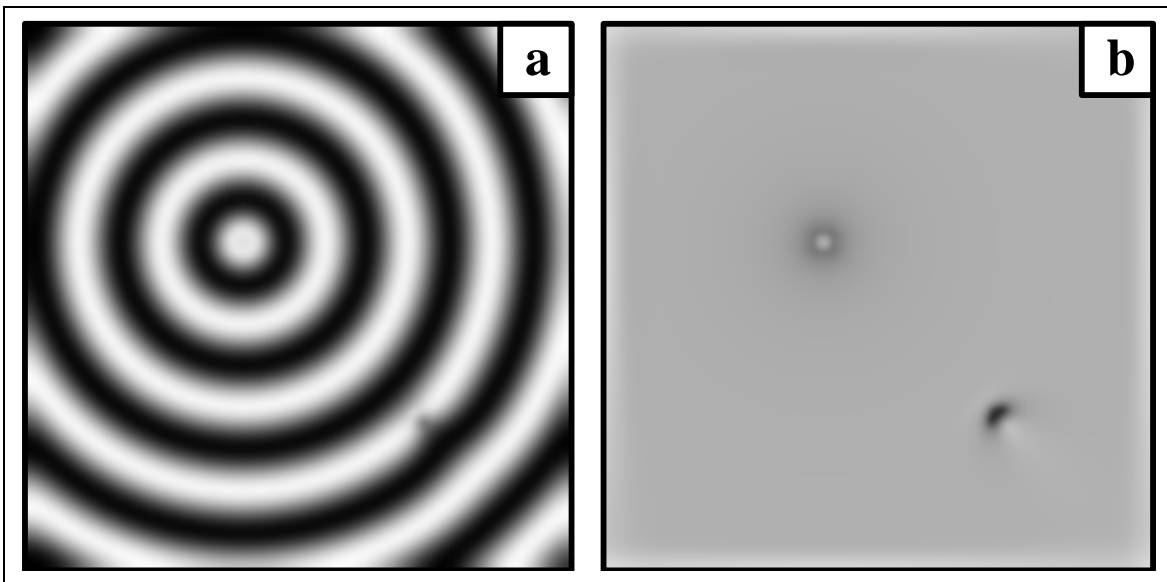

Figure 3.12: **Stable two-dimensional pacemaker with a wave sink.** *(a) shows an image of ReA, (b) an image of the $|A|$ at $t = 500$. The dark spot in (b) denotes the wave sink, where $|A|$ is decreased to its minimum value where $|A| = 0.67$. Note that here, black does not denote zero. The parameters are: $\omega = 0$, $\alpha = 1$, and $\beta = 0$. The two-dimensional domain has an extension given by $L_x = L_y = 100$. The pacemaker is characterized by $\Delta\omega = -0.6$ and $R = 1.6$, and the sink by $\Delta\omega = 0.7$ and $R = 1.6$.*

In the next simulation, the extension of the wave sink is greatly enlarged to find out how a strong wave sink behaves in two spatial dimensions. The results are displayed in Fig. 3.13.
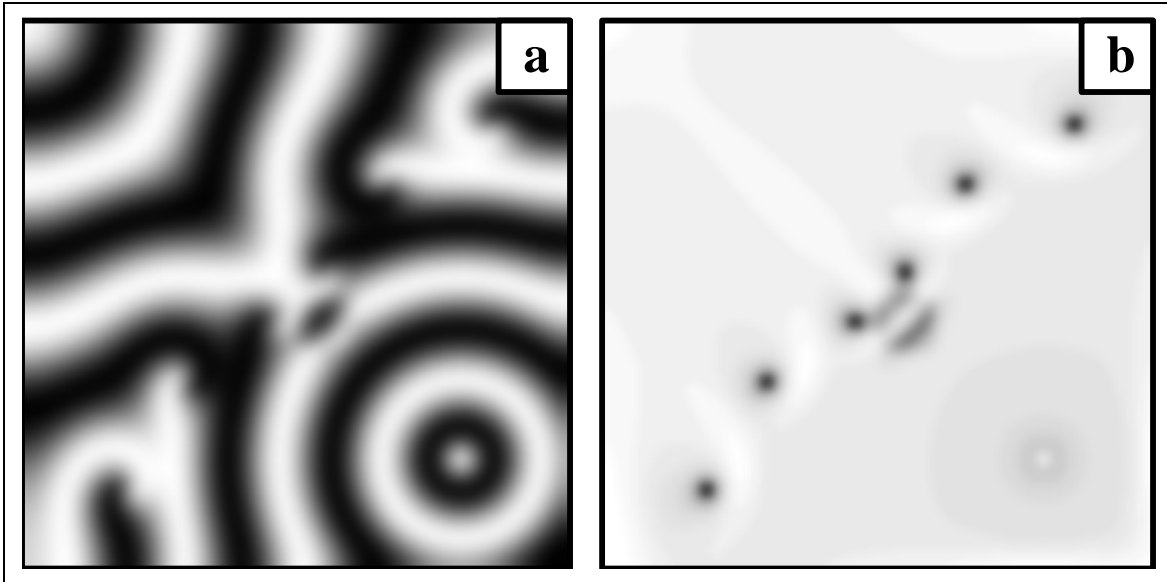
Figure 3.13: **Two-dimensional pacemaker generating open wave ends.** *(a) shows an image of ReA, (b) an image of $|A|$ at $t = 500$. The pacemaker is located close to the lower right corner while the sink is located in the center of the system. The dark spots in (b) denote open wave ends where the amplitude is vanishing. There, amplitude defects are present. The parameters are $\omega = 0$, $\alpha = -1$, $\beta = 0$, $L_x = L_y = 100$. The pacemaker is characterized by $R = 3.2$ and $\Delta\omega = 0.6$, and the wave sink by $R = 7.2$ and $\Delta\omega = -0.6$.*

It turns out that sufficiently deep and large wave sinks are able to break the waves that are emitted by a pacemaker (here in a system with positive dispersion). These broken waves have open ends which, in the absence of a pacemaker, would actually curl in and form a spiral (corresponding simulations are not shown here). The open ends constitute phase singularities which are associated with amplitude defects that can be easily detected in Fig. 3.13(b) as dark spots. Since the pacemaker periodically emits waves, the broken waves are pushed outward until they are annihilated at the no-flux boundary.

As the magnitude of the frequency shift $\Delta\omega$ of a pacemaker increases, phase slips are expected to develop in the expanding wave pattern. A simulation confirming this conjecture is shown in Fig. 3.14. There, a strongly negative frequency shift in a medium with negative dispersion leads to the emission of unstable target waves. In complete analogy with the one-dimensional simulations, phase slips are observed at a certain distance from the wave source. A phase slip is associated with an amplitude defect which has a circular geometry (*ring-shaped defect*). This is clearly seen in the image of the amplitude $|A|$ for such a time moment [Fig. 3.14(b)]. In addition, phase slips also occur at the boundary of the pacemaker, which may be due to the strong curvature of the waves in the center of the pattern. This shows that the appearance of phase slips is possible in different distances to the core. Both types of phase
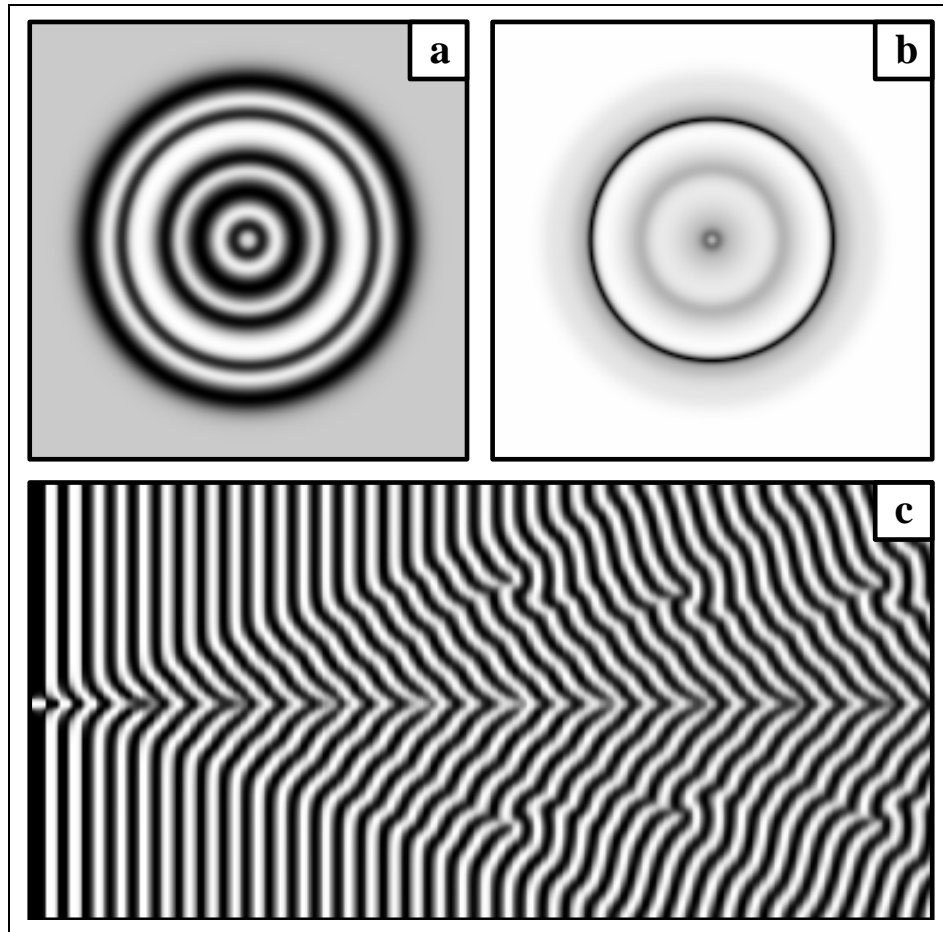
Figure 3.14: **Two-dimensional pacemaker with unstable target waves in a medium with negative dispersion.** *(a) shows an image of ReA, (b) an image of $|A|$ at $t = 131$. The black line in (b) denotes a circular defect line. A strong decrease of $|A|$ is also present close to the core. (c) shows a space-time diagram of ReA for a cross section through the center of the system parallel to the x-axis for a time interval $\Delta t = 250$. The parameters are $\omega = 0$, $\alpha = 1$, $\beta = 0$, $\Delta\omega = -0.7$, $R = 1.6$, and $L_x = L_y = 150$.*

slips can also be seen in the space-time diagram for a cross section through the center of the system [Fig. 3.14(c)]. Since the dispersion is negative, the target waves propagate toward the center. The phase slips periodically occurring far from the core and at the core boundary can be clearly identified.

The defect lines in the simulation presented in Fig. 3.14 show perfect circular symmetry. Next, a simulation is shown for the case that this symmetry is broken due to an interaction of the waves with the no-flux boundary. Figure 3.15 shows several time moments of the evolution of a wave pattern consisting of unstable target waves where the defect line appears close to the boundary of the system. As a result of the collision of the target wave with the border, the phase slip occurs first for the section of the wave which is directed toward
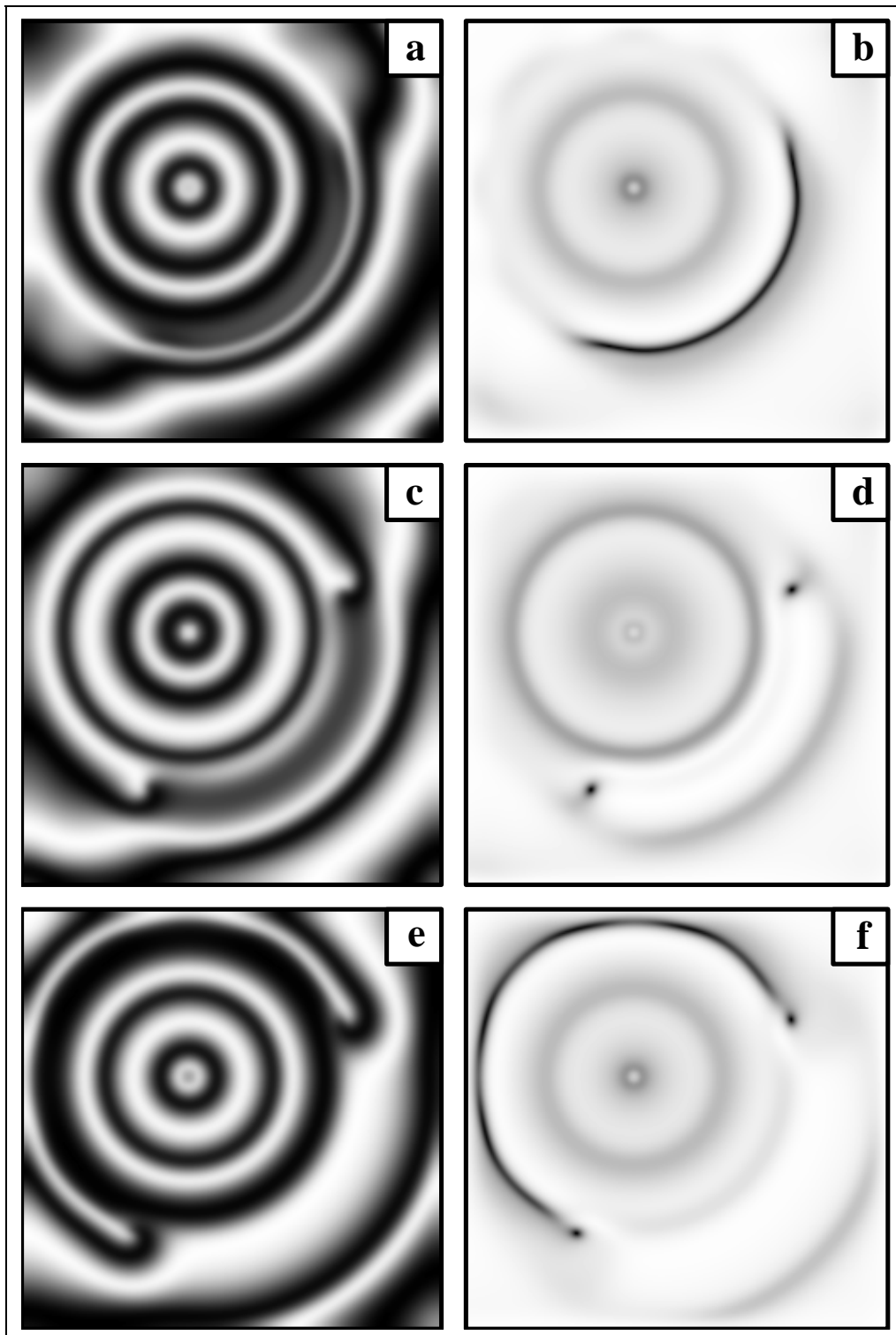
Figure 3.15: **Two-dimensional pacemaker generating line defects.** *(a,b)* $t = 537.5$; *(c,d)* $t = 546.5$; *(e,f)* $t = 586.0$. *The left column displays ReA, the right row shows* $|A|$. *The dark lines in the right column corresponds to line defects where phase slips occur (a,f), and the isolated dark dots to point defects (phase singularities) (d). The parameters are* $\omega = 0$, $\alpha = 1$, $\beta = 0$, $\Delta\omega = -0.7$, $R = 1.6$, *and* $L_x = L_y = 100$.

the center of the medium. Although this open defect line disappears after the phase slip, its open ends persist and form two point defects. At these point defects, a phase singularity is present, resembling the core of a spiral. Indeed, if the pacemaker is removed from the system, the point defects persist and form the cores of two spiral waves. However, if the pacemaker is kept within the system, the part of the target wave pattern which is interacting with the boundary also undergoes a phase slip process. This behavior is repeated periodically, leading to alternating phase slips occur in the center and at the border. The delay time between the two events is asymptotically constant.

3.3 Discussion

This chapter provides evidence that complex wave patterns with a rich variety of spatio-temporal behavior can be produced in oscillatory media by introducing a heterogeneity, i.e. a core region where the local oscillation frequency is modified. Depending on the parameters of the medium, which determine the dispersion of waves, and on the frequency shift of the heterogeneity, target patterns with outward and inward propagating waves can be observed. In particular, inward traveling target patterns are possible for a medium with negative dispersion. Whenever a heterogeneity is able to entrain the medium with propagating waves, i.e. form a target pattern, the heterogeneity represents a pacemaker, regardless of the direction of waves. If a heterogeneity is not capable of producing an extended target pattern but just a localized wave pattern, the heterogeneity represents a wave sink. The corresponding localized wave patterns may also consist of inward or outward traveling waves. When the radius of the heterogeneity is large compared to the wavelength of the generated waves, new effects may be observed, such as inward traveling waves inside the heterogeneity for a medium with positive dispersion.

Though some theoretical studies of inward traveling wave patterns in oscillatory (and excitable) media have been performed previously [113, 151, 152], this kinetic regime has remained less explored compared to outward traveling waves until recently, because no experimental evidence of inward traveling wave patterns in chemical reaction-diffusion systems was known. However, in 2001, Vanag and Epstein showed inward traveling target waves in a modified BZ reaction [27], triggering a growing interest in such patterns. Even more recently, inward traveling target patterns have also been found by Wolff in the CO oxidation reaction [110].

When the local frequency shift in the core region is increased, wave regimes with a

periodic formation of phase slips are observed. In these regimes, the effective oscillation frequency inside the core becomes different from the frequency of oscillations in the far region. The phase slips occur because the medium is no longer able to compensate the frequency shift by the propagation of waves. Hence, desynchronization takes place and oscillations in the core region become decoupled from the rest of the medium. While desynchronization is interpreted as an Eckhaus instability for intermediate values of the frequency shift (or equivalently for relatively small radii), a local desynchronization process is observed for large frequency shifts (or radii). Such effects have also been studied by Sakaguchi, who used mode truncation to analyze the onset of desynchronization in the CGLE [153].

Note that a specific form of the heterogeneity [Eq. (3.2)] has been assumed in order to derive the equation $k = k(R)$, which determines the wavenumber as a function of the spatial extension of the pacemaker. The analytical derivation of the properties of the pacemaker is general for all spatial dimensions and all possible frequency distributions until Eq. (3.19), which is valid for one spatial dimension only. The respective solutions for two and three spatial dimensions are considered in the book of Kuramoto [53]. Recently, Mahara *et al.* [58] investigated pacemakers in two spatial dimensions which have the shape of a ring.

For another modified version of the CGLE, properties of heterogeneous pacemakers have been studied by Hendrey and co-authors [59]. They assume that the heterogeneity not only changes the frequency, but also the amplitude of oscillations. Another major difference is that they have studied a heterogeneity with an exponentially decaying size. In spite of these differences, some of the numerical results found in their model are similar to the results presented here. For example, they also encounter periodically appearing phase slips if the frequency shift is large enough, a pattern they call *breathing target*. However, they do not provide an explanation for the appearance of phase slips in terms of the Eckhaus instability or a local desynchronization mechanism. A hysteresis between normal and breathing target patterns is observed. A substantial part of their work is devoted to spirals and the selection mechanism between spiral waves and target patterns, which are topics that have not been addressed in the present work. It may well be possible that hysteresis and a complex interaction of spirals and target patterns can also be found for the model studied in this chapter.

Though the analysis of pacemakers and wave sinks has been performed for a model system described by the CGLE, the results would probably remain qualitatively correct for other oscillatory media with anharmonic oscillations. In this context, experiments have recently been performed by Wolff for the CO oxidation reaction on platinum [110]. By pointing a laser beam on the surface, the temperature is locally increased and the desorption of CO

is enhanced. The temperature shift of the "heterogeneity" is controlled by the laser power. In this way, the kinetics of the system is changed locally by external means, as assumed in this chapter. The experiments in the oscillatory regime of the CO oxidation show outgoing and ingoing target patterns and localized outgoing waves. To date, no definite explanation of these observations is given, however it seems probable that at least the outgoing target patterns may be explained by the theory discussed in this chapter, since there, the frequency is locally increased and the dispersion is positive. An observation made in the excitable regime of this reaction deserves further attention. While a wave train consisting of nearly plane waves propagated along the surface, the laser spot was focused on a single point. The laser point was able to break the waves, whose open ends curled in. Qualitatively similar effects have been presented in Fig. 3.13.

Also in experiments with the light-sensitive Belousov-Zhabotinsky reaction, the oscillation frequency can easily be controlled by changing the local light intensity. In this way, heterogeneities with different shapes, sizes and strengths can be created. Experiments in this direction have been done by Petrov *et al.* [154] (see also Ref. [58]). By varying these parameters and the reaction conditions, it would be possible to create different pacemakers and maybe also observe the onset of desynchronization in this system.

It is well known that pacemakers which emit waves with different frequencies compete with each other. For a medium with positive dispersion, the pacemaker with the largest frequency suppresses all other pacemakers. However, this is only true as long as the waves are Eckhaus stable. If phase slips develop, the frequency and wavenumber of the waves decrease in the far field of the pacemaker, which is therefore not able to entrain the medium. Far from the heterogeneity, it effectively appears as a pacemaker with a lower frequency. For a medium with negative dispersion, the argument is modified. Then, the pacemaker with the lowest frequency would suppress all others. If phase slips appear in the wave pattern of such a pacemaker, it appears as having a higher frequency. Consequently, strong pacemakers which locally create large frequency differences may possibly not suppress the activity of other pacemakers which are located far enough. Of course, competition of target patterns and spirals may also be possible and proceeds according to the same arguments.

This chapter has been devoted to heterogeneous pacemakers and has presented in detail how a localized frequency increase yields the emission and propagation of waves. These results represent a useful basis for the systems where self-organized pacemakers are possible. Such systems are discussed in the following chapter.

Chapter 4

Self-organized pacemakers in oscillatory media

In this chapter, self-organized pacemakers in oscillatory media are discussed. Since simple oscillatory systems described by the complex Ginzburg-Landau equation are not capable of creating stable self-organized pacemakers, alternative models should be considered and analyzed. In Chapter 3, it has been shown that pacemakers and target patterns may be formed if two oscillation frequencies are present in the system. Therefore, a special type of oscillatory systems is investigated in this chapter, where two stable limit cycles corresponding to uniform oscillations with different frequencies coexist. Such systems are called birhythmic. The phenomenon of birhythmicity has been discussed in chemical and biochemical systems [15, 155–158], including important examples such as glycolytic oscillations [15], calcium oscillations [159], and the photo-sensitive BZ reaction [160]. One possible bifurcation which can give rise to birhythmicity is the supercritical pitchfork-Hopf bifurcation. Close to such a bifurcation, a general description of the spatio-temporal behavior in terms of amplitude equations is possible. In a system governed by such equations, self-organized pacemakers with extended wave patterns are generic and can be stable. Moreover, it is possible to construct an approximate analytical solution for self-organized pacemakers. It should be emphasized that such pacemakers are not formed by spatial inhomogeneities like the pacemakers considered in the previous chapter, but are entirely due to the intrinsic dynamics of the system.

After deriving the model and discussing its basic features in Sec. 4.1, the analytical solution for self-organized pacemakers in one-dimensional systems is presented in Sec. 4.2. Also, the drift of pacemakers caused by spatial parameter gradients is described. Results of numerical simulations are presented in Sec. 4.3. The existence and stability of self-organized pacemakers in one and two spatial dimensions are confirmed. The interaction between different pacemakers is subsequently analyzed and it will be demonstrated that stable pacemakers

globally inhibit the formation of other pacemakers in the system. Furthermore, kinetic instabilities leading to breathing and swinging pacemakers as well as instabilities induced by phase slips are numerically investigated. The chapter closes with a discussion of the obtained results (Sec. 4.4).

The derivation of the normal form and amplitude equations (Appendix A.2) is due to the close collaboration with Mads Ipsen. Some of the results presented in this chapter have been published in Refs. [161, 162].

4.1   The model

The model discussed in this chapter consists of two coupled amplitude equations valid in the vicinity of a supercritical pitchfork-Hopf bifurcation. These equations describe an oscillatory medium close to the soft onset of birhythmicity. In this section, the model is derived and a qualitative discussion of self-organized pacemakers based on the phase dynamics approximation is given.

4.1.1   The distributed pitchfork-Hopf bifurcation

The derivation of normal forms for reaction-diffusion systems close to certain bifurcations has recently been discussed by Ipsen *et al.* [163, 164]. Here, a system is considered which is close to a bifurcation where a stationary uniform state becomes unstable due to the simultaneous growth of a real uniform eigenmode and a pair of complex conjugate uniform eigenmodes. The generic bifurcation for this case is the fold-Hopf bifurcation. If pitchfork symmetry is additionally assumed, the dynamics of the system is governed by a pitchfork-Hopf bifurcation. Furthermore, if this bifurcation is supercritical, two stable limit cycles with different frequencies coexist in the vicinity of this bifurcation, which means that the medium is birhythmic.

Figure 4.1 illustrates how the combination of a supercritical pitchfork and a supercritical Hopf bifurcation yields birhythmicity. If one starts from the stable fixed point (shown in the upper left part of the figure) and increases the control parameter corresponding to the Hopf bifurcation, the stable fixed point is transformed into a stable limit cycle. On the other hand, if the parameter responsible for the pitchfork bifurcation is varied, the stable fixed point becomes unstable and two new stable fixed points are created. If both parameters are changed simultaneously, two stable limit cycles are obtained which generally have different
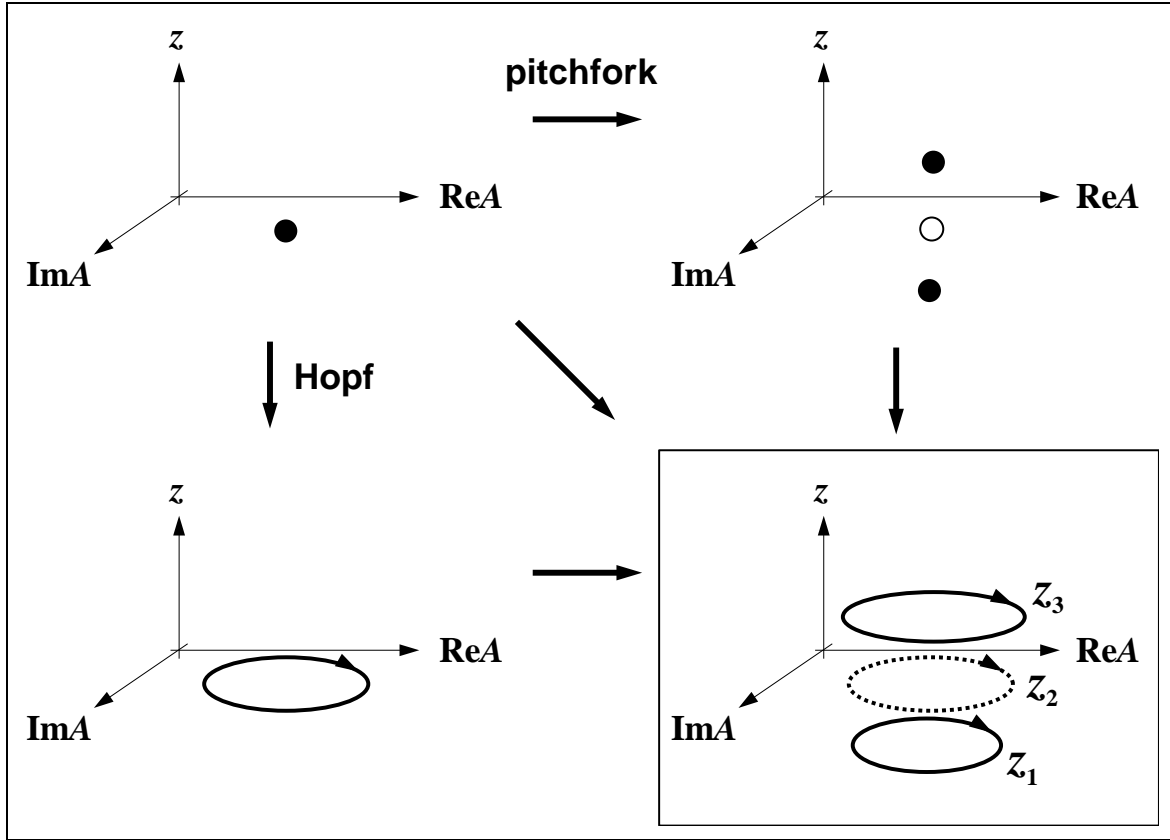
Figure 4.1: **Schematic view of the pitchfork-Hopf bifurcation.** *The black (white) dots represent stable (unstable) fixed points and the solid (dashed) lines indicate stable (unstable) limit cycles. Unstable fixed points are not displayed when limit cycles are present.*

frequencies and amplitudes.

The derivation of the normal form of the distributed pitchfork-Hopf bifurcation is presented in Appendix A.2. The normal form is given by

$$\dot{A} = \eta_1 A + g_0 A z + g_1 |A|^2 A + g_2 A z^2, \tag{4.1a}$$

$$\dot{z} = \eta_2 + \eta_3 z + c_0 |A|^2 + c_2 |A|^2 z + c_3 z^3, \tag{4.1b}$$

where A is the complex oscillation amplitude and z is the amplitude of the real mode. The coefficients in the equation for the complex amplitude are complex, the coefficients in the equation for the real amplitude are real. The real and imaginary parts of a parameter are denoted by the superscripts r and i. The real part η_1^r of the parameter η_1 is the Hopf bifurcation parameter and η_3 is the pitchfork bifurcation parameter. The parameter η_2 accounts for the imperfection of the pitchfork bifurcation, leading to a cusp scenario [44, 165]. For positive η_1^r, η_2, and η_3, there is a region in parameter space where birhythmicity is realized. Figure 4.2 shows a part of this region in the parameter subspace spanned by η_2 and η_3.
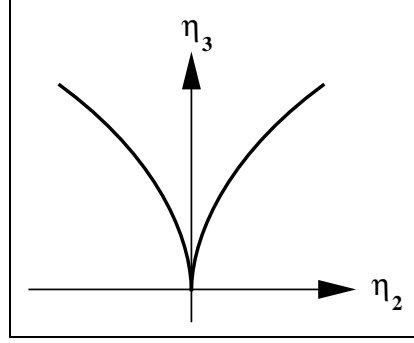
Figure 4.2: **The cusp in parameter space.** *The area between the curves denotes the region where birhythmicity is found in the parameter subspace spanned by η_2 and η_3.*

Under certain conditions, which are discussed in Appendix A.3, the terms proportional to Az^2 and $|A|^2 z$ can be dropped. Then, Eqs. (4.1) transform into

$$\dot{A} = \eta_1 A + g_0 A z + g_1 |A|^2 A, \tag{4.2a}$$

$$\dot{z} = \eta_2 + \eta_3 z + c_0 |A|^2 + c_3 z^3, \tag{4.2b}$$

which is the reduced normal form of a pitchfork-Hopf bifurcation. In order to obtain a set of amplitude equations describing the dynamics of a distributed system close to this bifurcation, the diffusion of all components must be taken into account. Appendix A.2 also shows the derivation of the diffusion terms. As a result, the amplitude equations read

$$\partial_t A = \eta_1 A + g_0 A z + g_1 |A|^2 A + d_A \nabla^2 A, \tag{4.3a}$$

$$\partial_t z = \eta_2 + \eta_3 z + c_0 |A|^2 + c_3 z^3 + d_z \nabla^2 z, \tag{4.3b}$$

where d_A is the complex diffusion coefficient for the mode A and d_z is the real diffusion coefficient for the mode z. Assuming that the pitchfork and Hopf bifurcations are crossed, i.e. $\eta_1^r > 0$ and $\eta_3 > 0$, and that these bifurcations appear in a supercritical way, i.e. $g_1^r < 0$ and $c_3 < 0$, it is convenient to transform spatial coordinates, time, and amplitude variables in the following way

$$A = \sqrt{\frac{\eta_1^r}{-g_1^r}}\, \tilde{A}, \qquad z = \frac{\eta_1^r}{g_0^r}\, \tilde{z}, \qquad x = \sqrt{\frac{d_A^r}{\eta_1^r}}\, \tilde{x}, \qquad t = \frac{1}{\eta_1^r}\, \tilde{t} \tag{4.4}$$

to obtain a rescaled version of the amplitude equations given by

$$\partial_t A = (1 - i\omega)A + (1 - i\epsilon)Az - (1 + i\alpha)|A|^2 A + (1 + i\beta)\nabla^2 A, \tag{4.5a}$$

$$\tau \partial_t z = \sigma - \gamma |A|^2 + z - \nu z^3 + l^2 \nabla^2 z. \tag{4.5b}$$

The tildes have been dropped here, and A and z are the rescaled amplitudes. The new parameters are given by

$$\omega = -\frac{\eta_1^i}{\eta_1^r}, \qquad \alpha = \frac{g_1^i}{g_1^r}, \qquad \epsilon = -\frac{g_0^i}{g_0^r}, \qquad \beta = \frac{d_A^i}{d_A^r},$$

$$\sigma = \frac{g_0^r \eta_2}{\eta_1^r \eta_3}, \qquad \gamma = \frac{g_0^r c_0}{g_1^r \eta_3}, \qquad \nu = -\frac{(\eta_1^r)^2 c_3}{(g_0^r)^2 \eta_3}, \qquad \tau = \frac{\eta_1^r}{\eta_3}, \qquad l = \sqrt{\frac{\eta_1^r d_z}{\eta_3 d_A^r}}. \tag{4.6}$$

The parameters ω, α, and β denote the linear and nonlinear frequency parameters, and the linear wave dispersion respectively. The parameter ϵ specifies the frequency shift of the oscillations due to the coupling of A to the real mode z, γ characterizes the strength of the feedback from the oscillatory to the real mode, and the positive parameter ν determines the nonlinear saturation of the amplitude of the real mode. The coefficients τ and l respectively describe the ratios of time and length scales of the real and oscillatory modes. The term $\sigma - \gamma |A|^2$ in Eq. (4.5b) is responsible for the imperfection of the pitchfork bifurcation. While the parameter σ is constant, $\gamma |A|^2$ is space- and time-dependent. This contribution represents the coupling to the oscillatory mode. As shown later, this term is important for the formation of stable self-organized pacemakers.

The system described by Eqs. (4.5) represents the model investigated in this chapter. It can be viewed as consisting of the usual complex Ginzburg-Landau equation (CGLE) coupled to an equation for a variable exhibiting bistable dynamics. Like the CGLE, Eq. (4.5a) is invariant with respect to a global phase shift $A \rightarrow A \exp(i\phi_0)$.

4.1.2 Birhythmicity

The system described by Eqs. (4.5) has two coexisting solutions corresponding to stable uniform oscillations. For further investigations, it is convenient to write the complex oscillation amplitude A in terms of the oscillation phase ϕ and the real oscillation amplitude ρ defined by $A = \rho \exp(-i\phi)$. Using $\nabla^2 A = \nabla^2 z = 0$ for uniform solutions, Eqs. (4.5) are transformed into

$$\dot{\rho} = (z + 1 - \rho^2)\rho, \tag{4.7a}$$

$$\dot{\phi} = \omega + \alpha \rho^2 + \epsilon z, \tag{4.7b}$$

$$\tau \dot{z} = \sigma - \gamma \rho^2 + z - \nu z^3. \tag{4.7c}$$

For harmonic limit cycle oscillations, the amplitudes ρ and z are constant in time and related through

$$\rho = \sqrt{z+1}, \tag{4.8}$$

as follows from Eq. (4.7a). Substituting this into Eq. (4.7c), the cubic equation

$$\nu z^3 - (1-\gamma)z = \sigma - \gamma \tag{4.9}$$

is obtained. Since the amplitudes of the limit cycles are completely determined by the stationary solutions of z, birhythmicity occurs if z exhibits bistability. For this case, the three roots of Eq. (4.9) must be real, as fulfilled when $4(\gamma-1)^3 + 27\nu(\gamma-\sigma)^2 < 0$. Since ν is positive, this means that the condition $\gamma < 1$ is necessary. The roots $z_1 < z_2 < z_3$ are found using the Cardan formula and are given by

$$z_1 = 2\rho_C^{1/3} \cos\left[(\phi_C + 2\pi)/3\right], \tag{4.10a}$$
$$z_2 = 2\rho_C^{1/3} \cos\left[(\phi_C + 4\pi)/3\right], \tag{4.10b}$$
$$z_3 = 2\rho_C^{1/3} \cos\left[\phi_C/3\right], \tag{4.10c}$$

where $\rho_C^{2/3} = (1-\gamma)/(3\nu)$ and $\cos\phi_C = (\sigma-\gamma)/(2\nu\rho_C)$. The roots z_1 and z_3 represent the stable stationary solutions of z while z_2 describes the unstable stationary solution.

The frequencies of uniform oscillations can be obtained directly from Eq. (4.7b) and Eq. (4.8) as

$$\omega_{1,2,3} = \omega + \alpha + (\alpha + \epsilon)z_{1,2,3}. \tag{4.11}$$

The limit cycle oscillations corresponding to ω_1 and ω_3 (ω_2) are stable (unstable) since the stability of the limit cycles is inherited from the stability of the bifurcating branches describing stationary solutions of z. When $\alpha + \epsilon > 0$, the smallest root z_1 corresponds to the slowest oscillations, i.e. $\omega_1 < \omega_2 < \omega_3$. In the opposite case $\alpha + \epsilon < 0$, the fastest oscillations are associated with the smallest root z_1. If $\nu \gg 1$, the three roots (4.10) are small, i.e. $|z| \ll 1$, and the respective amplitudes (4.8) and frequencies (4.11) differ only slightly from the respective values for uniform oscillations in the CGLE.

4.1.3 Phase dynamics approximation

Allowing for nonuniform distributions of the system variables, the system described by Eqs. (4.5) reads in terms of phase and amplitude

$$\partial_t \rho = (z + 1 - \rho^2)\rho + \nabla^2 \rho - \rho(\nabla\phi)^2 + \beta\rho\nabla^2\phi + 2\beta\nabla\phi\nabla\rho, \tag{4.12a}$$

$$\partial_t \phi = \omega + \alpha\rho^2 + \epsilon z + (2/\rho)\nabla\rho\nabla\phi + \nabla^2\phi - (\beta/\rho)\nabla^2\rho + \beta(\nabla\phi)^2, \tag{4.12b}$$

$$\tau\partial_t z = \sigma - \gamma\rho^2 + z - \nu z^3 + l^2\nabla^2 z. \tag{4.12c}$$

If phase perturbations are sufficiently smooth, i.e. if $|\nabla\phi| \ll 1$, small amplitude perturbations of a stable limit cycle decay much faster than phase perturbations (see Ref. [53] and Sec. 2.3). As a result, the amplitude ρ is approximately given by

$$\rho^2 = 1 + z - (\nabla\phi)^2 + \beta\nabla^2\phi, \tag{4.13}$$

and can be eliminated adiabatically from Eqs. (4.12), which then become

$$\partial_t \phi = \omega + \alpha + (\alpha + \epsilon)z + (\beta - \alpha)(\nabla\phi)^2 + (1 + \alpha\beta)\nabla^2\phi, \tag{4.14a}$$

$$\tau\partial_t z = [\sigma - \gamma + \gamma(\nabla\phi)^2 - \beta\gamma\nabla^2\phi] + (1 - \gamma)z - \nu z^3 + l^2\nabla^2 z. \tag{4.14b}$$

In Eq. (4.14a), two terms proportional to $\nabla^2 z$ and ∇z are neglected. The conditions under which this approximation is justified are discussed in Sec. 4.2.3.

The phase dynamics equations (4.14) constitute the basis of the analytical derivation in Sec. 4.2. Equation (4.14b) can be interpreted as describing the reaction and diffusion of a bistable component z. The typical solutions of such an equation are fronts connecting two stable uniform states. The presence of waves with nonvanishing phase gradients modifies the motion of these fronts. If the variable z is fixed, Eq. (4.14a) reduces to a phase dynamics equation of the type studied in Chapter 3. According to the Benjamin-Feir-Newell criterion, uniform oscillations in this system are modulationally stable if the phase diffusion coefficient $1 + \alpha\beta$ is positive, which is assumed throughout this chapter.

4.1.4 Self-organized pacemakers

Though a large variety of spatio-temporal patterns is described by Eqs. (4.14), the focus of the work presented here lies on solutions representing self-organized pacemakers. Figure 4.3 shows a schematic illustration of the pacemaker solution. The variable z is increased inside the central region of the target pattern, i.e. the pacemaker, which may be also called the core.
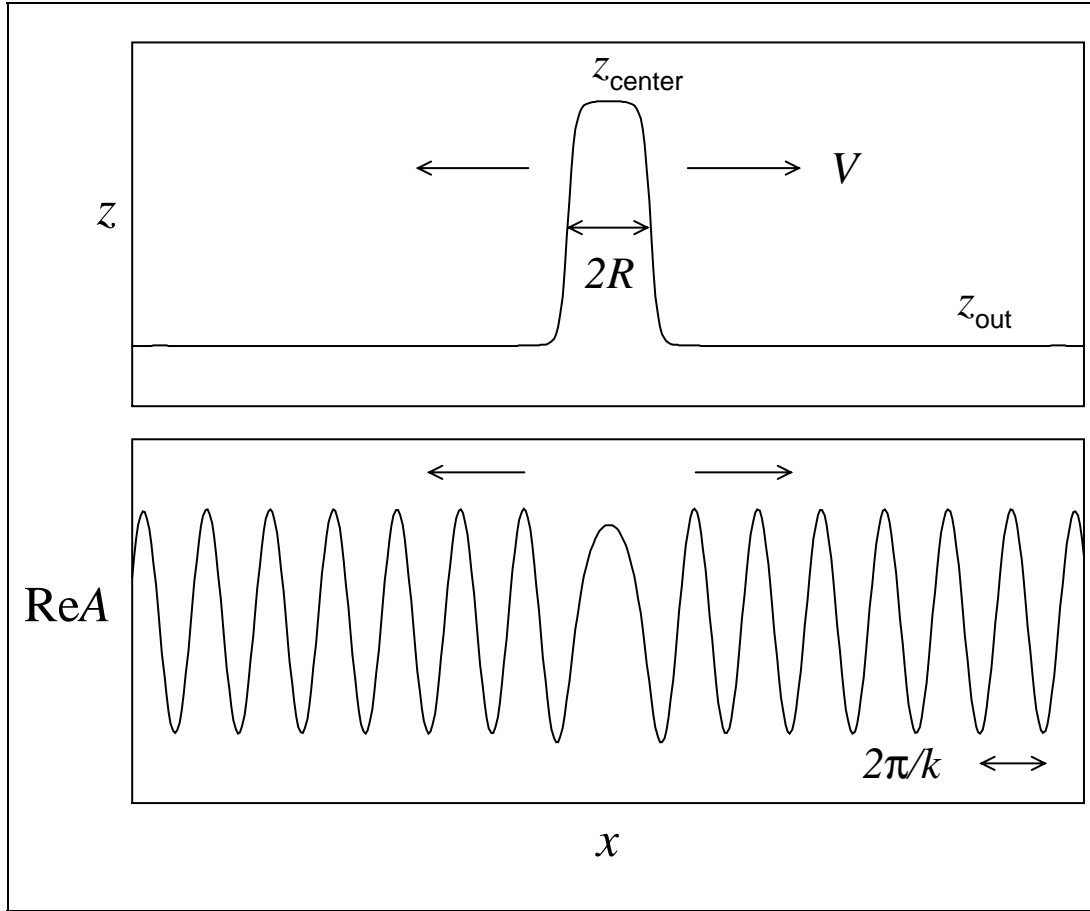
Figure 4.3: **Schematic view of a self-organized pacemaker.** *The figure shows typical distributions of z and ReA for a self-organized pacemaker.*

Suppose that this spatial distribution of $z(x)$ is fixed, i.e. constant in time, and approximated by the following expression

$$z(x) = \begin{cases} z_{\text{out}} & \text{for} \quad |x| > R, \\ z_{\text{center}} & \text{for} \quad |x| \leq R. \end{cases} \tag{4.15}$$

The values z_{center} and z_{out} of the variable z inside and outside the core and the radius R of the stationary core are determined later. According to Eq. (4.14a), the wave pattern generated by such a distribution of z is described within the phase dynamics approximation by

$$\partial_t \phi = \omega(x) + \alpha + (\beta - \alpha)(\nabla \phi)^2 + (1 + \alpha\beta)\nabla^2\phi, \tag{4.16}$$

where $\omega(x) = \omega + (\alpha + \epsilon)z(x)$ is defined in such a way that Eq. (4.16) becomes identical to Eq. (3.4), describing the phase equation for a medium with a heterogeneity. This means that, with respect to the oscillatory subsystem, a local heterogeneity is created, which approxi-

mately obeys

$$\omega(x) = \begin{cases} \omega_{\text{out}} & \text{for} \quad |x| > R, \\ \omega_{\text{out}} + \Delta\omega & \text{for} \quad |x| \leq R, \end{cases} \tag{4.17}$$

where $\omega_{\text{out}} = \omega + (\alpha + \epsilon)z_{\text{out}}$ and

$$\Delta\omega = (\alpha + \epsilon)(z_{\text{center}} - z_{\text{out}}) \tag{4.18}$$

corresponds to the frequency shift present inside the core region of width $2R$. Note that the nonlinear frequency coefficient α enters in Eq. (4.16) and is therefore not present in Eq. (4.17). Since the phase dynamics equation (4.16) has been studied as Eq. (3.4) in detail in Chapter 3, it is only briefly discussed here.

A necessary condition for the existence of pacemakers in such systems is given by $(\beta - \alpha)\Delta\omega > 0$ [Eq. (3.16)] or, using Eq. (4.18),

$$(\beta - \alpha)(\alpha + \epsilon)(z_{\text{center}} - z_{\text{out}}) > 0. \tag{4.19}$$

In the case of positive dispersion ($\beta - \alpha > 0$), there are two possible ways of fulfilling the condition (4.19). If z is increased inside the core (as assumed above), this implies that $\alpha + \epsilon$ must be positive. Obviously, if $\alpha + \epsilon < 0$, the variable z should instead exhibit a local decrease inside the core. On the other hand, if the dispersion is negative ($\beta - \alpha < 0$) and the parameters α and ϵ fulfill the condition $\alpha + \epsilon < 0$, the variable z should be increased inside the core. Accordingly, if $\alpha + \epsilon > 0$ in a system with negative dispersion, the variable z should be decreased inside the core. As explained in Chapter 3, the waves which form the target pattern are traveling toward the core in a medium with negative dispersion.

Although the analytical solution for self-organized pacemakers is presented in detail in the next section, the formation of pacemakers is already illustrated here for the specific case where z increases inside the core region (as shown in Fig. 4.3) and the parameters obey the conditions $\beta - \alpha > 0$ and $\alpha + \epsilon > 0$. To create a self-organized pacemaker, a sufficiently strong perturbation, leading to a local increase of the variable z, must be applied. Inside the core, the medium is then found in the state with a higher natural frequency. In this region, waves are initiated which propagate out of the core, giving rise to the formation of a target pattern. The core grows, accompanied by a simultaneous increase of the wavenumber k. The left and right boundaries of the core represent front solutions. If their velocity V is positive, the core expands, otherwise it contracts. A steady pacemaker is realized when $V = 0$. The front velocity V depends on the wavenumber k of the emitted waves and decreases for higher

wavenumbers. A feedback loop is therefore present: When a critical wavenumber is reached, the front velocity vanishes and a stationary pacemaker is formed.

4.2   Analytical solution

The analytical solution of a self-organized pacemaker in a one-dimensional system is constructed in this section. The approach is similar to a derivation for a different model system where, however, the background state corresponding to uniform oscillations was unstable and birhythmicity was absent [61]. First, the wave pattern corresponding to a fixed core is determined and the wavenumber of emitted waves is found. Then, the equation that determines the core front velocity as a function of the wavenumber is derived. Both results are then combined to obtain the properties of the stationary pacemaker and the conditions that ensure the existence and stability of the pacemaker solution. To be specific, the solution is constructed assuming that the conditions $\beta - \alpha > 0$ and $\alpha + \epsilon > 0$ are satisfied. Then, the variable z is increased inside the core, i.e. $z_{\text{center}} > z_{\text{out}}$. Also the other parameter regimes where self-organized pacemakers are possible are discussed. Finally, the motion of pacemakers in a spatial parameter gradient is considered and the resulting drift velocity is estimated.

4.2.1   Wave emission

Inside the core of a self-organized pacemaker, the variable z is increased under the above made conditions (see Fig. 4.3) and its distribution is approximately given by Eq. (4.15). If this distribution is fixed, the properties of the wave pattern can be calculated as in Chapter 3.

By applying the Cole-Hopf transformation

$$\phi = \frac{1 + \alpha\beta}{\beta - \alpha} \ln Q \tag{4.20}$$

to the phase equation (4.14a), the following equation for the new variable $Q(x, t)$,

$$\partial_t Q = \frac{\beta - \alpha}{1 + \alpha\beta}[\omega + \alpha + (\alpha + \epsilon)z(x)]Q + (1 + \alpha\beta)\nabla^2 Q, \tag{4.21}$$

is obtained. This equation can be solved exactly like Eq. (3.6) in Chapter 3. Therefore, the derivation is omitted and only the final results are given. The asymptotic solution of Q outside the core is

$$Q_0(x, t) \propto \exp(\lambda_0 t - \kappa|x|), \tag{4.22}$$

where $\lambda_0 = (\beta - \alpha)\Omega/(1 + \alpha\beta)$ and $\kappa = (\beta - \alpha)k/(1 + \alpha\beta)$. The phase distribution in the limit of large times outside of the core is

$$\phi(x, t) = [\omega + \alpha + (\alpha + \epsilon)z_{\text{out}}]t + (\beta - \alpha)k^2 t - k|x| + \text{const}, \qquad (4.23)$$

which corresponds to a pattern of propagating plane waves with the frequency Ω given by

$$\Omega = \omega + \alpha + (\alpha + \epsilon)z_{\text{out}} + (\beta - \alpha)k^2. \qquad (4.24)$$

The wavenumber k of the emitted waves is determined as a root of the equation

$$\sqrt{k_{\text{max}}^2 - k^2} \tan\left[\frac{\beta - \alpha}{1 + \alpha\beta}R\sqrt{k_{\text{max}}^2 - k^2}\right] = k, \qquad (4.25)$$

where

$$k_{\text{max}}^2 = \frac{\alpha + \epsilon}{\beta - \alpha}\left(z_{\text{center}} - z_{\text{out}}\right). \qquad (4.26)$$

In Fig. 4.4(a), the dependence of the wavenumber on the core radius is shown. The wavenumber k increases monotonously and approaches k_{max} as the radius diverges.
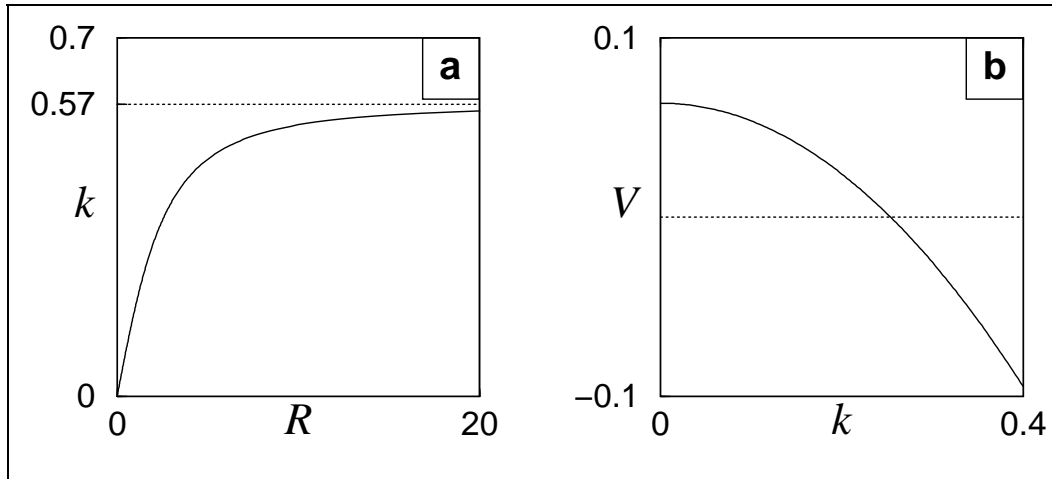

Figure 4.4: **Wavenumber and front velocity of a pacemaker.** *(a) Dependence of k on the core radius R. The maximum possible wavenumber $k_{\text{max}} = 0.57$ is denoted by the dashed line. (b) Dependence of the front velocity V (in units of l/τ) on the wavenumber k of emitted waves. The dashed line indicates $V = 0$. The parameters are $\alpha = 0.5$, $\beta = 1.5$, $\epsilon = 0.5$, $\nu = 40$, $\gamma = -0.075$, and $\sigma = -0.06$. The parameter ω can be chosen arbitrarily.*

4.2.2   Core dynamics

The core represents a region where the variable z is increased with respect to its value z_{out} in the outside region (Fig. 4.3). The boundaries of the core are formed by two interfaces,

or fronts, connecting the two states. For a steady pacemaker, the fronts should not move. The dynamics of the variable z is described by Eq. (4.14b). If the terms $(\nabla\phi)^2$ and $\nabla^2\phi$ are dropped in this equation, it takes the form of a standard equation describing front propagation in bistable media [45]. These terms, however, cannot be neglected because they lead to a significant renormalization of the front solutions. In the vicinity of a front, these terms can be determined as follows.

Assuming that the core is close to its stationary solution, the front velocities are very small. Therefore, the wave pattern adjusts to the instantaneous size of the core. The Cole-Hopf transformation (4.20) implies that the phase gradient $\nabla\phi$ and its derivative $\nabla^2\phi$ are given by

$$\nabla\phi = \frac{1+\alpha\beta}{(\beta-\alpha)Q}\nabla Q, \tag{4.27a}$$

$$\nabla^2\phi = \frac{1+\alpha\beta}{(\beta-\alpha)Q^2}[Q\nabla^2Q - (\nabla Q)^2]. \tag{4.27b}$$

As shown above, the distribution of Q_0 that corresponds to the asymptotic wave pattern [Eq. (4.22)] satisfies the equation

$$\lambda_0 Q_0 = \frac{\beta-\alpha}{1+\alpha\beta}[\omega + \alpha + (\alpha+\epsilon)z(x)]Q_0 + (1+\alpha\beta)\nabla^2 Q_0. \tag{4.28}$$

This equation can be used to express $\nabla^2 Q_0$ as a function of Q_0 and z, namely

$$\nabla^2 Q_0 = \kappa^2 Q_0 - \frac{(\alpha+\epsilon)(\beta-\alpha)}{(1+\alpha\beta)^2}[z(x) - z_{\text{out}}]Q_0. \tag{4.29}$$

On the other hand, the eigenfunction Q_0 of the rectangular potential well (4.15) and its derivative ∇Q_0 should be continuous at the well boundary, i.e. at $|x| = R$. Therefore, $\nabla Q_0 = -\kappa Q_0$ holds there. Thus, in the vicinity of the core boundary the phase gradient $\nabla\phi$ and its derivative $\nabla^2\phi$ are given by

$$\nabla\phi|_{\text{F}} = -k, \tag{4.30a}$$

$$\nabla^2\phi|_{\text{F}} = -\frac{\alpha+\epsilon}{1+\alpha\beta}[z_{\text{F}}(x) - z_{\text{out}}]. \tag{4.30b}$$

Note that the second derivative of the phase varies strongly within the core boundary. The subscript F indicates that $z_{\text{F}}(x)$ refers to the actual distribution of z close to the front and not to the approximative expression (4.15). Substituting Eqs. (4.30) into Eq. (4.14b), a closed equation is obtained that describes the slow motion of the fronts, namely

$$\tau\partial_t z_{\text{F}} = (\sigma - \gamma + \gamma k^2 - \gamma a z_{\text{out}}) + (1 - \gamma + \gamma a)z_{\text{F}} - \nu z_{\text{F}}^3 + l^2\nabla^2 z_{\text{F}}, \tag{4.31}$$

where $a = \beta(\alpha + \epsilon)(1 + \alpha\beta)^{-1}$. Equation (4.31) has the form of an equation for a bistable medium, but the coefficients are renormalized and depend on the wavenumber k of the emitted waves. The states of the medium on both sides of a front are given by the roots of the cubic equation

$$\nu z_{\mathrm{F}}^3 - (1 - \gamma + \gamma a)z_{\mathrm{F}} = \sigma - \gamma(1 + az_{\mathrm{out}} - k^2). \tag{4.32}$$

The smallest root of this equation corresponds to the value z_{out} of the variable z outside of the pacemaker core which depends on the wavenumber k.

The motion of the front that connects both stable states (*cf.* Ref. [45]) is determined by the roots of the cubic equation (4.32). Since there is no quadratic term for z in this equation, the sum of all three roots is zero and the front velocity V is determined by the middle root $z_{\mathrm{middle}}(k)$ of Eq. (4.32)

$$V(k) = -3\frac{l}{\tau}\sqrt{\frac{\nu}{2}}z_{\mathrm{middle}}(k). \tag{4.33}$$

The velocity V is a function of the wavenumber k and may vanish at a certain critical wavenumber k_0. In Fig. 4.4(b) a typical functional dependence is shown. It can be clearly seen that the velocity is positive for small values of k, corresponding to an expanding core, while the velocity is negative for large values of k, corresponding to a contracting core. A necessary condition for this behavior is that if $z_{\mathrm{middle}}(k < k_0) < 0$ (like the case studied here), $dz_{\mathrm{middle}}(k)/dk > 0$ should hold, which is fulfilled when $\gamma < 0$. This suggests that such self-organized pacemakers may have a stable stationary core. While expansion is present for small cores, large cores contract. This is indeed found and discussed further below.

On the other hand, the value of the variable z in the center of the core can be determined from the following arguments: Since the phase gradient $\nabla\phi$ vanishes at $x = 0$, Eq. (4.27b) there reduces to

$$\nabla^2\phi\,|_{x=0} = \frac{(1 + \alpha\beta)\nabla^2 Q}{(\beta - \alpha)Q}. \tag{4.34}$$

Using Eq. (4.29), the phase curvature at $x = 0$ is obtained as

$$\nabla^2\phi\,|_{x=0} = \frac{\beta - \alpha}{1 + \alpha\beta}k^2 - \frac{\alpha + \epsilon}{1 + \alpha\beta}(z_{\mathrm{center}} - z_{\mathrm{out}}), \tag{4.35}$$

where k is the wavenumber of the pattern outside the core. Substituting this expression into Eq. (4.14b) and using that $\nabla\phi = 0$ in the center of the core, it is found that the following equation holds at $x = 0$,

$$\tau\partial_t z = \sigma - \gamma - \gamma\left[\frac{\beta(\beta - \alpha)}{1 + \alpha\beta}k^2 - a(z_{\mathrm{center}} - z_{\mathrm{out}})\right] + (1 - \gamma)z - \nu z^3 + l^2\nabla^2 z. \tag{4.36}$$

Hence, the value z_{center} of the variable z in the center of the pacemaker is given by the largest root of the cubic equation

$$\nu z^3 - (1 - \gamma)z = \sigma - \gamma - \gamma \left[\frac{\beta(\beta - \alpha)}{1 + \alpha\beta} k^2 - a\left(z_{\text{center}} - z_{\text{out}}\right) \right]. \tag{4.37}$$

4.2.3 Stationary self-organized pacemakers

The results of the analysis in the two previous sections are now combined and the properties of self-organized pacemakers with stationary cores in a one-dimensional system are determined. The core boundaries of such pacemakers represent fronts whose velocity V is vanishing. According to Eq. (4.33), this implies that the middle root of Eq. (4.32) must be zero. Consequently, the wavenumber k_0 of the waves emitted by a stationary pacemaker must satisfy the equation

$$\sigma - \gamma + \gamma k_0^2 - \gamma a z_{\text{out}} = 0. \tag{4.38}$$

If $k = k_0$, the other two roots of the cubic equation (4.32) can easily be found as

$$z_{\text{out}} = -\sqrt{\frac{1 - \gamma(1 - a)}{\nu}}, \tag{4.39a}$$

$$z_{\text{in}} = +\sqrt{\frac{1 - \gamma(1 - a)}{\nu}}, \tag{4.39b}$$

with $a = \beta(\alpha + \epsilon)(1 + \alpha\beta)^{-1}$. Since z_{out} is now known, the wavenumber k_0 of the emitted waves can be determined from Eq. (4.38) as

$$k_0 = \sqrt{1 - \frac{\sigma}{\gamma} - a\sqrt{\frac{1 - \gamma(1 - a)}{\nu}}}. \tag{4.40}$$

Using Eq. (4.24), the frequency Ω_0 of generated waves is found as

$$\Omega_0 = \omega + \alpha - (\alpha + \epsilon)\sqrt{\frac{1 - \gamma(1 - a)}{\nu}} + (\beta - \alpha)k_0^2. \tag{4.41}$$

Finally, the core radius R_0 of a stationary pacemaker is determined by Eq. (4.25) as

$$R_0 = \frac{1 + \alpha\beta}{(\beta - \alpha)\sqrt{k_{\text{max}}^2 - k_0^2}} \tan^{-1}\left(\frac{k_0}{\sqrt{k_{\text{max}}^2 - k_0^2}}\right), \tag{4.42}$$

where $k_{\text{max}}^2 = (\alpha + \epsilon)(\beta - \alpha)^{-1}(z_{\text{center}} - z_{\text{out}})$ and z_{center} is given by the largest root of the cubic equation (4.37).

Analyzing the above results, it can be seen that the condition $\gamma(1 - a) < 1$ must be satisfied for a stationary pacemaker. Moreover, the wavenumber k_0 must not exceed $k_{\max}$, imposing additional restrictions on the model parameters, which are discussed further below.

In Fig. 4.5, the wavenumber k_0 of emitted waves, the radius R_0 of the pacemaker, and the pacemaker frequency Ω_0 are displayed as functions of the parameters γ, ϵ, and σ. These dependences are only shown within the intervals of the respective parameters where the pacemaker actually exists. It can be seen that large wavenumbers are always associated with high frequencies and large radii.

First, the dependences of k_0, R_0, and Ω_0 on σ are discussed in detail [Figs. 4.5(g-i)]. Then, the functional dependences of k_0, R_0, and Ω_0 on γ and ϵ are briefly considered.
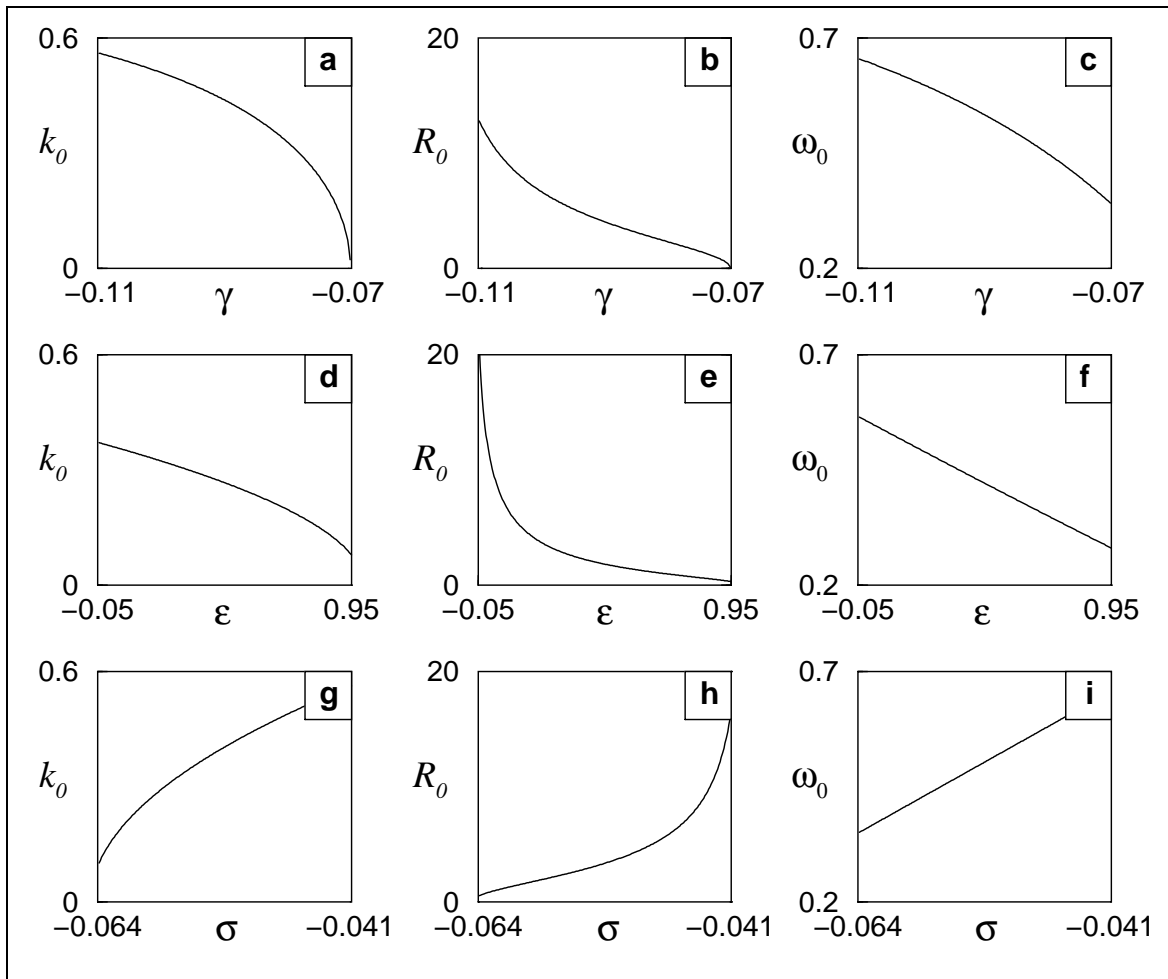

Figure 4.5: **Properties of self-organized pacemakers.** *The wavenumber k_0, the radius R_0, and the frequency ω_0 of a stationary pacemaker are shown as functions of the parameters γ, ϵ, and σ. The fixed parameters are $\omega = 0$, $\alpha = 0.5$, $\beta = 1.5$, and $\nu = 40$. If not varied, the other parameters are $\gamma = -0.075$, $\epsilon = 0.5$, and $\sigma = -0.06$.*

The wavenumber k_0 of the emitted waves can be written as

$$k_0 = \sqrt{\frac{\sigma_c - \sigma}{\gamma}}, \tag{4.43}$$

where

$$\sigma_c = \gamma - \gamma a \sqrt{\frac{1 - \gamma(1-a)}{\nu}}. \tag{4.44}$$

Note that pacemakers are found for $\sigma < \sigma_c$ if $\gamma > 0$ and for $\sigma > \sigma_c$ if $\gamma < 0$. In Figs. 4.5(g-i) the latter case is shown. Near $\sigma = \sigma_c$, i.e. for small σ, the value z_{center} in the center of the pacemaker is approximately given by

$$z_{center} \approx \sqrt{\frac{1 - \gamma(1-a)}{\nu}}. \tag{4.45}$$

In the limit $\sigma \to \sigma_c$, self-organized pacemakers have small cores [Fig. 4.5(h)], with a radius R_0 given by

$$R_0 \approx \frac{(1 + \alpha\beta) k_0}{(\beta - \alpha)k_{max}^2}. \tag{4.46}$$

The frequency Ω_0 of emitted waves is

$$\Omega_0 \approx \omega_1 + (\beta - \alpha) k_0^2, \tag{4.47}$$

where ω_1 is the frequency of the slow uniform oscillations, $\omega_1 = \omega + \alpha + (\alpha + \epsilon)z_1$. This is seen in Fig. 4.5(i) for small values of σ.

On the left border of the existence interval (at $\sigma = \sigma_c$), the radius R_0 of the core goes to zero, whereas the core size diverges on the right border (where $k_0 \to k_{max}$).

As σ departs from σ_c, the radius R_0 increases [Fig. 4.5(h)]. As seen from Eq. (4.42), the width of the pacemaker diverges when $k_0 \to k_{max}$. Rewriting Eq. (4.37) as

$$\nu z^3 - (1 - \gamma)z = \sigma - \gamma - \frac{\gamma\beta(\beta - \alpha)}{1 + \alpha\beta}(k_0^2 - k_{max}^2), \tag{4.48}$$

it is evident that for $k_0 \to k_{max}$, Eq. (4.37) reduces to Eq. (4.9), which determines the values of z in the uniform oscillatory states. Consequently, when $k_0 \to k_{max}$, the value z_{center} of the variable z in the center of the pacemaker is close to z_3, and the frequency Ω_0 of the emitted waves satisfies

$$\Omega_0 \approx \omega_3 - (\beta - \alpha)(k_{max}^2 - k_0^2), \tag{4.49}$$

where $\omega_3 = \omega + \alpha + (\alpha + \epsilon)z_3$.

Therefore, it follows that $\omega_1 < \Omega_0 < \omega_3$. When the radius R_0 becomes very large, i.e. $R_0 \to \infty$ and $k_0 \to k_{\max}$, the frequency Ω_0 approaches the frequency ω_3 of rapid uniform oscillations. On the other hand, when the core is small, k_0 is also small and the frequency Ω_0 is close to ω_1.

Equation (4.43) shows that the coupling parameter γ and the imperfection parameter σ must be of the same order of magnitude and have opposite effects on the dynamics: As σ is increased, k_0 and the other quantities also increase, while as γ increases, k_0 and the other quantities decrease. The larger the modulus $|\gamma|$ of the coupling parameter, the larger the stationary values of the wavenumber, radius, and frequency [Figs. 4.5(a-c)]. Obviously, the limits of large and small cores could also be discussed in terms of a critical value γ_c. However, this is omitted here because no fundamental new information is obtained by such an analysis.

The effect of an increased frequency shift ϵ is displayed in Figs. 4.5(d-f). The larger the frequency shift, the smaller the stationary values of the wavenumber, radius, and frequency. However, the wavenumber decreases slowly, i.e. for large values of ϵ small cores already emit waves with a relatively large wavenumber.

Now, the necessary assumptions which had to be made to derive the analytical solution of self-organized pacemakers [Eqs. (4.40), (4.41), and (4.42)] are examined.

As already pointed out, the amplitude equations (4.5) did not include the two terms proportional to Az^2 and $|A|^2z$ in the normal form (4.1), which is justified if $\nu \gg 1$. In addition, the phase gradients must be small ($|\nabla\phi| \ll 1$) in order to use the phase dynamics approximation (4.13). Since $\nabla\phi = -k$, this implies that the wavenumber k_0 of the emitted waves should be small, $|k_0| \ll 1$. As follows from the above analysis, $|k_0| < |k_{\max}|$ and $k_{\max} \propto \nu^{-1/4}$. Hence, $\nu^{1/4} \gg 1$ should hold.

In Eq. (4.14a) of the phase dynamics approximation, two terms proportional to $\nabla^2 z$ and ∇z have been neglected, which is justified if $|(\beta/2)\nabla^2 z| \ll |(\alpha + \epsilon)z|$ and $|\nabla z \nabla\phi| \ll |(\beta - \alpha)(\nabla\phi)^2|$. If the parameters α, β, and ϵ are of order unity (as assumed always), this implies that $|\nabla^2 z| \ll |z|$ and $|\nabla z| \ll |\nabla\phi|$. The gradients of the variable z are significant only within the boundaries of the core which represent standing fronts of width l. Hence, the condition $|\nabla^2 z| \ll |z|$ implies that $l \gg 1$. The other condition $|\nabla z| \ll |\nabla\phi|$ is then satisfied automatically (provided that $\nu^{1/4}$ is large).

On the other hand, the approximate analysis is valid only when the radius R_0 and the

wavelength $2\pi/k_0$ are much larger than the front width l. If the estimate (4.46) of the core size for small cores is used, it follows that $R_0 \approx \nu^{1/4}$. Therefore, $R_0 \gg l$ implies that $l \ll \nu^{1/4}$, which also follows from the requirement that $k_0 l \ll 1$. Combining all separate requirements, finally the condition

$$\nu^{1/4} \gg l \gg 1 \tag{4.50}$$

is obtained.

According to Eq. (4.46), pacemakers with vanishingly small core sizes R_0 are expected in the limit $\sigma \to \sigma_{\rm c}$. However, it must be recalled that the approximate analysis is only applicable if the radius R_0 is larger than the front width l. This means that σ should not be too close to $\sigma_{\rm c}$. In other words, $\sqrt{(\sigma_{\rm c} - \sigma)/\gamma} \gg l\nu^{-1/2}$ must hold.

The distribution of z inside the core was assumed to be flat, i.e. $z = z_{\rm center}$ for $|x| \leq R$ and not only in the center ($x = 0$). To check this approximation, the value of $z_{\rm center}$, given by the largest root of the cubic equation (4.48), is compared with the value $z_{\rm in}$ given by Eq. (4.39b), which describes the variable z at the inner side of the front. This flat distribution is justified if $|z_{\rm center} - z_{\rm in}| \ll |z_{\rm in}|$. As follows from Eq. (4.45), this condition is indeed valid for pacemakers with small cores ($k_0 \ll k_{\rm max}$). It becomes less accurate for pacemakers with larger cores, where k_0 approaches $k_{\rm max}$. In this case, the results of the above analytical derivation provide only a qualitative description.

In Sec. 4.2.1, the wavenumber of waves emitted by a pacemaker has been calculated assuming a quasi-stationary core. This is justified when the relaxation time for radial perturbations of the core is large compared to the characteristic time needed for the wave pattern to adjust to the core size. It can be expected that this is true when the dynamics of the variable z is slow compared to the characteristic time scale for the evolution of the wave pattern, i.e. when $\tau \gg 1$. The stability of self-organized pacemakers is investigated by means of numerical simulations in the next section.

The derivation of the pacemaker solution has been performed above assuming that the conditions $\beta - \alpha > 0$ and $\alpha + \epsilon > 0$ are fulfilled, implying that the variable z is increased inside the core. Now, it shall be discussed how the solution is modified in the other possible cases.

If $\beta - \alpha > 0$ and $\alpha + \epsilon < 0$, the variable z is decreased inside the core. Then, the right-hand sides of the expressions (4.39) for $z_{\rm out}$ and $z_{\rm in}$ are interchanged and Eqs. (4.40) and (4.41) for the wavenumber and the frequency must be modified accordingly. In this case, the value $z_{\rm center}$ is negative and given by the smallest root of Eq. (4.37).

When the dispersion is negative ($\beta - \alpha < 0$), the expression (4.42) for R_0 must be modified by replacing $\beta - \alpha$ by $\alpha - \beta$. If $\alpha + \epsilon > 0$, the variable z is decreased inside the core. To obtain final results in this case, the expressions (4.39) for z_{out} and z_{in} must be interchanged and the equations for the wavenumber and frequency [Eqs. (4.40,4.41)] must be modified respectively. Note that z_{center} is then given by the smallest root of Eq. (4.37). Finally, when $\alpha + \epsilon < 0$, the variable is increased inside the core. Aside from the already mentioned replacement of $\beta - \alpha$ by $\alpha - \beta$, no other modifications of the results are necessary. Recall that in the case of negative dispersion the waves which form the target pattern are traveling toward the core (*cf.* Chapter 3).

4.2.4 Drift induced by a parameter gradient

Self-organized pacemakers are not pinned and their positions are determined by the initial conditions only. Such self-organized structures are therefore able to move through the medium if its properties are not uniform. Suppose that one of the parameters of the model, for example γ, is not constant, but varies in space as $\gamma = \gamma(x)$. The variation of this parameter shall be so smooth that its change on a distance equal to the radius R_0 of the core is small. In this case, the velocity of the drift induced by the parameter gradient can be estimated by applying linear perturbation theory.

A stationary pacemaker forms in the zeroth-order approximation with respect to the parameter gradient. For convenience, its spatial position is chosen as the origin of the coordinate x, so that it is $\gamma(x) \approx \gamma_0 + \chi x$ in the vicinity of the center. As already noted, the boundaries of the core represent two fronts whose motion is described by Eq. (4.31). The velocity V of a front is determined by the middle root z_{middle} of the cubic polynomial (4.32), that is

$$V = -3\frac{l}{\tau}\sqrt{\frac{\nu}{2}} z_{\mathrm{middle}}(k). \tag{4.51}$$

The front velocity V and middle root z_{middle} are functions of the parameters and the wavenumber k of the emitted waves. For a stationary pacemaker, the core neither expands nor shrinks, and its boundaries must therefore represent standing fronts ($V = 0$). This condition fixes the wavenumber k_0 of the waves emitted by a stationary pacemaker. If the parameters are allowed to vary a little in space, the velocities of the two fronts, representing the left and right boundaries of the core, will be slightly different and do not vanish. As a result, the pacemaker slowly drifts in space.

For sufficiently small gradients, the front velocity is given by

$$V(\gamma(x)) \approx \left.\frac{\partial V}{\partial \gamma}\right|_{\gamma_0} \frac{\partial \gamma}{\partial x} x = V'(\gamma_0)\chi x, \tag{4.52}$$

where it must be taken into account that $V(\gamma_0) = 0$ for a stationary pacemaker with wavenumber k_0. Hence, the velocities of the left and right fronts are

$$V(\gamma(x = \pm R_0)) \approx \pm \chi R_0 V'(\gamma_0). \tag{4.53}$$

Therefore, these two fronts move with the same small absolute velocity, but in opposite directions with respect to the center of the pattern: One of them moves toward the center, whereas the other moves away from it. This means that the core is then drifting rigidly with the velocity

$$V_{\mathrm{D}} = -3\frac{l}{\tau}\sqrt{\frac{\nu}{2}}\chi R_0 z'_{\mathrm{middle}}(\gamma_0). \tag{4.54}$$

When the middle root z_{middle} of Eq. (4.32) is small, it can be estimated as

$$z_{\mathrm{middle}} = \frac{\gamma(1 + az_{\mathrm{out}} - k^2) - \sigma}{1 - \gamma + \gamma a}. \tag{4.55}$$

To determine the derivative of z_{middle} with respect to γ at $\gamma = \gamma_0$, it must be taken into account that the coefficient a is independent of γ and that to zeroth-order approximation, the values of z_{out} and k are given by Eqs. (4.39a) and (4.40) with $\gamma = \gamma_0$. The derivative $z'_{\mathrm{middle}}(\gamma_0)$ is then determined as

$$z'_{\mathrm{middle}}(\gamma_0) = \frac{1 + az_{\mathrm{out}} - k_0^2 + \sigma(a - 1)}{(1 - \gamma_0 + \gamma_0 a)^2}. \tag{4.56}$$

Using Eqs. (4.40), (4.51), and (4.54), the drift velocity finally is given by

$$V_{\mathrm{D}} = -3\frac{l}{\tau}\sqrt{\frac{\nu}{2}}\frac{\sigma \chi R_0}{\gamma_0(1 - \gamma_0 + \gamma_0 a)}. \tag{4.57}$$

Thus, the drift velocity is proportional to the gradient χ of the parameter γ.

The above analysis refers to the case when the variable z is increased inside the core. Obviously, the drift direction is reversed if the variable z is decreased inside the core region.

4.3   Numerical investigations

To check the existence of self-organized pacemakers, numerical simulations are performed in one- and two-dimensional systems. The instabilities of these patterns and the effects of global inhibition are also numerically investigated.

Equations (4.5) are integrated with an explicit Euler scheme where the Laplacian operator is discretized with a nearest-neighbor (*Five-point Laplacian*) approximation (see Appendix A.4). The numerical accuracy has been tested by repeating several simulations using a fourth-order explicit Runge-Kutta scheme and a stiff implicit Gear method. No significant differences are detected. No-flux boundary conditions are used. In the simulations, it is not possible to strictly satisfy the conditions (4.50) for the parameters of the model. Therefore, only the existence of stable self-organized pacemakers in one- and two-dimensional systems is confirmed, but without verifying the constructed analytical solutions quantitatively.

4.3.1   Stable pacemakers and their drift

In a distributed system with birhythmic dynamics, the two states associated with uniform oscillations with different frequencies represent two attractors. Moreover, stable self-organized pacemakers should also correspond to a certain attractor in the distributed dynamical system described by Eqs. (4.5). The coexistence of several attractors implies that the final state of the system may strongly depend on the initial conditions. When the conditions $\beta - \alpha > 0$ and $\alpha + \epsilon > 0$ are satisfied, a pacemaker can be created by starting from the uniform low-frequency oscillatory state and applying a sufficiently strong local perturbation of the variable z (increasing the variable z from z_1 close to z_3 inside a region of a certain radius R). Note that the basin of attraction for the pacemakers with small cores can be small, and only perturbations with a radius close to the stationary value R_0 of the core will therefore converge to the pacemaker solution.

Figure 4.6 shows the development of a pacemaker from a sufficiently large initial perturbation (a,b) and its asymptotic profile (c) in the one-dimensional system. It can be seen that the perturbation starts to expand and emit waves. The expansion speed decreases until the expansion finally terminates and a stationary core, emitting waves with a constant wavenumber, is formed. Snapshots of the spatial distributions of the real part ReA of the complex oscillatory amplitude A, the modulus $|A|$, and z for a stable stationary pacemaker are shown in Fig. 4.6(c).
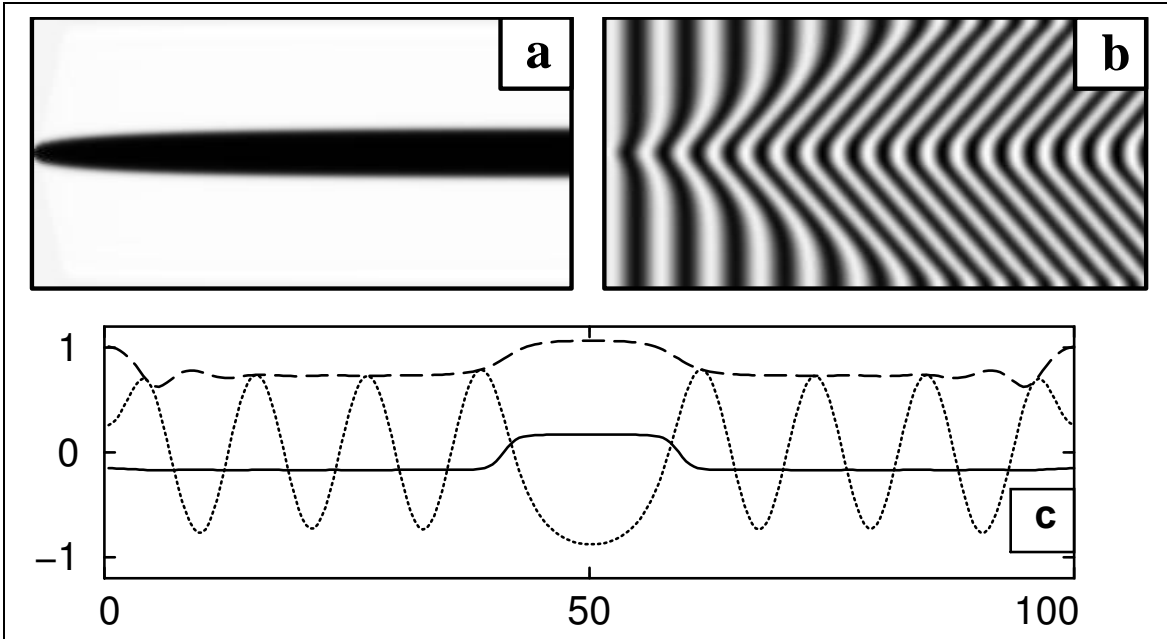
Figure 4.6: **Development of a stable stationary pacemaker (a,b) and its asymptotic profile (c).** *Frame (a) shows the evolution of the amplitude of the real mode z after an initial perturbation, whereas frame (b) displays the corresponding evolution of ReA. The system size is $L = 100$ and the displayed time interval is $\Delta t = 2000$ for z and $\Delta t = 200$ for ReA. In the space-time diagrams (a,b), time runs along the horizontal axis. In the gray scale representation used in this space-time diagram, dark regions correspond to large values of the displayed variables. In frame (c), the spatial distributions of the variables z (solid line), ReA (dotted line) and $|A|$ (dashed line) are presented. The parameters are $\alpha = 0.5$, $\beta = 1.5$, $\epsilon = 0.5$, $l = 1$, $\tau = 1$, $\nu = 40$, $\gamma = -0.075$, and $\sigma = -0.06$.*

If the conditions $\beta - \alpha > 0$ and $\alpha + \epsilon < 0$ are satisfied instead, the variable z is decreased inside the core and the initial perturbation must therefore be modified accordingly. This case is realized in the simulation for the two-dimensional medium shown in Fig. 4.7. The gray scale representation for the variable z is inverted, so that smaller values of z correspond to the darker areas here.

It has been shown in Sec. 4.2.4 that drifting pacemakers are expected when spatial parameter gradients are present. Figure 4.8 displays a simulation confirming this effect. The simulation is initiated with a stable stationary pacemaker. A constant gradient in the parameter γ is then introduced and the pacemaker starts to drift through the medium in the direction of increasing γ. When the gradient is removed, the motion of the pacemaker is terminated and a stationary pacemaker is recovered at a new position, as seen in Fig. 4.8(a). Emission and propagation of waves persist during the drift [Fig. 4.8(b)]. Note that the drift velocity is much smaller than the phase velocity of the waves.
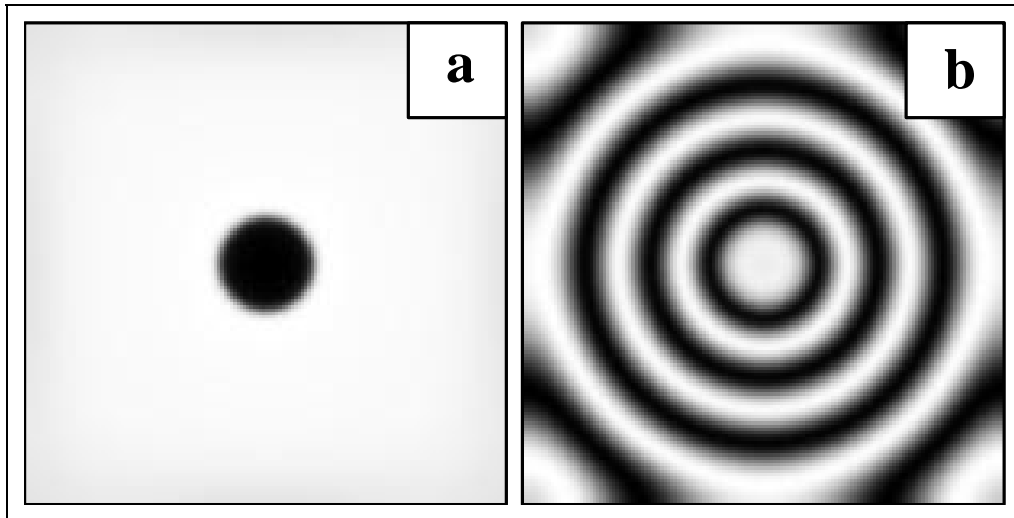
Figure 4.7: **Two-dimensional stable stationary pacemaker.** *The spatial distributions of variables z (a) and ReA (b) are displayed. The system size is $L_x = L_y = 120$; the parameters are $\alpha = -1.0$, $\beta = -0.5$, $\epsilon = 0.5$, $l = 1$, $\tau = 3$, $\nu = 40$, $\gamma = 0.20$, and $\sigma = 0.16$. The gray scale representation for the variable z is inverted here for esthetic reasons (small values of z correspond to the dark regions).*
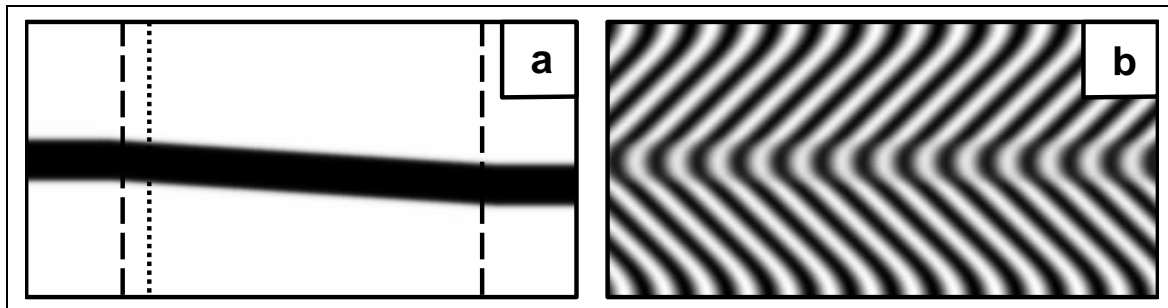

Figure 4.8: **Drift of a pacemaker.** *The spatial gradient of the parameter γ is applied inside the time interval indicated by the vertical dashed lines in frame (a), which shows the evolution of z in the time interval $\Delta t = 200000$. The pacemaker drifts in the direction of increasing γ. Frame (b) displays the drifting wave pattern within a narrow time interval $\Delta t = 500$ during the drift, marked by the dotted vertical line in frame (a). Small values of z correspond to the dark regions. The parameters are $\alpha = 1.38$, $\beta = 2.3$, $\epsilon = -3.18$, $l = 0.8$, $\tau = 2$, $\nu = 83$, $\gamma_0 = 5.59 \cdot 10^{-4}$, $\chi = 1.68 \cdot 10^{-6}$, and $\sigma = 3.4 \cdot 10^{-4}$.*

4.3.2 Global inhibition

In oscillatory media with positive dispersion, wave sources with a higher frequency suppress all less rapid sources. Therefore, the competition between usual pacemakers in heterogeneous media is always won by the most rapid pacemaker which suppresses all others (except the cases where phase slips take place, see Section 3.2). If two pacemakers have exactly the same frequency, they should coexist indefinitely. Since the frequencies of all self-organized

pacemakers in the same birhythmic medium are equal (they are uniquely determined by the parameters of the system), this suggests that such pacemakers must always coexist. The numerical simulations reveal, however, that the actual behavior is more complex.

To investigate interactions between pacemakers, a series of two-dimensional simulations is performed. In these simulations, a single pacemaker is created first. After its wave pattern has spread over the entire medium and the core has reached its stationary radius, another core is initiated by applying a strong local perturbation of z at some distance from the center of the pacemaker. Without the presence of the pacemaker, the new perturbation would evolve into a stationary pacemaker. A typical evolution, observed for a sufficiently large separation between the pacemaker and the new perturbation, is shown in Fig. 4.9. The perturbation creates a core (a) which starts to grow (b). However, at the same time, the core slowly drifts toward the pacemaker that remains immobile (c,d). Eventually, the two cores meet and fuse. Immediately after the fusion, the resulting pacemaker has a core which is larger than that of a stationary pacemaker and which does not have a circular shape. Subsequently, the core shrinks back to the size corresponding to a stable stationary pacemaker (d). A space-time diagram showing the evolution of the spatial distribution of z along the central vertical cross section of the medium is presented in Fig. 4.9(i). In Figs. 4.9(e-h) four snapshots of the wave patterns during this process are displayed. Note that the second core is not able to emit its own waves, but only modifies the wave pattern generated by the pacemaker. Therefore, that core effectively represents a suppressed pacemaker.

The development of the system is different for smaller spatial separations or weaker perturbations. Although the second perturbation would still be large enough to create a pacemaker in the absence of another core, it is immediately suppressed and does not give rise to a growing core. In Fig. 4.10, it is shown how the size of a small perturbation and the distance from a stationary pacemaker determine whether fusion (Fig. 4.9) or immediate suppression takes place. Note that for very small initial separations, the cores interact directly without mediation of the wave pattern, and fusion is observed.

This behavior can be characterized as *global inhibition*: If a pacemaker has developed and its wave pattern has covered the whole medium, the formation of further pacemakers becomes impossible in the entire medium. Perturbations which otherwise would be sufficient to create a pacemaker are either damped immediately or give rise to localized perturbations which then drift toward the dominant pacemaker and finally fuse with it.

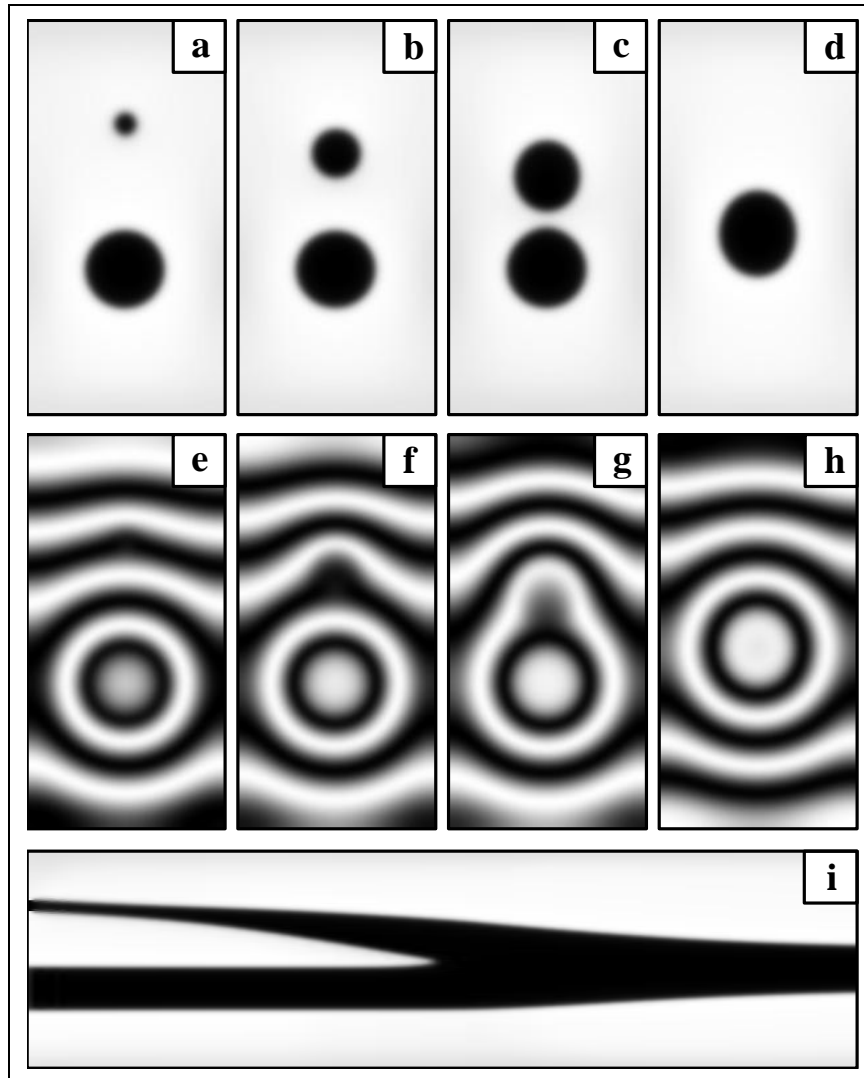The situation is different if the second perturbation is applied to a region which has not

Figure 4.9: **Interaction of cores.** *A stationary pacemaker interacts with another perturbation, leading to the fusion of the respective cores and global inhibition of other pacemakers. Snapshots of z are shown in frames (a-d), snapshots of ReA in frames (e-h). The displayed time moments are $t = 100$ (a,e), $t = 500$ (b,f), $t = 700$ (c,g), and $t = 1500$ (d,h). In frame (i) a space-time diagram of z for a cross section through the centers of the two cores is shown for the time interval $\Delta t = 2000$. The parameters are $L_x = 60$, $L_y = 120$, $\alpha = -1$, $\beta = -0.5$, $\epsilon = 0.5$, $l = 1$, $\tau = 9$, $\nu = 40$, $\gamma = 0.2$, and $\sigma = 0.16$. Small values of z correspond to the dark regions.*

yet been reached by the spreading wave pattern of the first pacemaker. In this case, the second pacemaker stabilizes and develops its own pattern of emitted waves, which eventually leads to the formation of a state of coexistence between the two pacemakers. In general, this occurs when the time interval between two subsequent perturbations (which are well separated in space) is relatively short.
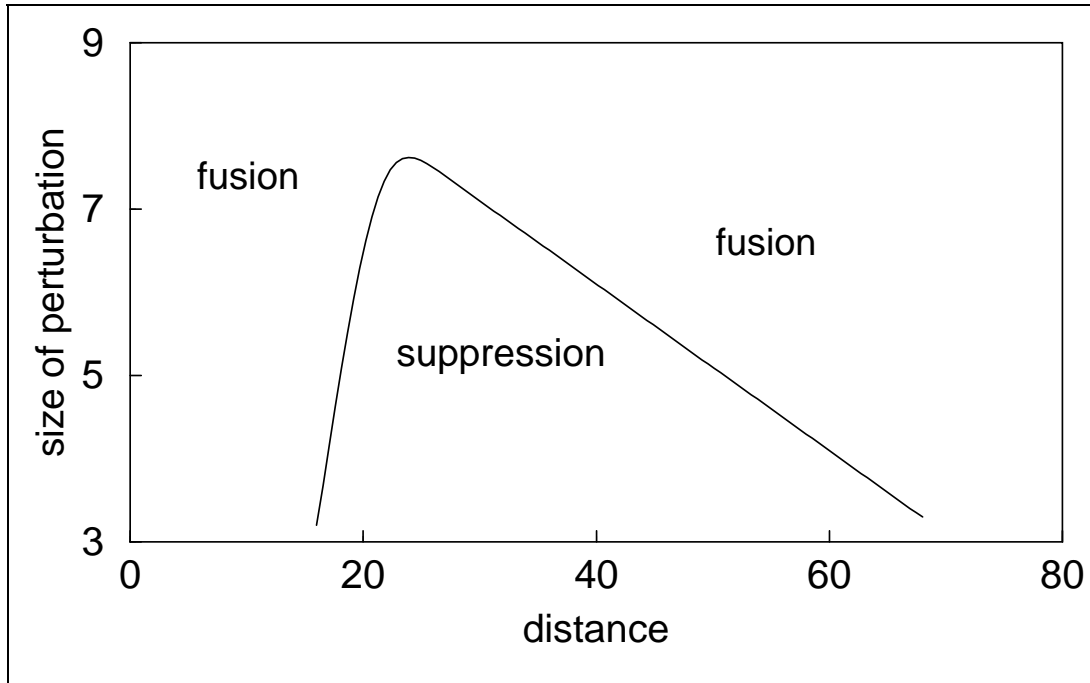
Figure 4.10: **Global inhibition.** *Regions of different behavior for two interacting cores in the two-dimensional system. The initial condition consists of a perturbation of a specified size located at a given distance from a stable self-organized pacemaker already present in the system. The parameters are the same as in Fig. 4.9.*

4.3.3   Instabilities of self-organized pacemakers

The stability of pacemakers is significantly affected by the ratio τ of the two characteristic times in the model equations (4.5). It has been shown in Sec. 4.3.1 that the cores are stable with respect to radial perturbations if the variable z is slow compared to the complex amplitude A of the oscillatory mode, i.e. if the ratio τ is relatively large. When $\tau = 1$ (Fig. 4.6), the transient leading to the stable pacemaker is monotonous. However, when τ is decreased, the transient ceases to be monotonous. The radius R of the core does not grow until its stationary value R_0 is reached, but first increases and then finally decreases to R_0. When τ is decreased further, damped oscillations of the core are observed. At still smaller τ, these oscillations become sustained and pacemakers with breathing cores are found, as shown in Figs. 4.11(a,b). This breathing behavior resembles breathing known for localized spot patterns in activator-inhibitor systems [166]. Swinging pacemakers are also observed in the simulations [Figs. 4.11(c,d)]. In this case, the radius of the core remains approximately constant whereas the position of the pacemaker oscillates in space. A decrease of τ for breathing pacemakers results in an increasing amplitude of core oscillations which become strongly anharmonic. For even lower values of τ, the core oscillations are so large that they either lead
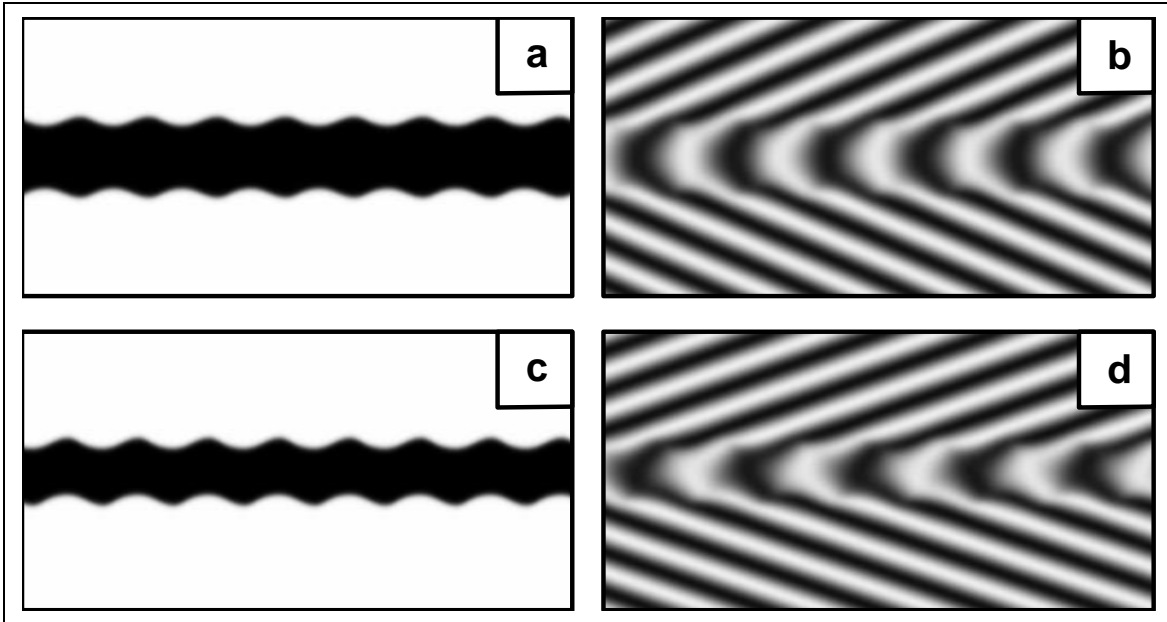
Figure 4.11: **Breathing (a-b) and swinging (c-d) pacemakers.** *Frames (a,c) show the evolution of z and frames (b,d) the corresponding evolution of ReA. The displayed coordinate and time intervals are $\Delta L = 100$, $\Delta t = 250$. In frames (a-b) $\beta = 3.0$ and in frames (c-d) $\beta = 2.65$. The other parameters are $L = 200$, $\alpha = 1.38$, $\epsilon = -3.18$, $l = 0.8$, $\tau = 0.001$, $\nu = 83$, $\gamma = 5.59 \cdot 10^{-4}$, $\sigma = 3.4 \cdot 10^{-4}$. Small values of z correspond to the dark regions.*

to a collapse and disappearance of the pacemaker, or result in a rapid expansion of the core until the whole medium is transformed into the other uniform oscillatory state. Which of the two possibilities is realized strongly depends on the initial conditions. Breathing pacemakers are also found in two-dimensional simulations. Figure 4.12 shows space-time diagrams along a cross section through the center of the medium. Breathing motion is clearly seen in
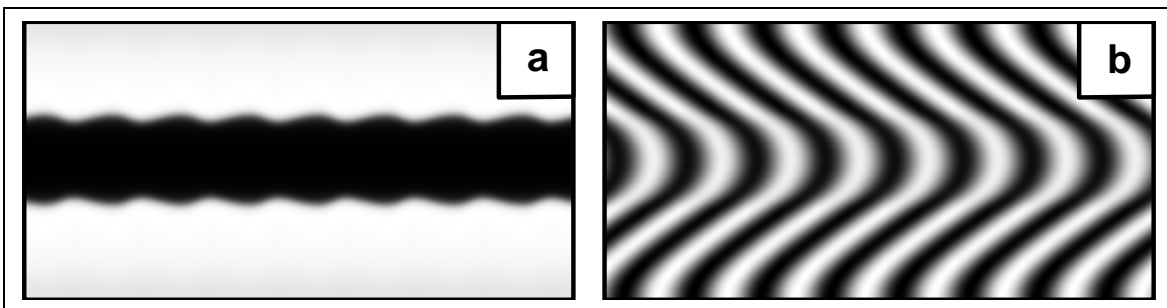

Figure 4.12: **Breathing pacemaker in two spatial dimensions.** *Space-time diagrams for a cross section through the center of the core are shown. The evolution of z is shown in (a), the one of ReA in (b). The system size is $L_x = L_y = 80$; the parameters are $\alpha = -1.0$, $\beta = -0.4$, $\epsilon = 0.5$, $l = 1$, $\tau = 0.075$, $\nu = 40$, $\gamma = 0.20$, and $\sigma = 0.16$. The displayed time interval is $\Delta t = 50$. Small values of z correspond to the dark regions.*

the diagram for z. Note that the simulation has been performed for a completely different set of parameters, indicating that the phenomenon is not restricted to a single small parameter regime.

Another mechanism leading to the destabilization of a pacemaker and the expansion of its core involves phase slips. Phase slips have been discussed in detail in Sec. 3.2. There, they appear as a result of a heterogeneous pacemaker close to the Hopf bifurcation. A similar effect can be expected for self-organized pacemakers in birhythmic media. The change of the oscillation frequency inside the core, however, is no longer determined by a fixed inhomogeneity, but by a local increase of the variable z. When phase slips are generated, this may have an effect on z and on the dynamics of the core itself. Numerical simulations show that the generation of phase slips may cause the core to destabilize. An example of this instability is displayed in Fig. 4.13. The oscillations inside the core are more rapid than in the
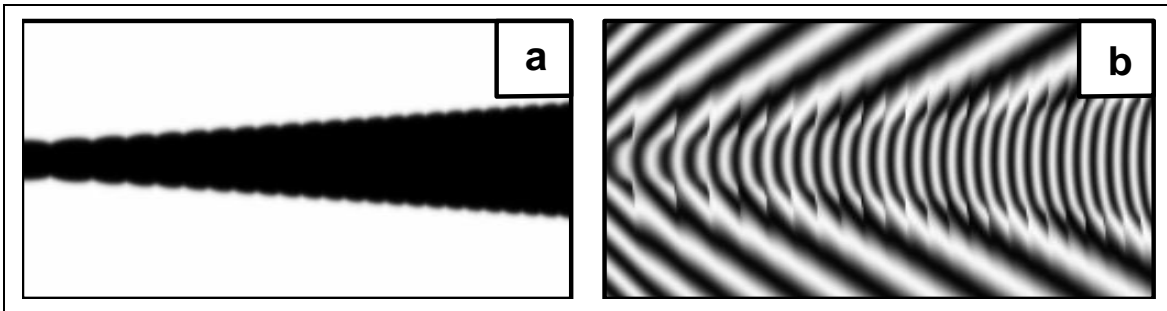

Figure 4.13: **Destabilization of a pacemaker by phase slips.** *The evolution of z is shown in (a), the one of $\mathrm{Re}A$ in (b). The displayed space and time intervals are $\Delta L = 100$ and $\Delta t = 625$. The parameters are $L = 100$, $\alpha = 1.38$, $\beta = 2.1$, $\epsilon = -3.18$, $\lambda = 0.8$, $\tau = 0.025$, $\nu = 83$, $\gamma = 5.59 \cdot 10^{-4}$, and $\sigma = 3.4 \cdot 10^{-4}$. Small values of z correspond to the dark regions.*

periphery and the zone where phase slips occur is located very close to the core boundary. Only some of these internal oscillations are able to emit waves [Fig. 4.13(b)]. Just like for the phase slips discussed in Sec. 3.2, the appearance of phase slips is associated with amplitude defects where $|A| = 0$, and therefore not shown here. Here, the phase slips occur so close to the core that the feedback loop that controls the front velocity is interrupted. The front effectively experiences a smaller wavenumber than that which corresponds to its radius. Therefore, the generation of phase slips is accompanied by the gradual growth of the core [Fig. 4.13(a)], which proceeds until the whole medium is dominated by the uniform state with the largest oscillation frequency.

Note that the width of the expanding core is weakly modulated: Just before the occurrence of a phase slip, the local wavenumber strongly increases, leading to a slight retreat of

the two core fronts. After the appearance of the phase slip, the local wavenumber decreases, implying that the core fronts move outward, giving rise to a core expansion. The expansion prevails over the contraction, and the net effect is a slow growth of the core.

4.4 Discussion

The principal result of this chapter is that self-organized pacemakers represent a generic wave pattern in oscillatory media near the soft onset of birhythmicity described by a supercritical pitchfork-Hopf bifurcation. The physical mechanism responsible for the stabilization of pacemakers in the considered system involves a long-range negative feedback, similar to the one necessary for the formation of stable localized spots in reaction-diffusion models with fast inhibitor diffusion [33]. An infinite-range inhibition, however, is caused here not by diffusion, but by the undamped propagation of waves emitted from the core region.

A solution for self-organized pacemakers in the vicinity of a pitchfork-Hopf bifurcation has been constructed analytically. Furthermore, the frequency and wavenumber of the waves emitted by a stationary self-organized pacemaker, and the size of its core, have been estimated. The analysis invokes arguments of the singular perturbation theory as strong separation of time and length scales have been assumed. The drift of self-organized pacemakers due to spatial parameter gradients has been predicted and the drift velocity has been estimated. The effect of the pacemaker drift in systems with spatial parameter gradients provides a convenient experimental method to identify self-organized pacemakers and distinguish them from target patterns caused by localized fixed heterogeneities in the medium. The numerical investigations have confirmed the existence of self-organized pacemakers and have shown that they are stable for a range of model parameters. Interactions between the pacemakers have been considered. Instabilities of pacemakers, leading to to their breathing, swinging, and expansion, have been numerically found. Breathing localized patterns were described long ago by Koga and Kuramoto [166] and have been found experimentally (e.g. [167]). Breathing and swinging behavior of spot patterns was investigated in detail for a three-component reaction-diffusion model by Suzuki *et al.* [168] and for two- and three-component models by Woesler *et al.* [169]. No analytical investigations have been done here for the pitchfork-Hopf model but it is expected that at the onset of breathing or swinging behavior the front solution undergoes a Hopf bifurcation. Note that swinging behavior is also denoted as *wiggling* or *rocking* in the literature.

Formally, the pitchfork-Hopf bifurcation as discussed here is a codimension-three bifurcation since three bifurcation parameters η_1^τ, η_2, and η_3 have been discussed. In the literature, bifurcations of high codimension are often considered as being difficult to observe in real systems. However, in complex chemical reaction-diffusion systems a codimension-one pitchfork bifurcation is less likely than a codimension-two imperfect pitchfork (or cusp) bifurcation. A perfect pitchfork bifurcation requires the presence of a special symmetry of the system. Furthermore, in a three-component system it seems not very probable that two stable limit cycles which have bifurcated from a fixed point are actually lying in a two-dimensional subspace of the phase space. These arguments lead to the conclusion that the bifurcation scenario discussed here may be actually found in reaction-diffusion systems.

Since the analysis is based on general amplitude equations, it is valid for any reaction-diffusion system near the soft onset of birhythmicity with small-amplitude limit cycles. As in the case of Hopf and Turing-Hopf bifurcations, it can be expected that the results of such an analysis based on amplitude equations would remain (at least, qualitatively) applicable even at larger distances from the bifurcation point, where amplitude equations are no longer strictly valid.

The model and the constructed solution of stable self-organized pacemakers is similar to a derivation performed for a different model [61]. However, that system has been introduced phenomenologically and does not represent a normal form. Moreover, uniform oscillations were unstable in that system and birhythmicity was absent. Nevertheless, extensive simulations performed for that model also display many of the patterns discussed here, such as stable self-organized pacemakers, drifting pacemakers, fusion, the suppression of cores, and phase slip patterns [170].

Aside from stable self-organized pacemakers, the amplitude equations for an oscillatory medium close to the onset of birhythmicity also give rise to other novel solutions, for example bistability of spirals: If the system is in one of its stable uniform states, with the distribution of z being approximately uniform, a spiral solution may exist and be stable. Since the amplitude of the oscillations drops down to zero in the core of the spiral and approaches a constant non-zero value far fromn the core, the distribution of z will not be strictly uniform. It is therefore possible that the core triggers transitions from one (metastable) state to the stable state mediated by fronts of z. If two spiral solutions associated with different values of z are present, the spirals have different frequencies and may compete. Future work may investigate such patterns in detail.

Not much seems to be known about the specific spatio-temporal dynamics of birhythmic media. To the author's knowledge, there is a publication on wave propagation in a model that displays birhythmicity [158]. However, the results presented in that paper were found for a parameter regime where birhythmicity was actually absent. The present work seems to report the first specific results on pattern formation in birhythmic systems.

Chapter 5

Self-organized pacemakers in excitable media

In this chapter, a three-component reaction-diffusion system is considered which shows self-organized pacemakers as stable solutions in the excitable regime. The model is an extension of the FitzHugh-Nagumo model presented in Sec. 2.4.

The chapter is organized as follows: After introducing the model in Sec. 5.1, the formation of stable self-organized pacemakers in the excitable regime is explained and demonstrated by simulations (Sec. 5.2). Unstable pacemakers are subsequently considered in Sec. 5.3. The chapter ends with a discussion of the obtained results (Sec. 5.4).

The results of the simulations have been discussed with Tsyoshi Mizuguchi and Yoshiki Kuramoto, who triggered the investigation of this model.

5.1 The model

This section introduces the model and discusses its basic properties. The model considered in this chapter is given by three coupled partial differential equations

$$\tau_u \partial_t u = u - u^3 - v + \kappa_u(s - u) + l_u^2 \nabla^2 u, \tag{5.1a}$$

$$\tau_v \partial_t v = \alpha u + \beta - v - \kappa_v(s - u) + l_v^2 \nabla^2 v, \tag{5.1b}$$

$$\tau_s \partial_t s = u - s + l_s^2 \nabla^2 s, \tag{5.1c}$$

which describe the evolution of three variables u, v, and s in a spatially extended system. The parameters l_u, l_v, and l_s represent the diffusion lengths, and τ_u, τ_v, and τ_s are the characteristic time scales of the system variables. The parameters α and β describe the local kinetics of the variable v which, together with the times scales, determine whether the local system is

in a monostable, Turing, excitable, or oscillatory regime. The variable s obeys simple linear kinetics and is coupled linearly to the variables u and v via the parameters κ_u and κ_v. For $s = u$ or $\kappa_u = \kappa_v = 0$, the coupling terms vanish and Eqs. (5.1a) and (5.1b) transform into the standard FitzHugh-Nagumo model, consisting of the variables u and v only. Therefore, the set of Eqs. (5.1) can be interpreted as a simple extension of the FitzHugh-Nagumo model. In the following, the case $\alpha > 0$ is considered, i.e. that the subsystem (5.1a, 5.1b) represents an activator-inhibitor system consisting of an activator u and an inhibitor v.

In the full system, the dynamics of the additional variable s only depends on itself and the activator u. The inhibitor v does not appear in Eq. (5.1c). The additional variable s plays the role of either an activator or an inhibitor, depending on the sign and magnitude of the coupling coefficients κ_u and κ_v. If $\kappa_u > 0$, the variable s activates the activator u; if $\kappa_v > 0$, it inhibits the inhibitor v. Since the coupling terms are proportional to the difference $s - u$, they also modify the activatory role of u. However, as long as the conditions $\kappa_u < 1$ and $\kappa_v > -\alpha$ are fulfilled, the variable u still behaves as an activator.

Local Dynamics

The model (5.1) without diffusive coupling reads

$$\tau_u \dot{u} = u - u^3 - v + \kappa_u(s - u), \tag{5.2a}$$

$$\tau_v \dot{v} = \alpha u + \beta - v - \kappa_v(s - u), \tag{5.2b}$$

$$\tau_s \dot{s} = u - s. \tag{5.2c}$$

The stationary states of system (5.2) are found with the condition $\dot{u} = \dot{v} = \dot{s} = 0$. From Eq. (5.2c) it follows that the variable s becomes equal to u as the system approaches a stationary uniform state. Then, the coupling terms vanish and the fixed points are identical to those of the standard FitzHugh-Nagumo model. Thus, the fixed points of the full model are given by the equations

$$0 = u_{\mathrm{s}}^3 + (\alpha - 1)u_{\mathrm{s}} + \beta, \tag{5.3a}$$

$$v_{\mathrm{s}} = \alpha u_{\mathrm{s}} + \beta, \tag{5.3b}$$

$$s_{\mathrm{s}} = u_{\mathrm{s}}, \tag{5.3c}$$

which do not depend on the coupling parameters κ_u and κ_v. Therefore, only the parameters α and β determine the number and position of stationary states. It has already been pointed out in Sec. 2.4 that excitable behavior of an activator-inhibitor system requires the presence

of a stable fixed point and a fast activator. Such a situation is realized for instance for $\alpha = 1$, $\beta = 0.2$, $\tau_u = 0.1$, and $\tau_v = 1$.

Nonlocality

It is an important feature of a reaction-diffusion system that the adiabatic elimination of a diffusing species may lead to nonlocal coupling terms in the remaining equations. This can be seen by the following analysis based on Ref. [171]. A similar discussion of these topics is also found, for instance, in Ref. [100].

For simplicity, it is assumed that only the variable s is diffusing, i.e. $l_u = l_v = 0$, and s is not coupled to v, i.e. $\kappa_v = 0$. Then, Eqs. (5.1) read

$$\tau_u \partial_t u = u - u^3 - v + \kappa_u(s - u), \tag{5.4a}$$

$$\tau_v \partial_t v = \alpha u + \beta - v, \tag{5.4b}$$

$$\tau_s \partial_t s = u - s + l_s^2 \nabla^2 s. \tag{5.4c}$$

If the variable s is changing on a much smaller time scale than u and v, it can be adiabatically eliminated. This means that Eq. (5.4c) becomes

$$0 = u - s + l_s^2 \nabla^2 s. \tag{5.5}$$

The solution to this linear equation can be found with Green's function method and is given by

$$s = u + \frac{1}{2l_s} \int_{-\infty}^{+\infty} dx' \exp\left(-\frac{|x - x'|}{l_s}\right) [u(x') - u(x)], \tag{5.6}$$

where the simple case of a one-dimensional, infinitely extended system has been considered. Equation (5.6) can be inserted into Eq. (5.4a) to replace the coupling term $\kappa_u(s - u)$. Finally, the following system is obtained

$$\tau_u \partial_t u = u - u^3 - v + F(u), \tag{5.7a}$$

$$\tau_v \partial_t v = \alpha u + \beta - v, \tag{5.7b}$$

where

$$F(u) = \frac{\kappa_u}{2l_s} \int_{-\infty}^{+\infty} dx' \exp\left(-\frac{|x - x'|}{l_s}\right) [u(x') - u(x)] \tag{5.8}$$

is the coupling function which describes the range and magnitude of the internal coupling of field u. The coupling is decaying exponentially. Its range is given by the diffusion length

l_s and its strength is proportional to κ_u. For a large coupling range l_s, the coupling becomes global, whereas for small l_s, the coupling is local and therefore of diffusive nature.

If diffusive coupling is present, the characteristic wavelength λ_P of observed patterns is much larger than the diffusion length, i.e. $\lambda_P \gg l_s$. Since in the diffusive limit of Eq. (5.8) the wavelength λ_P is given by $\lambda_P \propto \sqrt{\kappa_u}l_s$, this case is observed if the coupling strength κ_u is large. On the other hand, if $\kappa_u \approx 1$ (or smaller), the characteristic wavelength may be of the same order as the coupling range. Then, the approximation of diffusive coupling breaks down and the coupling is effectively nonlocal.

A similar analysis can be performed for $\kappa_v \neq 0$. Then, the coupling term $\kappa_v(s - u)$ in Eq. (5.4b) is replaced by a nonlocal coupling term. If $\kappa_v \gg 1$, this term corresponds to cross diffusion.

5.2   Stable pacemakers

This section studies the mechanism which enables the formation of stable self-organized pacemakers in the excitable regime. Since pulses are typical patterns for excitable systems, such solutions are compared to pacemakers. First, qualitative considerations are made before the results of one- and two-dimensional simulations are shown. Pulses are subsequently investigated in more detail. It turns out that two different pulse solutions may be stable at the same time and that the interaction of such pulses may also lead to stable pacemakers and target patterns.

5.2.1   Formation of pacemakers

The typical pattern for a one-dimensional excitable medium is the pulse solution, as discussed in Sec. 2.4. There, a sufficiently large perturbation of the fixed point leads to a pair of spreading pulses. The asymptotic pulse solution does not depend on the specific details of the perturbation once the threshold is crossed. If a perturbation does not reach the critical magnitude and the critical width, the perturbation directly decays to the steady state.

In the following, it is assumed that the subsystem (5.1a, 5.1b) is in the excitable regime close to relaxational oscillations. For simplicity, it is assumed that the inhibitor v does not diffuse ($l_v = 0$) and that s is only coupled to v and not to u ($\kappa_u = 0$). The coupling constant κ_v is assumed to be positive, i.e. the variable s inhibits the inhibitor v. Details of the numerical integration scheme are reported in Appendix A.4.

In such a system, self-organized pacemakers may occur if the diffusion length of the component s is much larger than the one of u, i.e. if $l_s \gg l_u$. Then, the width of a super-threshold perturbation determines whether this perturbation gives rise to a pulse pair or a pacemaker. On the one hand, a pair of pulses is created if the perturbation has a very large spatial extension. On the other hand, if the width of the perturbation is comparable to the diffusion length of the component s, a pacemaker is created. This is shown in Fig. 5.1 where the formation of a pair of pulses [Figs. 5.1(a,c)] is compared to the formation of a pacemaker [Figs. 5.1(b,d)]. The stable fixed point for these simulations is given by $u_s = s_s = -0.58$ and $v_s = -0.38$. The thin solid lines in Figs. 5.1(a,b) indicate the initial condition of u, where the perturbation consists of a constant shift to $u = 0$ within a region of width $2R$.
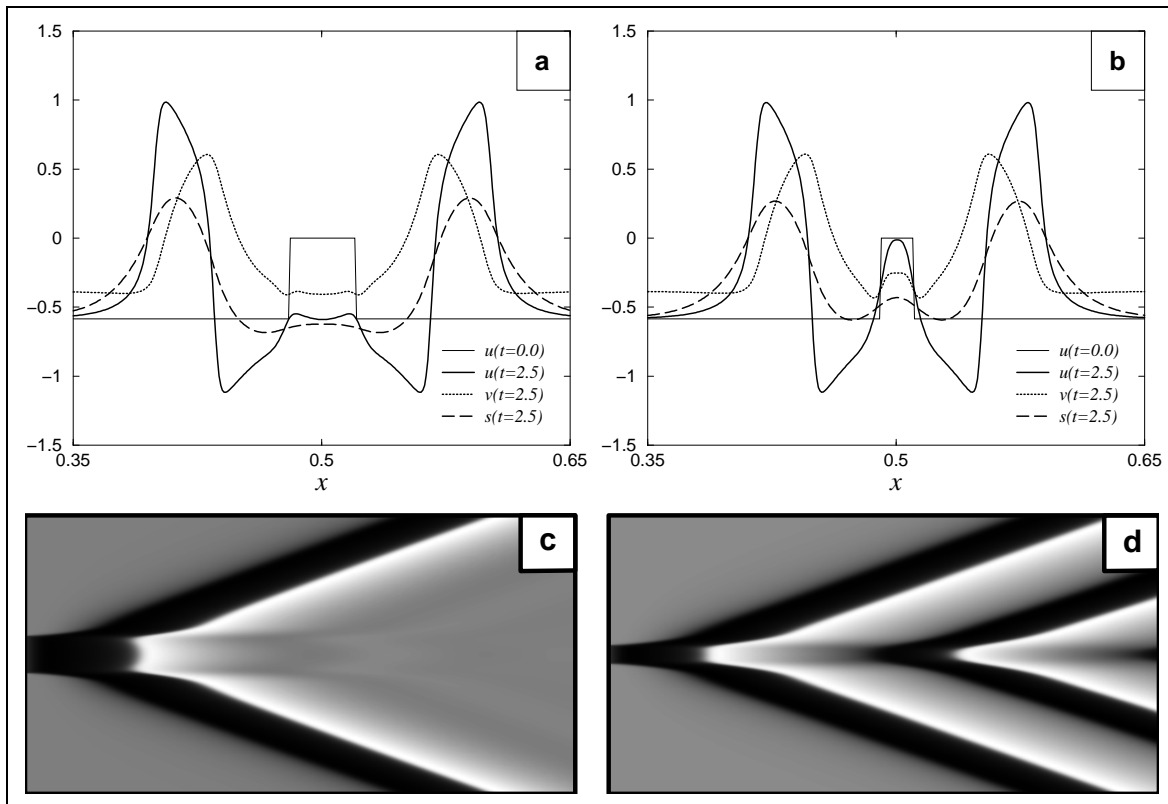

Figure 5.1: **Formation of pulse pairs and pacemakers.** *Characteristic stages in the development of a pulse pair (a) and a pacemaker (b) are displayed. The initial conditions for u are shown as thin solid lines. Space-time diagrams for the formation of a pulse pair and a pacemaker are displayed in (c) and (d) respectively. There, the variable u is shown in gray scale, where the black denotes large values. The color map is nonlinear to emphasize the increased values of u in the tail of the waves. The parameters are $\alpha = 1$, $\beta = 0.2$, $\kappa_v = 1$, $\tau_u = 0.1$, $\tau_v = 1$, $\tau_s = 0.1$, $l_u = 0.001$, and $l_s = 0.017$. The displayed system size is $L = 0.3$ and the shown time interval in (c,d) is $\Delta t = 5$.*

If the perturbation is wide [Figs. 5.1(a,c)], a pair of pulses is emitted. The thick lines in

Fig. 5.1(a) denote the distributions of u, v, and s shortly after the emission of the pair of pulses. The subsequent evolution in the central region is characterized by a decay to the stationary state and the two pulses remain the only excited regions in the system. Note that the distribution of the activator u possesses two local maxima at positions where the boundaries of the initial perturbation were located before. These maxima are associated with the non-monotonous, oscillatory tail of each pulse and are typical for a pulse in an excitable regime close to the onset of oscillations. In the space-time diagram that shows the formation of a pulse pair [Fig. 5.1(c)], the local maxima of u can be clearly identified as dark lines in the middle of the displayed time interval. For later time moments, these maxima correspond to the first maxima in the tails of the pulses. The inhibitor v also shows two maxima at these positions which, however, are less pronounced. The component s, on the other hand, shows a broad profile and has its maximum in the center of the pattern. This is not surprising because the diffusion length l_s is relatively large.

In Figs. 5.1(b,d), the same system is shown where the width of the initial perturbation of u is smaller, but still large enough to trigger the formation of waves. After the emission of the first waves, the distribution of u first shows the same two maxima like Figs. 5.1(a,c). Then, the maxima merge in the central part of the pattern because they are located sufficiently close to each other. This local increase in the activator u in the center constitutes a super-threshold perturbation which creates a new pair of waves. This scenario is repeated and a pacemaker is established. Comparing Fig. 5.1(c) with Fig. 5.1(d), it can be seen that the location of the pacemaker approximately coincides with the location where the first maxima of the tails of the emitted waves merge. The width of the wave source is approximately given by the size of the initial perturbation. It should be noted that the profile of the first wave emitted by a pacemaker [Fig. 5.1(b)] strongly resembles the profile of the pulse solution [Fig. 5.1(a)].

Figure 5.2 displays the evolution of a system, where a pacemaker is formed, for a longer time interval. Since periodic boundary conditions have been applied, not only the pacemaker is observed (which can be seen in the upper part of the figure), but also the location where the waves collide (in the lower part of the figure). The first waves emitted by the pacemaker strongly resemble pulses. Later, and in particular in the asymptotic regime, the waves have other properties, i.e. different wavelength, frequency, and amplitude of the variable s. It can be seen that the wavenumber and the frequency of the waves increase with time. However, the pulse-like waves emitted first are faster than the subsequent ones, i.e. the wave speed decreases with time. As indicated by the different gray levels for s in Fig. 5.2(a), the maximum value of s within a pulse-like wave is significantly larger than in those waves which form
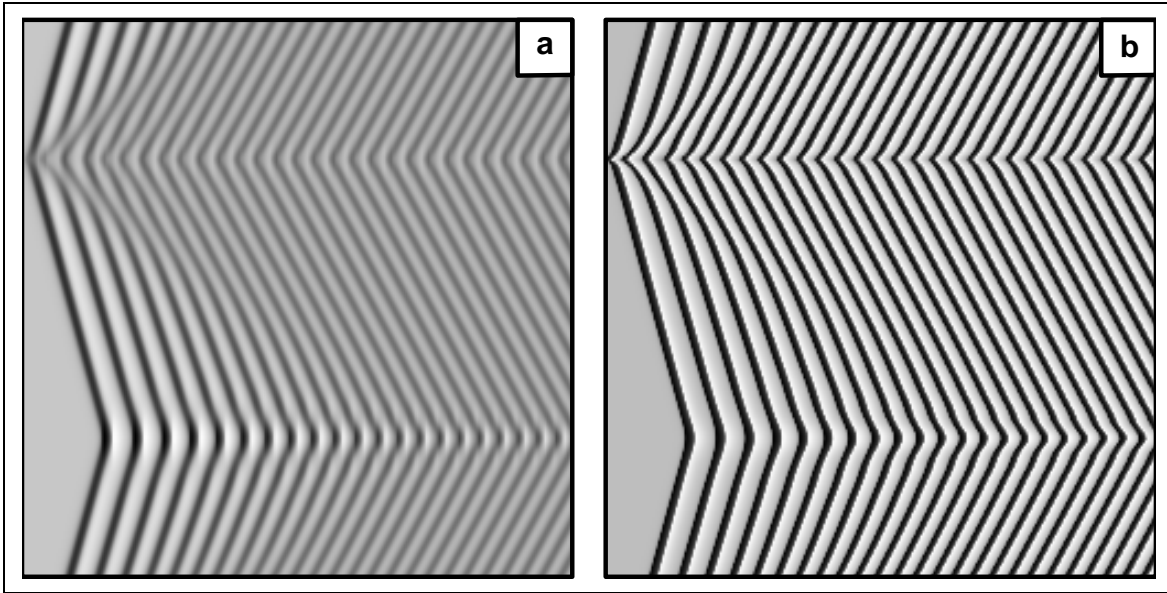
Figure 5.2: **Stable self-organized pacemaker in one spatial dimension.** *Space-time diagrams for s (a) and u (b) are shown. The parameters are $\alpha = 1$, $\beta = 0.2$, $\kappa_v = 1$, $\tau_u = 0.05$, $\tau_v = 1$, $\tau_s = 0.1$, $l_u = 0.00071$, and $l_s = 0.017$. The displayed time interval is $\Delta t = 50$ and the system size is $L = 1$. Periodic boundary conditions are used.*

the asymptotic wave train. Furthermore, the amplitude of s within the collision zone of the waves is also much larger than within the wave train. The difference in amplitude between the first (pulse-like) waves and the asymptotic wave train are restricted to the variable s. The values of u in a pulse and in the asymptotic wave train are very similar [Fig. 5.2(b)].

In the asymptotic regime, the wavenumber of the propagating waves is constant. Within the range of perturbations that lead to pacemakers, no dependence of the asymptotic wavenumber on the specific width of perturbation is detected.

Simulations of two-dimensional systems have also been performed. Figure 5.3 shows an example of a target wave pattern present in a system with no-flux boundary conditions. The perturbation has been applied in a corner of the system to show as many waves as possible. In Fig. 5.3(a), the variable s is shown. As with the one-dimensional system, the variable s has an intermediate amplitude within the wave train and a large amplitude where the waves collide (here with the no-flux boundary). Figure 5.3(b) shows that the amplitude of the activator u does not undergo any significant changes at the boundary. The evolution of that pattern is qualitatively similar to the one-dimensional case, i.e. a pacemaker arises only for appropriate perturbations and the amplitude of s in the asymptotic pattern is smaller than in the beginning.
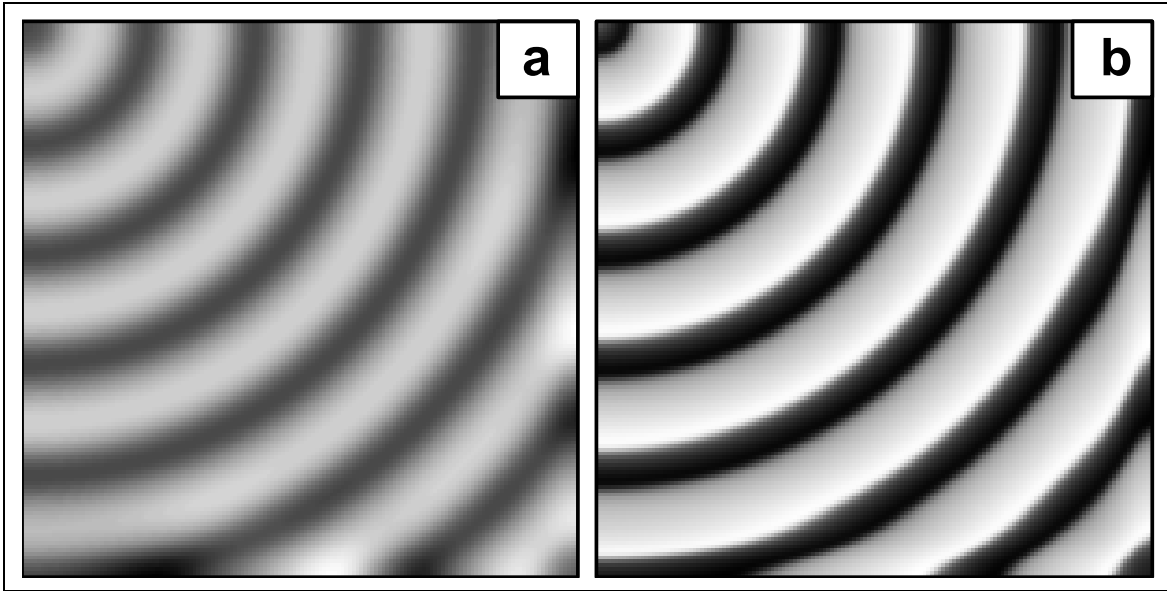
Figure 5.3: **Stable self-organized pacemaker in two spatial dimensions.** *Snapshots of the distributions of s (a) and u (b) are displayed. The parameters are* $\alpha = 1$, $\beta = 0.2$, $\kappa_v = 1$, $\tau_u = 0.1$, $\tau_v = 1$, $\tau_s = 0.1$, $l_u = 0.05$, $l_s = 1$, $L_x = L_y = 15$, *and* $t = 500$. *No-flux boundary conditions are used. Black denotes large values.*

5.2.2   Bistability of pulse solutions

In the previous section, it has been shown that pacemakers are not the only type of pattern that can occur in system (5.1). In this section, it is shown that the system admits two stable types of pulse solutions. The pulse solutions are compared and their relationship to the pacemakers is studied in more detail.

Figure 5.4 shows the profiles of three different patterns found in one-dimensional systems: a target pattern with pacemaker (a), a small pulse (b, left), and a large pulse (b, right). All these patterns are stable with respect to small perturbations. In particular, both the small and the large pulse may propagate indefinitely in a medium with periodic boundary conditions. These patterns are characterized in more detail in the following.

The large pulse corresponds to the pulse already seen in Fig. 5.1. It is created by applying a sufficiently large perturbation of u to the uniform steady state. Its velocity V_{lp} is the largest among the velocities of the three solutions and the pattern is characterized by the largest amplitude S_{lp} within the pulse, where S_{lp} is defined as the difference between the maximum of s and its value in the fixed point. If this pulse solution is slightly perturbed, the perturbation is damped out quickly. Simulations indicate that this also holds for relatively strong perturbations, showing that this pulse solution is quite robust.
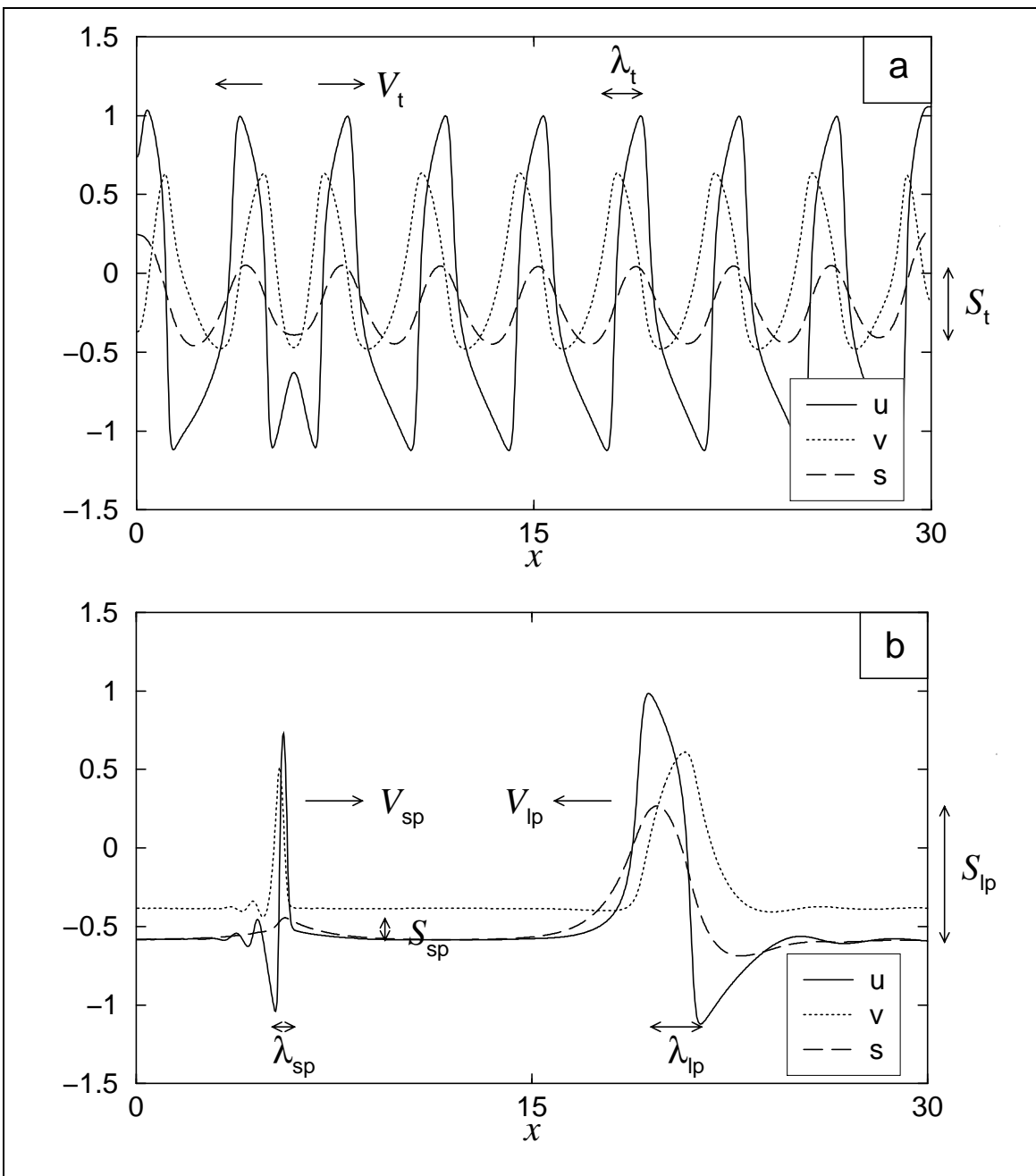
Figure 5.4: **Pacemaker and pulse solutions.** *The profiles of the variables are shown for a pacemaker (a) and the two pulse solutions (b). The parameters are $\alpha = 1$, $\beta = 0.2$, $\kappa_v = 1$, $\tau_u = 0.1$, $\tau_v = 1$, $\tau_s = 0.1$, $l_u = 0.05$, $l_s = 1$, and $L = 30$. The velocities V of the waves, the amplitude S of the variable s, and the characteristic width λ of the waves are displayed. The solid, dotted, and dashed lines correspond to u, v, and s respectively. No-flux boundary conditions are present in (a), being responsible for the increase of s at the boundary. Further explanations are found in the text.*

The small pulse is closely related to the pulse solution known for the standard FitzHugh-Nagumo model. It can be obtained by performing a simulation where the FitzHugh-Nagumo system is decoupled from the variable s, i.e. for $\kappa_v = 0$. Then, the coupling parameter κ_v may be increased slowly without destroying the pulse (here, to $\kappa_v = 1$). This pulse solution is not only short but also slow compared to the large pulse. Remarkably, the distribution of s within the pulse only shows a small deviation from the stationary value, i.e. S_{sp} is relatively small. This pulse solution is also stable with respect to small perturbations. However, it can easily be destabilized with moderate perturbations. A transition into the large pulse solution is typically observed in such cases.

The target pattern is formed by a wave train with a wave speed V_{t}, which lies between the velocities of the two pulse solutions. The amplitude S_{t} of s within the wave train, i.e. the difference between the maximum and minimum values of s, also lies between the large amplitude for the large pulse and the small amplitude for the small pulse, for which the amplitude is defined as the difference between the maximum and the value of the rest state. In order to compare the widths of the pulses with the width of a single wave in the target pattern, it is convenient to define the half-width λ of a wave as the distance between the maximum and minimum of the profile of the activator u, i.e. the half-width λ is measured in the decreasing part of the profile. In the case of the wave train, the half-width is approximately half of one wavelength. In summary, it is found that

$$V_{\mathrm{sp}} < V_{\mathrm{t}} < V_{\mathrm{lp}}, \tag{5.9a}$$

$$S_{\mathrm{sp}} < S_{\mathrm{t}} < S_{\mathrm{lp}}, \tag{5.9b}$$

$$\lambda_{\mathrm{sp}} < \lambda_{\mathrm{t}} < \lambda_{\mathrm{lp}}, \tag{5.9c}$$

where the subscripts refer to small (sp) and large (lp) pulses, and to target waves (t) respectively. All pacemakers and pulses that have been observed in the simulations fulfill Eqs. (5.9). For the set of parameters $\alpha = 1$, $\beta = 0.2$, $\tau_u = \tau_s = 0.1$, $\tau_v = 1$, $l_u = 0.05$, and $l_s = 1$, bistability of pulses is observed for $0.73 < \kappa_v < 1.09$. For $\kappa_v < 0.73$, only the small pulse is stable, while for $\kappa_v > 1.09$ only the large pulse is stable (larger values than $\kappa_v = 1.2$ have not been considered in the simulations).

5.2.3 Interaction of pulses and pacemakers

The two different kinds of pulse solutions are stable with respect to small perturbations and travel persistently on the background of the steady state in a one-dimensional medium with periodic boundary conditions. However, when pulses of both types are present in such a medium, they necessarily interact because they travel with different velocities. Furthermore, pulses of the same kind may collide and give rise to complex spatio-temporal patterns. Following interactions are discussed in this section for a fixed set of parameters: Two large pulses, a large pulse and waves from a pacemaker, two small pulses, a large and a small pulse, and a small pulse with waves from a pacemaker.

When two large pulses meet, they annihilate in the collision and the system returns to the stationary state. This corresponds to the typical behavior of pulses in excitable media and is therefore not further discussed here. If a large pulse collides with the waves emitted by a pacemaker, the large pulse is annihilated and the pacemaker entrains the medium.

At the location where two small pulses collide [Fig. 5.5], the amplitude of s increases strongly, as displayed in Fig. 5.5(a). Subsequently, slightly apart from the collision zone,
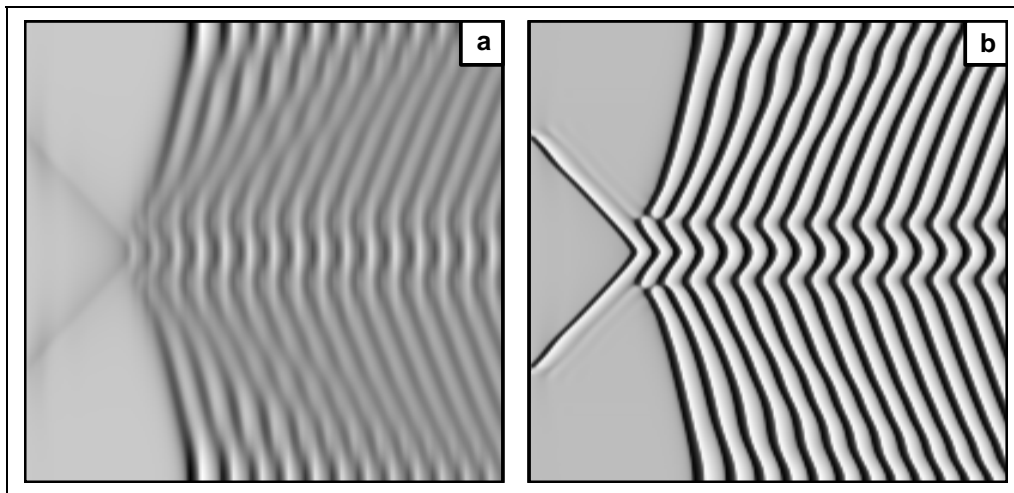

Figure 5.5: **Two colliding small pulses lead to a bound state of two pacemakers and a wave sink.** *Space-time diagrams for s (a) and u (b). The parameters are $\alpha = 1$, $\beta = 0.2$, $\kappa_v = 1$, $\tau_u = 0.1$, $\tau_v = 1$, $\tau_s = 0.1$, $l_u = 0.05$, and $l_s = 1$. Black denotes large values. The displayed time interval is $\Delta t = 40$ and the system size is $L = 20$. No-flux boundary conditions are used.*

two symmetrically shifted pacemakers are formed. As a result, a bound state of two pacemakers is created. Between the two wave sources, there is a small region where the waves collide. There, the component s performs large amplitude oscillations. The frequency and

wavenumber of the waves emitted by such a bound state of two pacemakers are larger than the corresponding values of the waves emitted by only one pacemaker. The bound state of two pacemakers emits hundreds of waves, but it is actually found to be unstable for the studied sets of parameters and the system finally returns to the rest state. This is shown for a different simulation in Fig. 5.6. The instability develops as an increasing asymmetry between the two wave sources. Finally, one destroys the other and subsequently decays itself.
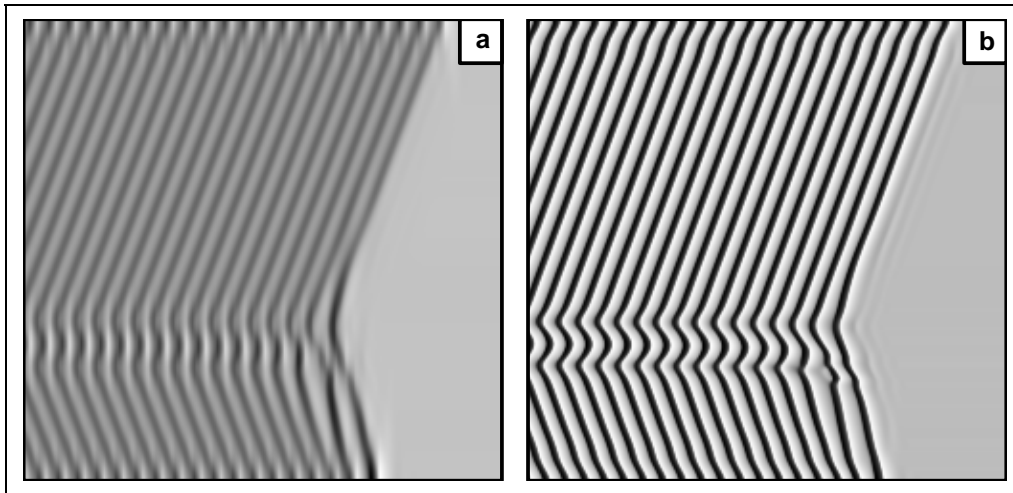

Figure 5.6: **Unstable bound state of pacemakers.** *Space-time diagrams for s (a) and u (b) are shown. The parameters are like in Fig. 5.5. Black denotes large values. The displayed time interval is $\Delta t = 50$ and the system size is $L = 25$. No-flux boundary conditions are imposed.*

If a large and a small pulse interact, as displayed in Fig. 5.7, the waves first seem to annihilate. However, the large pulse actually reappears and proceeds into its initial direction. Also the small pulse reappears and first seems to proceed as before. Yet it becomes unstable and transforms into a large pulse. Moreover, in the tail of this pulse, a pacemaker appears. In the wave pattern subsequently formed, the impact of the small pulse is still seen as a local decrease of the amplitude of the component s of the target waves. This modulation is advected toward the border and finally decays there. The asymptotic state consists of a stable pacemaker located close to the collision zone of the pulses.

If the different pulses do not meet in a head-on collision, but if the fast (large) pulse runs into the tail of the slow (short) one, the asymptotic state also consists of a pacemaker that is created at the location of the collision. Corresponding simulations are not shown here.

The next interaction scenario is the case of a small pulse colliding with the waves emitted by a pacemaker. The result of such interaction is shown in Fig. 5.8. Within the collision zone,
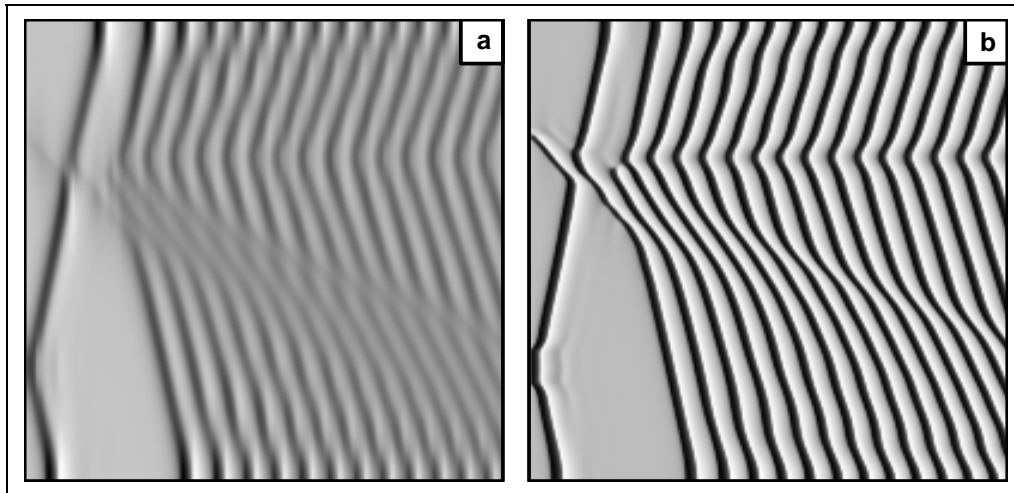
Figure 5.7: **Interaction of a small pulse with a large pulse.** *A stable pacemaker is formed. Space-time diagrams for s (a) and u (b) for the initial evolution of the system are shown. The parameters of the system are as in Fig. 5.5.*

large amplitude oscillations of s appear, forming a localized pattern which can be clearly identified. This localized pattern can be interpreted as a bound state of a pacemaker and a collision zone of waves. However, this pattern is not stationary. It travels at very low speed toward the original pacemaker. Finally, the bound state of pacemaker and collision zone reaches the initial pacemaker and form the type of bound state of two pacemakers already discussed in Fig. 5.5. This pattern is unstable, the pacemaker is finally destroyed, and the stationary state is recovered (*cf.* Fig. 5.6). The transient, however, is long and comprises hundreds of wave emissions.
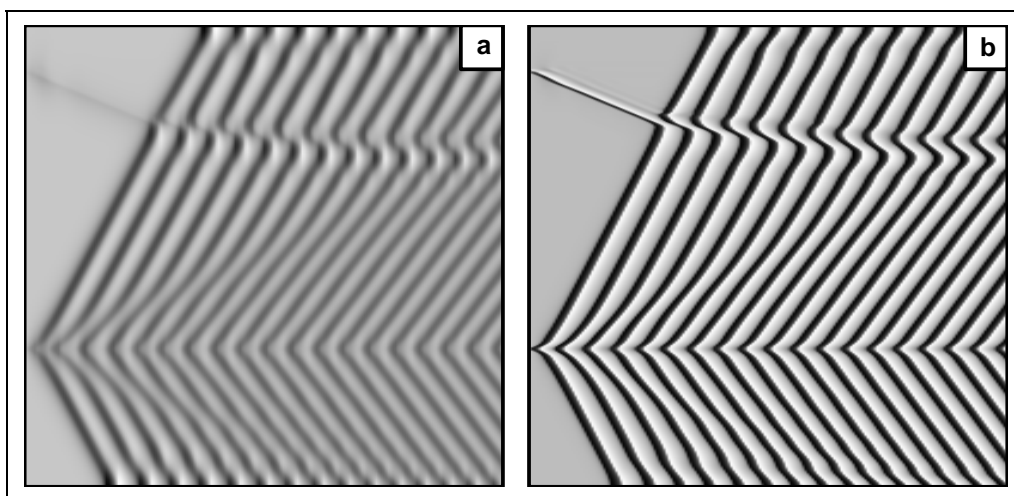

Figure 5.8: **Interaction of a small pulse with a pacemaker.** *Space-time diagrams for the initial evolution of s (a) and u (b) are displayed. The parameters of the system are as in Fig. 5.5, except the system size, which is $L = 50$.*

The bound state of the pacemaker and the collision zone can be studied without the initial pacemaker. In a one-dimensional system with periodic boundary conditions, the waves emitted by the pacemaker may be identical to the waves which are received in the collision zone. This is shown in Fig. 5.9. This pattern may be interpreted as a pacemaker that emits waves only in one direction. The localized pattern drifts at a low constant speed through the medium. The width of the localized pattern can be defined as the distance between the centers of the pacemaker and the collision zone. Then, an interesting phenomenon can be reported: This width is half of the wavelength of the waves and a wave needs half the period to cross such a distance. This means that the pacemaker emits a wave exactly at that moment that a wave would have needed to cross the localized pattern. However, the phase difference between these two waves is 2π. This is illustrated by the white dotted lines in Figs. 5.9(a,b).
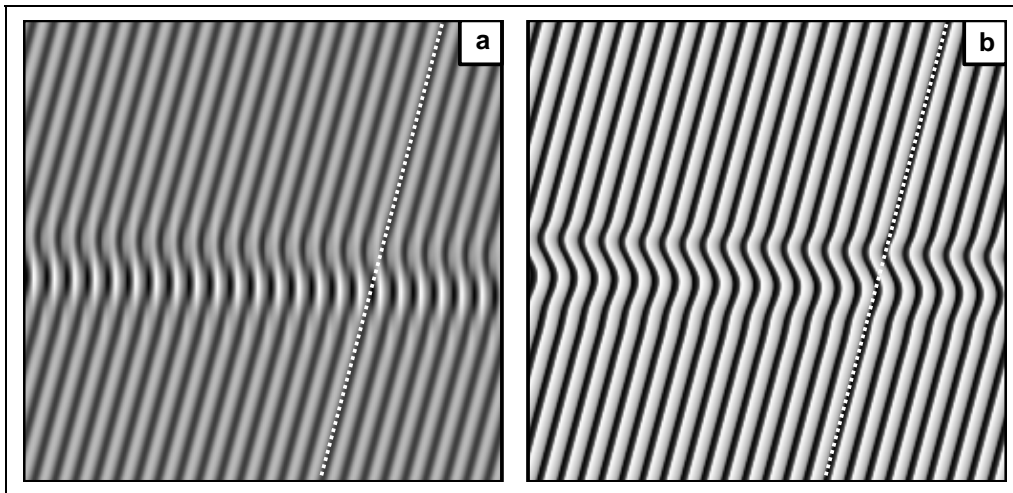

Figure 5.9: **Stable bound state of a pacemaker with a collision zone.** *Space-time diagrams for s (a) and u (b) are shown. The parameters of the system are as in Fig. 5.5, except the system size which is $L = 22.625$ and the displayed time interval, which is $\Delta t = 50$. Periodic boundary conditions are used.*

The last interaction scenario that is discussed consists of waves emitted by a pacemaker which run into the tail of the small pulse. Simulations not displayed here show that the waves from the pacemaker overtake the pulse and entrain the rest of the system. This means that the asymptotic state consists of the initial pacemaker. The small pulse produces a local perturbation which is advected to the no-flux boundary and decays there.

5.3 Unstable pacemakers

In the previous section, stable self-organized pacemakers and several other structures like pulses and localized states have been discussed. However, even single pacemakers are not stable under all conditions. Unstable pacemakers are considered in this section.

Up to now, two diffusing components u and s have been considered where $l_u \ll l_s$. Now, the case of vanishing activator diffusion ($l_u = 0$) is discussed, i.e. s is the only diffusing component. Then, the simulations show a qualitatively different behavior compared to the previous section. An example is displayed in Fig. 5.10. First, a pacemaker is formed since the width of a perturbation is comparable to the diffusion length of the component s [Figs. 5.10(a,e)]. The pacemaker starts to emit waves. Then, as time proceeds, the wave-
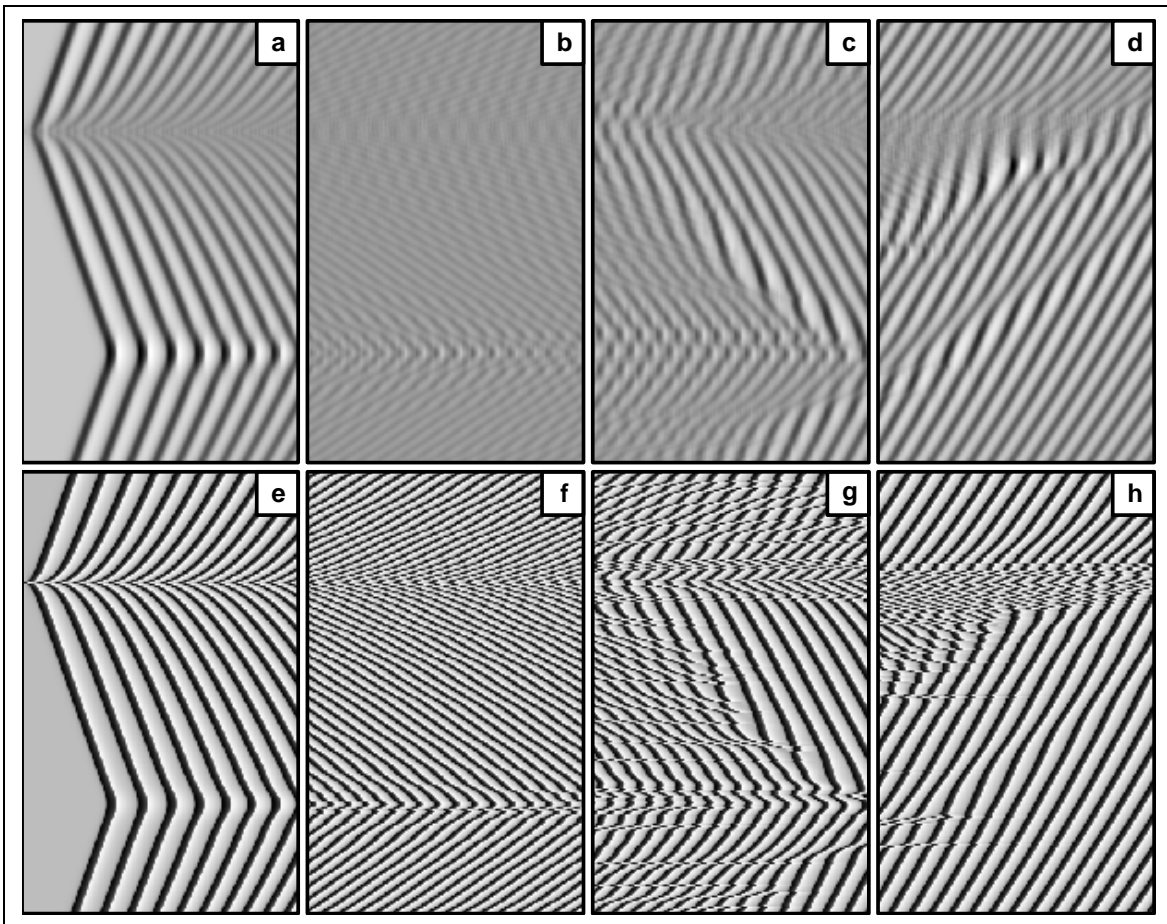

Figure 5.10: **Unstable pacemaker.** *Space-time diagrams for s (a-d) and u (e-h) are shown. The displayed time intervals are $\Delta t = 25$, starting at $t = 0$ (a,e), $t = 350$ (b,f), $t = 443$ (c,g), and $t = 1513$ (d,h). The parameters are $\alpha = 1$, $\beta = 0.2$, $\kappa_v = 1$, $\tau_u = 0.05$, $\tau_v = 1$, $\tau_s = 0.1$, $l_u = 0$, and $l_s = 0.017$. The system size is $L = 1$ and periodic boundary conditions are used.*

length of the emitted waves decreases. In parallel, also the amplitude of s within the wave train decreases, as seen in Fig. 5.10(b). There, almost no waves can be identified and the value of s hardly deviates from its mean value. However, waves are still present and can be clearly identified in the space-time diagrams for u, since the activator always displays waves with large amplitudes [Fig. 5.10(f)]. The simulation show that the wave pattern subsequently decomposes into small wave fragments which are separated by phase jumps. These phase discontinuities are seen for example in Fig. 5.10(f) in the center of the collision zone or in Fig. 5.10(g) for $t = 443$ almost everywhere.

This irregular wave pattern resembles spatio-temporal chaos, as seen in Fig. 5.10(g) for $t = 443$ to $t = 455$. The behavior is intermittent since waves are occasionally formed that have a large amplitude in the variable s, propagate with a high velocity, and are able to destroy the small amplitude wave patches [Figs. 5.10(c,g), $t = 455$ to $t = 468$]. In this way, the regular pacemaker can be clearly seen again, also in the diagram for s [Fig. 5.10(c)]. The state of large amplitude target waves is unstable and the whole scenario is repeated.

The wave source which creates the irregular wave pattern is denoted as unstable pacemaker, emphasizing that the regular wave source has become unstable. Therefore, an unstable pacemaker still produces target waves, although regular, large-amplitude waves as considered in the previous sections are absent.

If the medium has periodic boundary conditions, a large amplitude wave may reach the pacemaker and destroy it [Fig. 5.10(d,h)]. Then, a periodic train of pulses is formed which travels along the one-dimensional medium. A pulse train formed in this way does not decompose into small wave patches. Several simulations have been carried out for periodic boundary conditions, showing always the formation of pulse trains. However, the number of pulses present in such a system may vary. The traveling waves do not have an intrinsic wavelength. Furthermore, if no-flux boundary conditions are applied to such a pulse train, the pulses decay at the boundary. This demonstrates that the observed wave train should indeed be interpreted as a train of pulses in an excitable medium and that the system is not close to a wave bifurcation.

Simulations performed for a system with no-flux boundary conditions show different dynamics for long integration times. Although large-amplitude wave trains may also be created, such patterns decay at the border and give rise to irregular dynamics. Then, either the unstable pacemaker may persist or it may decay and give way to spatio-temporal chaos without any pacemaker. Such regimes are not in the focus of this thesis and hence not discussed here.

It seems obvious that the absence of diffusion of u leads to the instability of the regular pacemaker solution. To check this hypothesis, the variable u is allowed to diffuse weakly in a moment where the pattern consists of small-amplitude, irregular wave patches. As Fig. 5.11 demonstrates, a pacemaker that emits regular target waves is established. Therefore, activator diffusion seems indeed to be crucial for the stability of the regular pacemaker solution. However, a stable pacemaker does not always appear in such a situation. For another simulation (not shown here), a bound state of two pacemakers is created instead, which becomes unstable and decays to the rest state after a long transient, as discussed above.
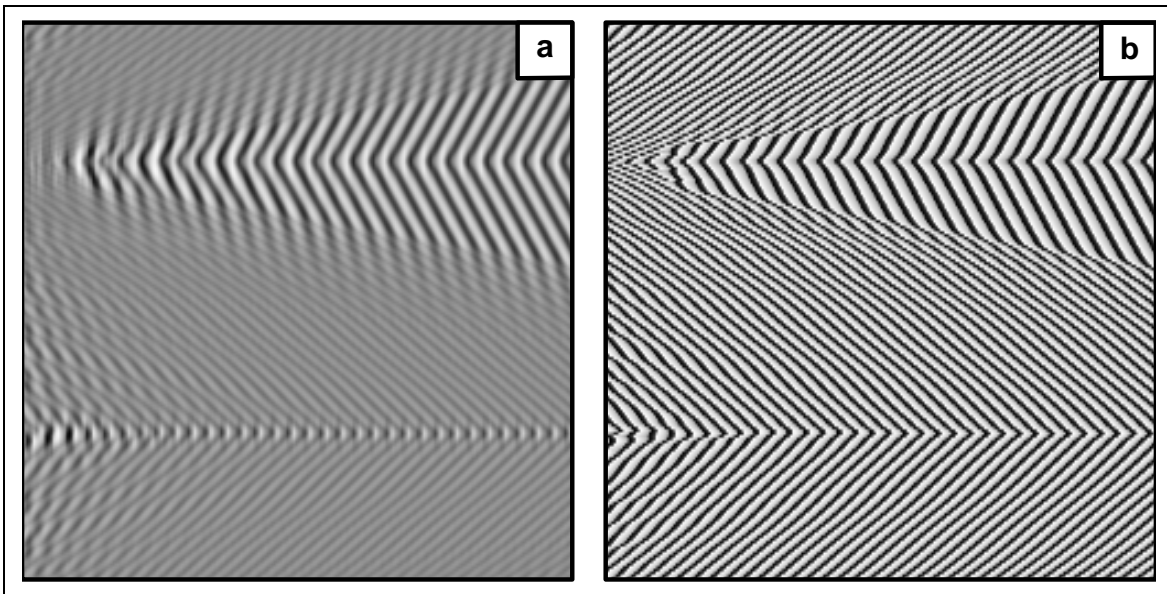

Figure 5.11: **Stabilized pacemaker.** *Space-time diagrams for s (a) and u (b) are shown. The displayed time interval is $\Delta t = 50$. The system is as in Fig. 5.10 but with $l_u = 0.00071$.*

Above, the pulse solutions have been considered for the case of small activator diffusion. Here, their behavior is discussed for vanishing diffusion of u. Numerical simulations have been performed where stable pulses are present and the parameter l_u is set to zero. The result is that the large pulses remain stable in this case while the small pulses become unstable and quickly decay to the stationary state. Since the small pulse corresponds to the pulse that exists in the standard FitzHugh-Nagumo model, it is not surprising that this pulse solution is not observed in the case where $l_u = l_v = 0$. If the diffusion length l_s of the component s is set to zero, the small pulse remains stable while the large pulse becomes unstable. Therefore, the stability of the small pulse solution strongly depends on activator diffusion, while the stability of the large pulse depends mainly on diffusion of the third variable s.

5.4   Discussion

The main result of this chapter is the observation of stable self-organized pacemakers in an excitable medium. The system consists of a FitzHugh-Nagumo model which is extended by an additional diffusing variable s. This component obeys linear kinetics and has been introduced to extend the standard two-component FitzHugh-Nagumo model in a minimal way. The following conditions are sufficient to create a stable self-organized pacemaker: strong diffusion of the variable s, proximity to the regime of relaxational oscillations, and sufficiently strong coupling of s to the inhibitor v. Then, whether a pacemaker or a pair of pulses develops, depends on the initial condition. The principal mechanism is identified as the width of a critical perturbation, which should be of the order of the diffusion length of the component s. Simulations not shown here demonstrate that if the parameters are chosen such that the system is in the regime of relaxational oscillations but still close to the regime discussed here, the formation of pacemakers is also observed. Thus, the mechanism leading to these structures is more general and not restricted to the excitable regime.

Beside the solution corresponding to a pacemaker, other solutions in the excitable regime of the extended FitzHugh-Nagumo model have also been discussed. Here, pulse solutions are of particular interest. For the studied sets of parameters, two stable types of pulses have been found, namely a pulse resembling the pulse solution for the standard FitzHugh-Nagumo model, and a novel pulse solution that has considerably larger velocity, amplitude, and width. If the waves emitted by a pacemaker are characterized in terms of these quantities, the result is that such waves have intermediate values compared to the two pulse solutions.

The model studied here consists of three independent variables. Several years ago, Ohta *et al.* [135–137] reported self-organized pacemakers in a two-component activator-inhibitor model with a coexistence of excitable kinetics and stable uniform oscillations. In their system, pacemakers were also created by appropriate initial conditions. The wave sources, however, were unstable and uniform oscillations were approached asymptotically. Two main differences between their system and the system studied here can be pointed out. First, the local dynamics of their system is characterized by the presence of a limit cycle while here, the only local attractor consists of the stationary state. Second, the pacemakers studied here do not decay to uniform oscillations, but remain stable, at least as long as activator diffusion is present.

The three-component model studied here is not designed to explain the behavior of a specific reaction-diffusion system. However, it represents a simple extension of a general

two-component model that is often used to describe the behavior of systems of various origins. Similar three-component models based on the FitzHugh-Nagumo model have been proposed to describe spiral formation in aggregating *Dictyostelium Discoideum* colonies [172] or traveling spots in gas-discharge systems [33]. In such systems, the additional component is always assumed to be strongly diffusive. Applications of the results of the present model to those or other systems may be possible.

The role of activator diffusion has been identified to be crucial for the stability of the pacemaker and the corresponding wave train. If the diffusion of u is absent, the only stable pattern is the large pulse solution. The pacemaker solution remains present, but a transition to irregular dynamics with wave patches at a small length scale is observed. Dislocations develop and a transition to spatio-temporal chaos is observed. The small scale patterns indicate that according to the argument presented in Sec. 5.1, the effective coupling is nonlocal. The coupling terms introduce nonlocal coupling which has no obvious impact on the dynamics as long as diffusion of u is present. Even very small diffusion is sufficient to stabilize the pacemaker solution and give rise to large-scale patterns. Further simulations for the present model may clarify the question whether unstable (irregular) pacemakers are also possible for very small activator diffusion. The influence of nonlocal coupling on pattern formation in one-dimensional and disc-shaped media has been intensively investigated by Middya, Sheintuch, and others in a series of papers [113, 114, 173, 174]. They describe many patterns, among them stable target patterns, for global coupling and long-range interaction. However, they do not report such unstable pacemakers giving rise to irregular wave patterns.

As a result of the different types of interaction between the pulses and pacemakers, not only stable pacemakers may appear, but also localized patterns representing bound states of pacemakers, or bound states of a pacemaker with a collision zone. This demonstrates that the class of initial conditions giving rise to pacemakers is not small, and also provides an opportunity to characterize the wave train emitted by a pacemaker as an intermediate structure between the two different pulse solutions. Although the localized states are unstable in the simulations, their transients are very long. Therefore, these patterns may be stable for other sets of parameters and may also have long-lasting counterparts in experiments. Future work may search for stable bound state of two pacemakers. Since the bound state of two pacemakers emits waves with a larger frequency than one pacemaker only, competition and interaction of pacemakers may be studied. Finding a stable bound state of pacemakers would mean that this pattern could be interpreted as a self-organized wave source. This means that bistability of different pacemaker solutions could be possible.

The bistability of pulse solutions is a rare phenomenon in reaction-diffusion systems. Winfree showed that multiple spiral wave solutions are possible in an excitable system [175, 176]. There, the dispersion relation of the waves, i.e. the dependence of the velocity on the wavelength, shows an oscillatory behavior. The local minima of the dispersion relation determine the stable spiral solutions. Consequently, several spirals with different wavelengths and speeds may coexist in such a system. Another type of bistability of pulse solutions was recently presented by Bordiougov [177]. There, pulse trains with identical wavelengths and different velocities may coexist. In this work, the pulse solutions are very different in wavelengths and speed. While one pulse corresponds to the pulse solution known for the FitzHugh-Nagumo system, the other is genuine for the whole, coupled system and exists only for sufficiently large coupling strengths κ_v. This chapter has been focused on the formation of pacemakers, but further investigation of pulses in the three-component extension of the FitzHugh-Nagumo model seem to be an interesting topic in its own right.

The localized pattern which corresponds to a bound state of a pacemaker and a collision zone of waves closely resembles drifting patterns found by Nicola [100]. He investigated systems near a Turing-wave bifurcation described by a two-component model with nonlocal coupling or the respective amplitude equations. However, Nicola's results are not directly applicable since the simulations for the system studied here are not carried out close to a Turing or wave bifurcation. Nevertheless, the approaches used by Nicola may be useful to characterize the drifting bound state pattern in terms of interfaces that connect different states of traveling waves.

Chapter 6

Conclusions and perspectives

The aim of this thesis has been to investigate target patterns and pacemakers in oscillatory and excitable reaction-diffusion systems. Heterogeneous and self-organized pacemakers and the corresponding target patterns have been studied analytically and numerically. While heterogeneous pacemakers have been discussed for a medium close to a Hopf bifurcation, self-organized pacemakers have been discussed for a birhythmic medium close to a pitchfork-Hopf bifurcation and for an excitable system described by an extended FitzHugh-Nagumo model.

The investigation of heterogeneous pacemakers in oscillatory systems has focused on two aspects. First, the conditions for creating pacemakers and extended target patterns versus the creation of wave sinks and localized wave patterns have been derived systematically. Systems with both positive and negative dispersion have been considered. Inward traveling target patterns and large heterogeneities have been discussed. Second, heterogeneities with large frequency shifts have been investigated. In this case, the waves become Eckhaus unstable and amplitude defects appear with either ring-shaped or more complex topologies. For pacemakers with very large frequency shifts, the amplitude defects already occur at the boundaries of the heterogeneities, giving rise to the local desynchronization of oscillations. Wave sinks can also have a significant impact on the spatio-temporal dynamics of the system by breaking the waves arriving from other wave sources.

It has been shown in this thesis that a system close to a pitchfork-Hopf bifurcation is able to create stable self-organized pacemakers. The normal form and amplitude equations of the pitchfork-Hopf bifurcation have been derived. Such a system displays birhythmicity, i.e. bistability of limit cycles, and it has been demonstrated analytically that stable self-organized pacemakers are possible. Simulations have confirmed the existence of stable self-organized

pacemakers. In the presence of a parameter gradient, such patterns drift, as has been shown analytically and numerically. The interaction between pacemakers has been studied numerically, giving rise either to coexisting pacemakers or to a new phenomenon called global inhibition: Established pacemakers suppress new cores or merge with them. When the frequencies of the limit cycles differ strongly, the waves may become Eckhaus unstable and the pacemaker may destabilize. Furthermore, kinetic instabilities of pacemakers are possible, creating breathing and swinging pacemakers.

A pacemaker in an excitable medium consists of a small localized region where the system is effectively oscillatory. No stable self-organized pacemakers for excitable media have previously been reported. In this thesis, a three-component model has been proposed on the basis of the FitzHugh-Nagumo equations, consisting of an activator, an inhibitor, and an additional variable. The formation of stable self-organized pacemakers in the excitable regime of that model has been demonstrated if several conditions are fulfilled: The system is close to relaxational oscillations, the additional component is strongly diffusive, and the additional component inhibits the inhibitor. Moreover, bistability of pulse solutions has been observed in such a system. Different pulses can interact and may create pacemakers or localized patterns. If the diffusion of the activator vanishes, the waves emitted by the wave source are unstable and spatio-temporal chaos appears, which is interpreted as a result of nonlocal coupling.

If amplitude equations are derived for a specific bifurcation, they are applicable to all systems which are close to this bifurcation. Therefore, the phenomena reported in this thesis for heterogeneous pacemakers in oscillatory media and self-organized pacemakers in birhythmic media may be found in many reaction-diffusion systems. The analytical derivations in Chapters 3 and 4 are based on the phase dynamics approximations of the respective amplitude equations. Since phase equations may be derived independently from bifurcations for systems displaying harmonic oscillations, the results found here may hold for general systems displaying harmonic oscillations. As known for Hopf or Turing bifurcations, it can be expected that the results based on amplitude equations remain (at least, qualitatively) applicable even at larger distances from the bifurcation point, where the oscillations become anharmonic. From these arguments the conclusion may be drawn that the results for heterogeneous and self-organized pacemakers as described in this thesis may be generally found for oscillatory and birhythmic media.

Since the FitzHugh-Nagumo model is a paradigmatic model for excitable systems, the simple extension of the FitzHugh-Nagumo equations discussed in this thesis may also be

applicable to many excitable media. The fact that stable self-organized pacemakers have not only been found in the excitable regime of that model, but also in the regime of relaxational oscillations strongly suggest that the appearance of such patterns is not restricted to a small parameter regime.

Summarizing the results from this point of view, it seems possible that stable self-organized pacemakers are generic for three-component reaction-diffusion systems in both oscillatory and excitable media.

This thesis opens perspectives for experimental investigations. The findings for excitable pacemakers may stimulate the search for such patterns in the excitable, close to oscillatory regimes of various reaction-diffusion systems. Some experiments, where heterogeneous pacemakers have been created in the light-sensitive BZ reaction and the CO oxidation reaction, have already been performed. Further studies could try to explore large or high-frequency pacemakers. Since the Oregonator model of the BZ reaction is known to have a birhythmic regime, it may be of interest to search for birhythmicity and the formation of self-organized pacemakers in this reaction.

Chapter A

Appendix

A.1 Remarks on the parameter ω in the CGLE

It is useful to make a remark on the choice of the frequency parameter ω in the simulations. In principle, ω can be determined from the underlying reaction-diffusion system. However, it has been made clear in Sec. 2.3 that ω can be scaled out of the CGLE. This means that if this parameter is present in the equation, it can be chosen freely. Then, of course, the parameter ω does not correspond to a frequency of the original reaction-diffusion system but to the frequency at which an arbitrarily chosen coordinate frame is rotating. Four possible cases are of interest here:

- $\omega \gg 1$

  This choice of ω would closely resemble a reaction-diffusion system close to a Hopf bifurcation (see Sec. 2.3). However, the numerical time integration step becomes very small in this case, and simulations become inefficient. The numerical advantage to use a rescaled amplitude equation instead of a full reaction-diffusion model vanishes in this limit since the simulation time for a reaction-diffusion model may be $20 - 50$ times larger than for a corresponding amplitude equation [178].

- $\omega = -\alpha$

  The frequency of uniform oscillations is $\omega_{\mathrm{SL}} = \omega + \alpha$. If $\omega = -\alpha$, then a coordinate frame is chosen that rotates with the frequency of uniform oscillations. This means that in such a system the waves propagate in different directions depending on whether their frequency is increased or decreased with respect to the frequency of uniform oscillations.

- $\omega = 0$

  This possibility corresponds to a complete rescaling of CGLE (and not to a vanishing Hopf frequency) and is the typical case which is discussed in large part of the literature on the CGLE. Then, the waves may also propagate in different directions depending on the parameters and the wavenumber of the waves. It should be emphasized that these effects do not reflect the real behavior of a reaction-diffusion system.

- $\omega > \max(-\alpha, -\beta)$

  If this condition is fulfilled, all plane waves propagate into the same direction, independent of their wavenumber and the specific parameters. The artificial effects described in the previous two cases are avoided. If ω is still of the same order as α and β, the numerical simulation is not slowed down as in the case $\omega \gg 1$. Furthermore, space-time diagrams obtained for such a parameter choice correspond qualitatively to real reaction-diffusion systems and nevertheless display the interesting effects in a convenient way.

In the simulations of Chapter 3, the parameter ω usually is chosen such that the last criterion is fulfilled. In the simulations of Chapter 4, usually $\omega = 0$ is chosen.

A.2 Derivation of the normal form and the amplitude equations

The derivation of the normal form and the amplitude equations for the pitchfork-Hopf bifurcation is spilt into two parts. First, systems without diffusion are discussed, which are described by sets of ordinary differential equations. Subsequently, the terms corresponding to the effects of diffusion are calculated. This derivation is due to the collaboration with Mads Ipsen who recently discussed the derivation of the normal form coefficients for bifurcations of stationary points in the context of reaction-diffusion systems [74]. The notations in this part of the appendix are chosen in accordance with these works.

The normal form of the pitchfork-Hopf bifurcation

Consider a dynamical system, described by a vector $\mathbf{x} \in \mathbb{R}^n$, and depending on a set of parameters $\boldsymbol{\mu} \in \mathbb{R}^s$. The system is supposed to have a stationary point $\mathbf{x}_{\mathrm{s}}(\boldsymbol{\mu})$ at which a local bifurcation occurs at $\boldsymbol{\mu} = \mathbf{0}$. This stationary point shall be chosen as the origin of the phase space. The system evolves with time according to the equation

$$\dot{\mathbf{x}} = \mathbf{F}(\mathbf{x}; \boldsymbol{\mu}) = \mathbf{J} \cdot \mathbf{x} + \mathbf{f}(\mathbf{x}, \boldsymbol{\mu}). \tag{A.1}$$

It is assumed that the Jacobian matrix at the stationary point at the bifurcation, $\mathbf{J} = D\mathbf{F}(\mathbf{0}, \mathbf{0})$, has r semisimple critical eigenvalues λ_i whose real parts are zero. These eigenvalues are associated with r linearly independent pairs of right and left eigenvectors $\mathbf{u}_i$ and $\mathbf{u}_i^*$, normalized according to

$$\mathbf{u}_i^* \cdot \mathbf{u}_j = \delta_{ij}, \quad \text{for} \ \ i, j = 1, \ldots, r. \tag{A.2}$$

The r-dimensional center manifold W^{c} at $\boldsymbol{\mu} = \mathbf{0}$ is tangent to the center subspace E^{c} at $\mathbf{x} = \mathbf{0}$, which is spanned by the r right eigenvectors $\mathbf{u}_i$.

For $\boldsymbol{\mu} \neq 0$, the expression for the unfolded center manifold $W^{\mathrm{c}}(\boldsymbol{\mu})$ in terms of coordinates y_i of $\mathbf{y} \in E^{\mathrm{c}}$ in a basis of critical eigenvectors $\mathbf{u}_i$ is given by

$$\mathbf{x} = \mathbf{y} + \mathbf{h}(\mathbf{y}, \boldsymbol{\mu}) = \sum_{i=1}^{r} y_i \mathbf{u}_i + \sum_{\mathbf{pq}} \mathbf{h}_{\mathbf{pq}} \mathbf{y}^{\mathbf{p}} \boldsymbol{\mu}^{\mathbf{q}}, \tag{A.3}$$

with integer sets $\mathbf{p} = (p_1, \ldots, p_r)$, $\mathbf{q} = (q_1, \ldots, q_s)$, and $\mathbf{y}^{\mathbf{p}} = \prod_i y_i^{p_i}$, $\boldsymbol{\mu}^{\mathbf{q}} = \prod_j \mu_j^{q_j}$.

The normal form, determining the dynamics on the unfolded center manifold, is given by a system of coupled equations

$$\dot{y}_i = \lambda_i y_i + \sum_{\mathbf{pq}}^{i} \mathbf{u}_i^* \cdot \mathbf{f_{pq}} \mathbf{y}^\mathbf{p} \boldsymbol{\mu}^\mathbf{q} \Delta(\mathbf{p} \cdot \boldsymbol{\lambda} - \lambda_i), \tag{A.4}$$

where $\Delta(s) = 1$ for $s = 0$, and $\Delta(s) = 0$ otherwise. Thus, the sum in Eq. (A.4) is effectively taken over all possible sets $\mathbf{p}$ for which the resonance condition for this i'th component is satisfied, i.e.

$$\mathbf{p} \cdot \boldsymbol{\lambda} = \sum_{j=1}^{r} p_j \lambda_j = \lambda_i. \tag{A.5}$$

In the following, a set $\mathbf{p}$ is called *resonant*, if the condition (A.5) is satisfied for at least one component $i = 1, \ldots, r$. In Eq. (A.4), the vectors $\mathbf{f_{pq}}$ are coefficients in the expansion of the vector field $\mathbf{f}(\mathbf{x}, \boldsymbol{\mu})$ on the unfolded center manifold $W^c(\boldsymbol{\mu})$ defined as

$$\mathbf{f}(\mathbf{y} + \mathbf{h}(\mathbf{y}, \boldsymbol{\mu}), \boldsymbol{\mu}) = \sum_{\mathbf{pq}} \mathbf{f_{pq}} \mathbf{y}^\mathbf{p} \boldsymbol{\mu}^\mathbf{q}. \tag{A.6}$$

The procedure that should be used to determine the coefficient vectors $\mathbf{h_{pq}}$ in Eq. (A.3) is systematically presented in Ref. [74].

For any nonresonant set $\mathbf{p}$, these vectors are solutions of the system linear equations

$$\mathbf{A_p} \cdot \mathbf{h_{pq}} = -\boldsymbol{\Phi_{pq}}, \tag{A.7}$$

where the matrix $\mathbf{A_p}$ is given by

$$\mathbf{A}_p = \mathbf{J} - \sum_{j=1}^{r} p_j \lambda_j \mathbf{I}, \tag{A.8}$$

and $\mathbf{I}$ is the unity matrix. Here, the "source term" $\boldsymbol{\Phi_{pq}}$ is a complicated function of the lower-order solutions $\mathbf{h_{p'q'}}$ for which a general closed expression is given in Ref. [74]. The order p of any given set $\mathbf{p}$ is defined as $p = \sum_{i=1}^{r} p_i$. The order of a set $\mathbf{q}$ is defined similarly.

For a resonant set $\mathbf{p}$, the matrix $\mathbf{J} - \sum_{j=1}^{r} p_j \lambda_j \mathbf{I}$ is singular. In this case, operators $\mathbf{R_p}$ and $\mathbf{Q_p}$ are introduced such that $\mathbf{R_p}$ projects onto the null-space of $\mathbf{A_p}$ and $\mathbf{Q_p} = \mathbf{I} - \mathbf{R_p}$, namely

$$\mathbf{R_p} \cdot \mathbf{x} = (\mathbf{I} - \mathbf{Q_p}) \cdot \mathbf{x} = \sum_{i=1}^{r} (\mathbf{u}_i^* \cdot \mathbf{x}) \mathbf{u}_i \Delta(\mathbf{p} \cdot \boldsymbol{\lambda} - \lambda_i). \tag{A.9}$$

Under resonance conditions, the vectors $\mathbf{h_{pq}}$ are given by solutions of the equations

$$\mathbf{A_p} \cdot \mathbf{h_{pq}} = -\mathbf{Q_p} \cdot \boldsymbol{\Phi_{pq}}, \tag{A.10}$$

with the additional constraint that $\mathbf{h_{pq}}$ should be orthogonal to the null-space of $\mathbf{A_p}$, i.e.

$$\mathbf{R_p} \cdot \mathbf{h_{pq}} = 0. \tag{A.11}$$

Since $\boldsymbol{\Phi_{pq}}$ depends on lower order solutions $\mathbf{h_{p'q'}}$, the system of equations (A.7) and (A.10) should be solved iteratively starting from the lowest order.

Now, the specific bifurcation is considered at which the spectrum of critical eigenvalues consists of one pair of complex conjugate, imaginary eigenvalues and one real eigenvalue equal to zero. First, the generic case is discussed, which is a fold-Hopf bifurcation, and then the additional requirements necessary for a pitchfork-Hopf bifurcation to take place are described.

Only terms up to linear order in the bifurcation parameters $\boldsymbol{\mu}$ (i.e. $|\mathbf{q}| = 0, 1$) are kept. In this case, contributions of different components μ_i of $\boldsymbol{\mu}$ are additive, and for simplicity a single parameter μ corresponding to the case where $\mathbf{q}$ is a simple scalar q is considered: The generalization to several parameters is straightforward. In addition, the notation is simplified by assigning

$$\lambda_{1,2} = \pm \mathrm{i}\omega_0 \quad \text{and} \quad \lambda_3 = 0 \tag{A.12}$$

for the eigenvalues at the bifurcation point. The notation $\mathbf{u}_1 = \mathbf{u}$, $\mathbf{u}_2 = \overline{\mathbf{u}}$, and $\mathbf{u}_3 = \mathbf{v}$ is used for the corresponding right eigenvectors. In this case, only the amplitudes for y_1 and y_3 need to be considered, because complex conjugation gives $y_2 = \overline{y_1}$ (to simplify the notation, $A = y_1 \mathrm{e}^{-\mathrm{i}\omega_0 t}$ and $z = y_3$ is defined). Generically, this situation corresponds to a fold-Hopf bifurcation, for which the general structure of the normal form can be found immediately using Eq. (A.4) and Eq. (A.5)

$$\dot{A} = \sigma_1 \mu A + g_0 A z + g_1 |A|^2 A + g_2 A z^2, \tag{A.13a}$$

$$\dot{z} = \sigma_2 \mu + \sigma_3 \mu z + c_0 |A|^2 + c_1 z^2 + c_2 |A|^2 z + c_3 z^3, \tag{A.13b}$$

where all terms up to third order in A and z are included for $q = 0$ and only terms essential to the unfolding for $q = 1$. The coefficients in the equation for A are complex (although the imaginary part of $\sigma_1 \mu$ can always be scaled out), the coefficients appearing in the equation for z are real.

To find the coefficients in Eq. (A.13) explicitly, first the expressions for the coefficient vectors $\mathbf{f_{pq}}$ given by Eq. (A.6) are determined. To third order, the expansion of the center

manifold given by Eq. (A.3) becomes

$$
\begin{aligned}
\mathbf{x} = &\mathbf{u}A + \overline{\mathbf{u}}\,\overline{A} + \mathbf{v}z + (\mathbf{h}_{2000}A^2 + \text{c.c.}) + \mathbf{h}_{1100}|A|^2 + \mathbf{h}_{0020}z^2 + (\mathbf{h}_{1010}Az + \text{c.c.}) + \\
&(\mathbf{h}_{3000}A^3 + \mathbf{h}_{2100}|A|^2A + \text{c.c.}) + (\mathbf{h}_{2010}A^2z + \mathbf{h}_{1020}Az^2 + \text{c.c.}) + \\
&\mathbf{h}_{1110}|A|^2z + \mathbf{h}_{0030}z^3 + (\mathbf{h}_{0001} + \mathbf{h}_{1001}A + \mathbf{h}_{0101}\overline{A} + \mathbf{h}_{0011}z)\mu,
\end{aligned}
$$

$$(A.14)$$

where "c.c." denotes the complex conjugate of all preceding terms within a given bracket.

Substituting Eq. (A.14) into the Taylor expansion of the expression on the right-hand side of Eq. (A.1), and collecting terms of the same order in A, $\overline{A}$, z, and μ, the following contributions to the coefficient vectors $\mathbf{f}_{\mathbf{pq}}$ are found:

$$
\begin{aligned}
\mathbf{f}_{1010} &= \mathbf{F}_{\mathbf{xx}}(\mathbf{u}, \mathbf{v}), \\
\mathbf{f}_{2100} &= \mathbf{F}_{\mathbf{xx}}(\mathbf{u}, \mathbf{h}_{1100}) + \mathbf{F}_{\mathbf{xx}}(\overline{\mathbf{u}}, \mathbf{h}_{2000}) + \tfrac{1}{2}\mathbf{F}_{\mathbf{xxx}}(\mathbf{u}, \mathbf{u}, \overline{\mathbf{u}}), \\
\mathbf{f}_{1020} &= \mathbf{F}_{\mathbf{xx}}(\mathbf{u}, \mathbf{h}_{0020}) + \mathbf{F}_{\mathbf{xx}}(\mathbf{v}, \mathbf{h}_{1010}) + \tfrac{1}{2}\mathbf{F}_{\mathbf{xxx}}(\mathbf{u}, \mathbf{v}, \mathbf{v}), \\
\mathbf{f}_{1010} &= \mathbf{F}_{\mathbf{xx}}(\mathbf{u}, \overline{\mathbf{u}}), \\
\mathbf{f}_{0020} &= \tfrac{1}{2}\mathbf{F}_{\mathbf{xx}}(\mathbf{v}, \mathbf{v}), \\
\mathbf{f}_{1110} &= \mathbf{F}_{\mathbf{xx}}(\mathbf{u}, \mathbf{h}_{0110}) + \mathbf{F}_{\mathbf{xx}}(\overline{\mathbf{u}}, \mathbf{h}_{1010}) + \mathbf{F}_{\mathbf{xx}}(\mathbf{v}, \mathbf{h}_{1100}) + \mathbf{F}_{\mathbf{xxx}}(\mathbf{u}, \overline{\mathbf{u}}, \mathbf{v}), \\
\mathbf{f}_{0030} &= \mathbf{F}_{\mathbf{xx}}(\mathbf{v}, \mathbf{h}_{0020}) + \tfrac{1}{6}\mathbf{F}_{\mathbf{xxx}}(\mathbf{v}, \mathbf{v}, \mathbf{v}), \\
\mathbf{f}_{0001} &= \mathbf{F}_{\mu}, \\
\mathbf{f}_{1001} &= \mathbf{F}_{\mathbf{x}\mu}\cdot\mathbf{u} + \mathbf{F}_{\mathbf{xx}}(\mathbf{u}, \mathbf{h}_{0001}), \\
\mathbf{f}_{0011} &= \mathbf{F}_{\mathbf{x}\mu}\cdot\mathbf{v} + \mathbf{F}_{\mathbf{xx}}(\mathbf{v}, \mathbf{h}_{0001}),
\end{aligned}
$$

$$(A.15)$$

where the following notations are used

$$
\mathbf{F}_{\mathbf{xx}}(\mathbf{x}, \mathbf{x}) = \sum_{i,j=1}^{n} \frac{\partial^2 \mathbf{F}}{\partial x_i \partial x_j} x_i x_j, \qquad \mathbf{F}_{\mathbf{xxx}}(\mathbf{x}, \mathbf{x}, \mathbf{x}) = \sum_{i,j,k=1}^{n} \frac{\partial^3 \mathbf{F}}{\partial x_i \partial x_j \partial x_k} x_i x_j x_k,
$$

$$
\mathbf{F}_{\mu} = \frac{\partial \mathbf{F}}{\partial \mu}, \qquad \mathbf{F}_{\mathbf{x}\mu}\cdot\mathbf{x} = \sum_{i=1}^{n} \frac{\partial^2 \mathbf{F}}{\partial x_i \partial \mu} x_i, \quad \text{etc.}
$$

$$(A.16)$$

The coefficient vectors $\mathbf{h}_{ijkl}$ are determined by solving the corresponding system of linear equations (A.7) and (A.10). Using Eq. (A.4), the expressions for the coefficients in Eq. (A.13) can be written as

$$
\begin{aligned}
g_0 &= \mathbf{u}^*\cdot\mathbf{f}_{1010}, & g_1 &= \mathbf{u}^*\cdot\mathbf{f}_{2100}, & g_2 &= \mathbf{u}^*\cdot\mathbf{f}_{1020}, \\
c_0 &= \mathbf{v}^*\cdot\mathbf{f}_{1100}, & c_1 &= \mathbf{v}^*\cdot\mathbf{f}_{0020}, & c_2 &= \mathbf{v}^*\cdot\mathbf{f}_{1110}, & c_3 &= \mathbf{v}^*\cdot\mathbf{f}_{0030}, \\
\sigma_1 &= \mathbf{u}^*\cdot\mathbf{f}_{1001}, & \sigma_2 &= \mathbf{v}^*\cdot\mathbf{f}_{0001}, & \sigma_3 &= \mathbf{v}^*\cdot\mathbf{f}_{0011}.
\end{aligned}
$$

$$(A.17)$$

The case of a pitchfork-Hopf bifurcation is a special case of the fold-Hopf bifurcation, which satisfies

$$c_1 = \tfrac{1}{2}\mathbf{v}^* \cdot \mathbf{F_{xx}}(\mathbf{v}, \mathbf{v}) = 0. \tag{A.18}$$

Defining $\eta_i = \sigma_i \mu$ for $i = 1, 2, 3$, system (A.13) transforms into

$$\dot{A} = \eta_1 A + g_0 A z + g_1 |A|^2 A + g_2 A z^2, \tag{A.19a}$$

$$\dot{z} = \eta_2 + \eta_3 z + c_0 |A|^2 + c_2 |A|^2 z + c_3 z^3, \tag{A.19b}$$

which is the complete unrescaled normal form of the pitchfork-Hopf bifurcation.

The amplitude equations of the pitchfork-Hopf bifurcation

When the system described by Eq. (A.1) is modified by introducing diffusion of the involved species, the time evolution of the system is governed by a reaction-diffusion equation

$$\partial_t \mathbf{x} = \mathbf{F}(\mathbf{x}; \boldsymbol{\mu}) + \mathbf{D} \cdot \nabla^2 \mathbf{x}, \tag{A.20}$$

where $\mathbf{x} = \mathbf{x}(\mathbf{r}, t)$ and $\mathbf{D}$ is a diagonal diffusion matrix.

In reaction-diffusion systems, diffusion may take the local concentrations away from the center manifold W^c even if they initially were on W^c everywhere. However, close to the bifurcation, the motion on the unfolded center manifold due to local interactions typically is much slower than the motion transverse to it. Consequently, diffusion never takes the system far away from that "slow manifold", so the evolution of the spatially extended system may be approximately described by Eq. (A.20) with $\mathbf{x}$ restrained to move on the slow manifold $W^c(\boldsymbol{\mu})$ given by Ref. (A.3).

Therefore, to get a differential equation in $\mathbf{y}$, the right-hand side of Eq. (A.3) may be substituted in Eq. (A.20). The appropriate solution to the resulting equation is then transformed by Eq. (A.3) to the motion in the center manifold, the approximate solution to the reaction-diffusion equation (A.20).

Just as in the derivation of the normal form (A.13), the discussion is restricted to a bifurcation with a single pair of complex conjugate imaginary eigenvalues $\pm i\omega_0$ together with any number of semisimple eigenvalues. There are r such critical eigenvalues (counting multiplicity) and r linearly independent right eigenvectors and corresponding left eigenvectors satisfying the biorthonormality relations (A.2). The period of the oscillations near $\mathbf{x} = \mathbf{0}$ at $\boldsymbol{\mu} = \mathbf{0}$ is $T = 2\pi/\omega_0$.

The solution $\mathbf{y}(\mathbf{r}, t)$ may be expressed as the modulation of harmonic oscillations of frequency ω_0 for the oscillatory mode. To find an equation for the modulation, it is convenient to view $\mathbf{y}$ as a function of two independent time variables, τ and θ, with θ accounting for the (fast) harmonic oscillation and τ describing the (slow) modulation of the dynamics. Specifically, it is possible to define

$$\mathbf{y}(\mathbf{r}, \tau, \theta) = e^{\mathbf{J}\theta} \cdot \mathbf{z}(\mathbf{r}, \tau) = \sum_{i=1}^{r} e^{\lambda_i \theta} z_i(\mathbf{r}, \tau) \mathbf{u}_i, \tag{A.21}$$

where z_i are newly introduced amplitudes that should not be confounded with the amplitude z of the real mode introduced above. At the end of the calculation, $\tau = \theta = t$ shall be chosen. Through Eq. (A.1) and in terms of the new time variables, the reaction-diffusion equation (A.20) may be written as

$$\partial_\tau \mathbf{x} = (\mathbf{J} \cdot \mathbf{x} - \partial_\theta \mathbf{x}) + \mathbf{f}(\mathbf{x}, \boldsymbol{\mu}) + \mathbf{D} \cdot \nabla^2 \mathbf{x}. \tag{A.22}$$

The linear operators P_i are now defined as

$$P_i[\mathbf{g}(\theta)] = \frac{1}{T} \int_0^T e^{-\lambda_i \theta} \mathbf{u}_i^* \cdot \mathbf{g}(\theta) d\theta. \tag{A.23}$$

Since

$$\partial_\tau \mathbf{y} = e^{\mathbf{J}\theta} \cdot \partial_\tau \mathbf{z} = \sum_{i=1}^{r} \partial_\tau z_i e^{\lambda_i \theta} \mathbf{u}_i, \tag{A.24}$$

it is $P_i[\partial_\tau \mathbf{y}] = \partial_\tau z_i$, and therefore it is possible to extract an equation for $\partial_\tau z_i$ by applying P_i to both sides of Eq. (A.22). As shown in Ref. [163], the following identities hold for P_i

$$P_i[\partial_\tau \mathbf{h}] = 0 \quad \text{and} \quad P_i[\mathbf{J} \cdot \mathbf{x} - \partial_\theta \mathbf{x}] = 0, \tag{A.25}$$

and application of P_i to Eq. (A.22) therefore gives

$$\partial_\tau z_i = \frac{1}{T} \int_0^T e^{-\lambda_i \theta} \mathbf{u}_i^* \cdot \mathbf{f}(\mathbf{y} + \mathbf{h}(\mathbf{y}, \boldsymbol{\mu})) d\theta + \frac{1}{T} \int_0^T e^{-\lambda_i \theta} \mathbf{u}_i^* \cdot \mathbf{D} \cdot \nabla^2 (\mathbf{y} + \mathbf{h}(\mathbf{y}, \boldsymbol{\mu})) d\theta. \tag{A.26}$$

By observing

$$\mathbf{y}^{\mathbf{P}} = \prod_i y_i^{p_i} = \exp\left(\sum_i p_i \lambda_i \theta\right) \prod_i z_i^{p_i} = e^{\mathbf{p} \cdot \boldsymbol{\lambda} \theta} \mathbf{z}^{\mathbf{P}}, \tag{A.27}$$

the first integral term in Eq. (A.26) involving $\mathbf{f}(\mathbf{x}, \boldsymbol{\mu})$ can be determined as

$$\frac{1}{T} \int_0^T e^{-\lambda_i \theta} \mathbf{u}_i^* \cdot \mathbf{f}(\mathbf{y} + \mathbf{h}(\mathbf{y}, \boldsymbol{\mu})) d\theta = \frac{1}{T} \sum_{\mathbf{pq}} \mathbf{u}_i^* \cdot \mathbf{f}_{\mathbf{pq}} \mathbf{z}^{\mathbf{P}} \boldsymbol{\mu}^{\mathbf{q}} \int_0^T e^{(\mathbf{p} \cdot \boldsymbol{\lambda} - \lambda_i)\theta} d\theta$$

$$= \sum_{\mathbf{pq}}^{i} \mathbf{u}_i^* \cdot \mathbf{f}_{\mathbf{pq}} \mathbf{z}^{\mathbf{P}} \boldsymbol{\mu}^{\mathbf{q}}, \tag{A.28}$$

where the last sum is taken over all sets $(\mathbf{p}, \mathbf{q})$ for which the resonance condition (A.5) for the i'th component is satisfied. All other terms vanish because of the integral of the exponential in Eq. (A.28).

For the diffusion part of Eq. (A.26), a nonlinear term arises because the motion is restrained to the slow manifold. Diffusion is linear in $\mathbf{x}$ but since the dynamics is described in terms of points $\mathbf{y} \in E^c$, diffusion is not linear in $\mathbf{y}$. However, it can be expected that the linear diffusion terms will dominate over the nonlinear diffusion, and these higher order terms may therefore be neglected in first approximation. For the diffusion term of Eq. (A.22), it follows

$$
\frac{1}{T} \int_0^T e^{-\lambda_i \theta} \mathbf{u}_i^* \cdot \mathbf{D} \cdot \nabla^2 (\mathbf{y} + \mathbf{h}(\mathbf{y}, \boldsymbol{\mu})) d\theta = \frac{1}{T} \int_0^T e^{-\lambda_i \theta} \mathbf{u}_i^* \cdot \mathbf{D} \cdot \nabla^2 \mathbf{y} d\theta
$$
$$
= \sum_j \mathbf{u}_i^* \cdot \mathbf{D} \cdot \mathbf{u}_j \nabla^2 z_j \frac{1}{T} \int_0^T e^{(\lambda_j - \lambda_i)\theta} d\theta
$$
$$
= \mathbf{u}_i^* \cdot \mathbf{D} \cdot \mathbf{u}_i. \tag{A.29}
$$

By using Eqs. (A.28) and (A.29), an amplitude equation for the modulation is obtained as a set of coupled equations for the set of all coefficients $z_i(\mathbf{r}, \tau)$ defined in Eq. (A.21),

$$
\partial_t z_i = \sum_{\mathbf{pq}}^i \mathbf{u}_i^* \cdot \mathbf{f_{pq}} \mathbf{z^p} \boldsymbol{\mu^q} + d_i \nabla^2 z_j, \quad \text{where } d_i = \mathbf{u}_i^* \cdot \mathbf{D} \cdot \mathbf{u}_i, \tag{A.30}
$$

where the sum is taken over all sets $(\mathbf{p}, \mathbf{q})$ for which the resonance condition (A.5) for the i'th component is satisfied. Here, τ is identified with the "real" time t, since there is no longer a need to distinguish between the two formal time variables t and τ. An equivalent rescaled normal form, similar to Eq. (A.30), may also be expressed for the uniform system given by Eq. (A.1). This is obtained by insertion of the rescaling (A.21) in Eq. (A.4), which then yields an expression for the normal form in terms of the amplitudes z_i, namely

$$
\dot{z}_i = \sum_{\mathbf{pq}}^i \mathbf{u}_i^* \cdot \mathbf{f_{pq}} \mathbf{z^p} \boldsymbol{\mu^q}. \tag{A.31}
$$

From a solution $z_i(\mathbf{r}, t)$ $(i = 1, \dots, r)$ to Eq. (A.30), an approximate solution to the reaction-diffusion equation (A.20) is obtained as

$$
\mathbf{x}(\mathbf{r}, t) = \mathbf{y}(\mathbf{r}, t) + \mathbf{h}(\mathbf{y}(\mathbf{r}, t), \boldsymbol{\mu}), \tag{A.32a}
$$

$$
\mathbf{y}(\mathbf{r}, t) = \sum_{i=1}^r z_i(\mathbf{r}, t) e^{\lambda_i t} \mathbf{u}_i. \tag{A.32b}
$$

Note that the transformation $\mathbf{h}$ produces higher-order harmonics of the form $\mathrm{e}^{\mathrm{i}k\omega_0 t}$ ($|k| \neq 1$) in the plane of oscillations and also generates components off the center subspace E^c. Of course, these terms are also modulated (by products of powers of the amplitudes z_i) and are therefore not periodic in t.

The only difference between the amplitude equation (A.30) derived for a reaction-diffusion system and the normal form (A.31) for the ODE system is the presence of the additional diffusion term. The derivation of the particular amplitude equation for a distributed system undergoing a pitchfork-Hopf bifurcation is therefore a relatively simple task, since the result (A.19) for the ODE system only needs to be modified by addition of the diffusion terms $d_i = \mathbf{u}_i^* \cdot \mathbf{D} \cdot \mathbf{u}_i$. In accordance with the notation used in Sec. 4.1.1, the amplitude equation for the distributed pitchfork-Hopf bifurcation is given by

$$\partial_t A = \eta_1 A + g_0 A z + g_1 |A|^2 A + g_2 A z^2 + d_A \nabla^2 A, \qquad d_A = \mathbf{u}^* \cdot \mathbf{D} \cdot \mathbf{u}, \qquad \text{(A.33a)}$$

$$\partial_t z = \eta_2 + \eta_3 z + c_0 |A|^2 + c_2 |A|^2 z + c_3 z^3 + d_z \nabla^2 z, \qquad d_z = \mathbf{v}^* \cdot \mathbf{D} \cdot \mathbf{v}. \qquad \text{(A.33b)}$$

A.3   Simplification of the amplitude equations

Here, the conditions are discussed under which the normal form Eq. (4.1) (or Eq. (A.19)) for the pitchfork-Hopf bifurcation can be reduced to the simpler case given by Eq. (4.2).

The normal form of a uniform reaction-diffusion system close to the pitchfork-Hopf bifurcation is given by Eq. (A.19),

$$\dot{A} = \eta_1 A + g_0 A z + g_1 |A|^2 A + g_2 A z^2, \tag{A.34a}$$

$$\dot{z} = \eta_2 + \eta_3 z + c_0 |A|^2 + c_2 |A|^2 z + c_3 z^3, \tag{A.34b}$$

where η_1, g_0, g_1 and g_2 are complex, η_2, η_3, c_0, c_2, and c_3 real coefficients. Real and imaginary parts are denoted as $\eta_1 = \eta_1^r + i\eta_1^i$; no confusion with the index i and the number r of eigenvalues (both used above), or the amplitude of oscillations r (used below) should occur. A simple rescaling $A = \exp(i\eta_1^i t)\tilde{A}$ and subsequent dropping of tildes and suppressing of the superscript r for η_1 then lead to Eqs. (A.34), where η_1 is now a real-valued parameter. In the following, the parameters η_1, η_2 and η_3 are regarded as the independent bifurcation parameters of the system, which are assumed to be small.

The usual transformation $A = r\exp(-i\phi)$ to phase ϕ and amplitude r yields

$$\dot{r} = \eta_1 r + g_0^r r z + g_1^r r^3 + g_2^r r z^2, \tag{A.35a}$$

$$\dot{z} = \eta_2 + \eta_3 z + c_0 r^2 + c_2 r^2 z + c_3 z^3, \tag{A.35b}$$

where the equation of the phase is omitted. In the following it is assumed that the Hopf and pitchfork bifurcations are supercritical, i.e. $g_1^r < 0$ and $c_3 < 0$.

Rescaling amplitude $r = \sqrt{-1/g_1^r}\,\tilde{r}$ and real mode $z = (1/g_0^r)\tilde{z}$, Eqs. (A.35) transform into

$$\dot{r} = \eta_1 r + rz - r^3 + \kappa_1 r z^2, \tag{A.36a}$$

$$\dot{z} = \tilde{\eta}_2 + \eta_3 z - \tilde{\gamma} r^2 + \kappa_2 r^2 z - \tilde{\nu} z^3, \tag{A.36b}$$

where the tildes of the amplitudes are dropped and $\kappa_1 = g_2^r/(g_0^r)^2$, $\kappa_2 = -c_2/g_1^r$, $\tilde{\eta}_2 = \eta_2 g_0^r$, $\tilde{\gamma} = g_0^r c_0/g_1^r$, and $\tilde{\nu} = -c_3/(g_0^r)^2$. The parameters that could be confounded with the parameters defined in Sec. 4.1.1 have tildes now. In the following, the effect of the terms κ_1 and κ_2 on the solutions obeying $\dot{r} = 0$ and $\dot{z} = 0$ is investigated. In particular, is must be ensured that the terms containing κ_1 and κ_2 do not contribute in a significant way to the solution in the birhythmic regime near the bifurcation point, i.e. for $|\eta_{1,2,3}| \ll 1$.

Limit cycles with a constant amplitude require $\dot{r} = 0$ and fulfill therefore

$$r^2 = \eta_1 + z + \kappa_1 z^2. \tag{A.37}$$

Note that the right-hand side of this equation must be positive. Inserting Eq. (A.37) into Eq. (A.36b), the following equation is yielded

$$\tilde{\eta}_2 - \tilde{\gamma}\eta_1 + (\eta_3 - \tilde{\gamma} + \kappa_2\eta_1)z + (\kappa_2 - \tilde{\gamma}\kappa_1)z^2 - (\tilde{\nu} - \kappa_1\kappa_2)z^3 = 0, \tag{A.38}$$

which is equivalent to

$$z^3 - \frac{\kappa_2 - \tilde{\gamma}\kappa_1}{\tilde{\nu} - \kappa_1\kappa_2}z^2 - \frac{\eta_3 - \tilde{\gamma} + \kappa_2\eta_1}{\tilde{\nu} - \kappa_1\kappa_2}z - \frac{\tilde{\eta}_2 - \tilde{\gamma}\eta_1}{\tilde{\nu} - \kappa_1\kappa_2} = 0. \tag{A.39}$$

The main argument is that in the appropriate limit for $\eta_{1,2,3}$, the three roots of Eq. (A.39) and the associated amplitudes of the limit cycles vanish simultaneously.

Reduced system

The argument is outlined first for the simple reduced system, where $\kappa_1 = \kappa_2 = 0$. In this case, Eq. (A.39) becomes

$$z^3 - \frac{\eta_3 - \tilde{\gamma}}{\tilde{\nu}}z - \frac{\tilde{\eta}_2 - \tilde{\gamma}\eta_1}{\tilde{\nu}} = 0. \tag{A.40}$$

A sufficient (not necessary) condition for bistability of z is that in Eq. (A.40) the constant term is zero and the coefficient of the linear term negative. This means

$$\tilde{\eta}_2 = \tilde{\gamma}\eta_1, \tag{A.41a}$$

$$\frac{\eta_3 - \tilde{\gamma}}{\tilde{\nu}} > 0. \tag{A.41b}$$

In general, the roots of z are calculated with the Cardan formula (*cf.* Sec. 4.1.2). Here, however, the constant term of Eq. (A.40) and one of its roots, z_2, are zero, and the roots $z_{1,3}$ are determined easily as

$$z_{1,3} = \mp\sqrt{\frac{\eta_3 - \tilde{\gamma}}{\tilde{\nu}}}. \tag{A.42}$$

Assuming that $|z| \ll 1$ for $|\eta_3| \ll 1$, i.e. the coupling of the amplitude to the real mode should not be too strong (the cusp points of the fixed point and the limit cycle shall not be separated too far from each other), means

$$\frac{|\tilde{\gamma}|}{\tilde{\nu}} \ll 1. \tag{A.43}$$

Also, since only small values of $\eta_{1,2,3}$ should be allowed, it has to be required that η_3 and $|\tilde{\gamma}|$ are of the same order because otherwise the roots $z_{1,3}$ cannot become zero, i.e.

$$|\tilde{\gamma}| \ll 1. \tag{A.44}$$

The condition of having a limit cycle with amplitude r associated with the roots $z_{1,3}$ is

$$\eta_1 \geq \sqrt{\frac{\eta_3 - \tilde{\gamma}}{\tilde{\nu}}}. \tag{A.45}$$

Therefore, if $\eta_3 \to \tilde{\gamma}$, then $z \to 0$ and $r \to \eta_1$. To every η_1 there exists an $\tilde{\eta}_2$ that fulfills Eq. (A.41a). Furthermore, for $\eta_1 \to 0$, the amplitude $r \to 0$ and $\tilde{\eta}_2 \to 0$ simultaneously.

Full system

Now, the coefficients κ_1 and κ_2 are nonvanishing. Equation (A.39) is rewritten as

$$z^3 - p_2 z^2 - p_1 z - p_0 = 0, \tag{A.46}$$

where

$$p_2 = \frac{\kappa_2 - \tilde{\gamma}\kappa_1}{\tilde{\nu} - \kappa_1\kappa_2}, \tag{A.47a}$$

$$p_1 = \frac{\eta_3 - \tilde{\gamma} + \kappa_2\eta_1}{\tilde{\nu} - \kappa_1\kappa_2}, \tag{A.47b}$$

$$p_0 = \frac{\tilde{\eta}_2 - \tilde{\gamma}\eta_1}{\tilde{\nu} - \kappa_1\kappa_2}. \tag{A.47c}$$

The main difference to the reduced model is the term p_2 which is nonvanishing and independent from the bifurcation parameters. In particular, it is not possible to have all three roots of z being exactly zero at the same time.

The bifurcation parameter $\tilde{\eta}_2$ can be chosen such that

$$\tilde{\eta}_2 = \tilde{\gamma}\eta_1, \tag{A.48}$$

is fulfilled and therefore $p_0 = 0$. In this case, one of the roots of Eq. (A.46), z_2, is zero. Then, the equation $z^2 - p_2 z - p_1 = 0$ gives two roots $z_{1,3} = \pm c + p_2/2$ (where $c = \sqrt{p_1 + p_2^2/4}$) which cannot be exactly zero at the same time. However, it is possible to tune c to zero by choosing

$$\eta_3 = \tilde{\gamma} - \kappa_2\eta_1 - (\kappa_2 - \tilde{\gamma}\kappa_1)^2/4. \tag{A.49}$$

In this case, the roots $z_{1,3}$ approach the common value $z_{1,3} \to p_2/2$. The roots $z_{1,3}$ become arbitrarily small for $|p_2| \ll 1$. This condition means that

$$\left| \frac{\kappa_2 - \tilde{\gamma}\kappa_1}{\tilde{\nu} - \kappa_1\kappa_2} \right| \ll 1. \tag{A.50}$$

For all coefficients κ_1 and κ_2 there is a value of $\tilde{\nu}$ that fulfills this condition. If the coefficients κ_1 and κ_2 are not larger than of order unity, the condition (A.50) becomes $\tilde{\nu} \gg 1$, which is assumed in this work. To summarize, the conditions

$$|\tilde{\gamma}| \ll 1 \qquad \text{and} \qquad \tilde{\nu} \gg 1 \tag{A.51}$$

should be fulfilled in order that the reduction of Eq. (4.1) to Eq. (4.2) holds.

A.4   Details of the numerical integration

The simulations presented in this thesis were obtained using a variety of software. In particular, following applications have been used:

- *The Virtual Laboratory.* This simulation platform was developed by Alexander von Oertzen in the Fritz Haber Institute of the Max Planck Society for the interactive simulation and graphical representation of reaction-diffusion systems in one and two spatial dimensions. The author of this thesis has maintained this software during the last two years. The software is based on PV-WAVE, a product of VISUAL NUMERICS. The specific integration kernels must be written by the respective user of the platform, in this case by the author of this thesis. More details on the Virtual Laboratory can be found in Ref. [179].

- *Simulations of the amplitude equations.* The models discussed in Chapters 3 and 4 have been integrated with an explicit Euler method. The Laplacian operator is discretized with a nearest-neighbor (*Five-point Laplacian*) approximation and the Virtual Laboratory is used throughout. For the amplitude equations of the pitchfork-Hopf bifurcation, the numerical accuracy has been tested by repeating several simulations using a fourth-order explicit Runge-Kutta scheme and a stiff implicit Gear method.

- *Simulations of the extended FitzHugh-Nagumo model.* The model of Chapter 5 has been integrated with an explicit Euler method in the one-dimensional domain, using the Virtual Laboratory. Two-dimensional simulations have been performed using the DVODE solver of ODEPACK, a collection of FORTRAN solvers. The Laplacian operator is again discretized with a nearest-neighbor approximation.

Bibliography

[1] M. C. Cross and P. C. Hohenberg, Rev. Mod. Phys. **65**, 851 (1993).

[2] *Chemical Waves and Patterns*, edited by R. Kapral and K. Showalter (Kluwer Academic Publishers, Dordrecht, 1995).

[3] D. Walgraef, *Spatio-Temporal Pattern Formation* (Springer, New York, 1997).

[4] *Nonlinear Evolution of Spatio-Temporal Structures in Dissipative Continuous Systems*, edited by F. H. Busse and L. Kramer (Plenum Press, New York, 1990).

[5] Y. J. Li, J. Oslonovitch, N. Mazouz, F. Plenge, K. Krischer, and G. Ertl, Science **291**, 2395 (2001).

[6] E. Schöll, *Nonlinear Spatio-Temporal Dynamics and Chaos in Semiconductors* (Cambridge University Press, Cambridge, 2001).

[7] *Self-organization in activator-inhibitor-systems: semiconductors, gas-discharge and chemical active media*, edited by H. Engel, F. Niedernostheide, H. Purwins, and E. Schöll (Wissenschaft und Technik, Berlin, 1996).

[8] T. Ackemann and W. Lange, Appl. Phys. B **72**, 21 (2001).

[9] P. B. Umbanhowar, F. Melo, and H. L. Swinney, Nature **382**, 793 (1996).

[10] A. T. Winfree, J. Biosci. **27**, 465 (2002).

[11] A. V. Holden, Physics World, November 1998, 29 (1998).

[12] H. Haken, *Brain Dynamics* (Springer, Berlin, 2002).

[13] M. A. Dahlem, Ph.D. thesis, Otto-von-Guericke-Universität Magdeburg, 2000.

[14] J. D. Murray, *Mathematical Biology* (Springer, Berlin, 1989).

[15] A. Goldbeter, *Biochemical Oscillations and Cellular Rhythms* (Cambridge University Press, Cambridge, 1996).

[16] P. Ball, *The Self-Made Tapestry: Pattern Formation in Nature* (Oxford University Press, Oxford, 1999).

[17] J. Lechleiter, S. Girard, E. Peralta, and D. Clapham, Science **252**, 123 (1991).

[18] O. Steinbock and S. C. Müller, Z. Naturforsch. C **50**, 275 (1995).

[19] B. Blasius, A. Huppert, and L. Stone, Nature **399**, 354 (1999).

[20] S. H. Strogatz, *Nonlinear Dynamics and Chaos* (Addison-Wesley, Reading, Massachusetts, 1994).

[21] B. P. Belousov, *Sbornik referatov po Radiatsionnoi Meditsine* (Medgiz, Moscow, 1959), p. 145, collections of abstracts on radiation medicine (in Russian).

[22] A. N. Zaikin and A. M. Zhabotinsky, Nature **255**, 535 (1970).

[23] A. M. Zhabotinsky and A. N. Zaikin, in *Oscillatory Processes in Biological and Chemical Systems*, Vol. 2 of *Transactions of All-Union Symposium*, edited by E. E. Sel'kov (Nauka, Pushchino on Oka, 1971), pp. 279–283, (in Russian).

[24] A. M. Zhabotinsky and A. N. Zaikin, J. Theor. Biol. **40**, 45 (1973).

[25] A. T. Winfree, Science **175**, 634 (1972).

[26] A. T. Winfree, Science **181**, 937 (1973).

[27] V. K. Vanag and I. R. Epstein, Science **294**, 835 (2001).

[28] V. K. Vanag and I. R. Epstein, Phys. Rev. Lett. **87**, 2283011 (2001).

[29] S. Jakubith, H. H. Rotermund, W. Engel, A. v. Oertzen, and G. Ertl, Phys. Rev. Lett. **65**, 3013 (1990).

[30] H. H. Rotermund, Surf. Sci. Rep. **29**, 265 (1997).

[31] M. Kim, M. Bertram, M. Pollmann, A. von Oertzen, A. S. Mikhailov, H. H. Rotermund, and G. Ertl, Science **292**, 1357 (2001).

[32] Y. A. Astrov and Y. A. Logvin, Phys. Rev. Lett. **79**, 2983 (1997).

[33] C. P. Schenk, M. Or-Guil, M. Bode, and H.-G. Purwins, Phys. Rev. Lett. **78**, 3781 (1997).

[34] J. J. Tyson, K. A. Alexander, V. S. Manoranjan, and J. D. Murray, Physica D **34**, 193 (1989).

[35] H. Haken, *Synergetics. An Introduction* (Springer, Berlin, 1977).

[36] P. Glandsdorff and I. Prigogine, *Thermodynamic Theory of Structure, Stability and Fluctuations* (Wiley, New York, 1971).

[37] G. Nicolis and I. Prigogine, *Self-Organization in Nonequilibrium Systems* (Wiley, New York, 1977).

[38] E. Schrödinger, *What is Life?* (Cambridge University Press, Cambridge, 1944).

[39] A. Turing, Phil. Trans. Roy. Soc. B **237**, 37 (1952).

[40] V. Castets, E. Dulos, J. Boissonade, and P. De Kepper, Phys. Rev. Lett. **64**, 2953 (1990).

[41] H. G. Schuster, *Deterministic Chaos* (Physik-Verlag, Weinheim, 1984).

[42] J. Guckenheimer and P. J. Holmes, *Nonlinear Oscillations, Dynamical Systems and Bifurcations of Vector Fields* (Springer, New York, 1983).

[43] J. H. Poincaré, *Les Méthodes Nouvelles de la Méchanique Céléste* (Gauthier-Villars, Paris, 1892–1899).

[44] Y. A. Kuznetsov, *Elements of Applied Bifurcation Theory* (Springer, New York, 1995).

[45] A. S. Mikhailov, *Foundations of Synergetics I*, 2 ed. (Springer, Berlin, 1994).

[46] E. Meron, Phys. Rep. **218**, 1 (1992).

[47] I. S. Aranson and L. Kramer, Rev. Mod. Phys. **74**, 99 (2002).

[48] S. Nasuno, M. Sano, and Y. Sawada, J. Phys. Soc. Jpn. **58**, 1875 (1989).

[49] M. Assenheimer and V. Steinberg, Phys. Rev. Lett. **70**, 3888 (1993).

[50] G. Gerisch, Roux Arch. Entwicklungsmech. Organismen **116**, 127 (1965).

[51] Y. A. Astrov, I. Müller, E. Ammelt, and H.-G. Purwins, Phys. Rev. Lett. **80**, 5341 (1998).

[52] J. Christoph, R. D. Otterstedt, M. Eiswirth, N. I. Jaeger, and J. L. Hudson, J. Chem. Phys. **110**, 8614 (1999).

[53] Y. Kuramoto, *Chemical Oscillations, Waves, and Turbulence* (Springer, Berlin, 1984).

[54] J. J. Tyson and P. C. Fife, J. Chem. Phys. **73**, 2224 (1980).

[55] J. A. Sepulchre and A. Babloyantz, Phys. Rev. Lett. **66**, 1314 (1991).

[56] H. Nagashima, J. Phys. Soc. Jpn. **60**, 2797 (1991).

[57] A. E. Bugrim, M. Dolnik, A. M. Zhabotinsky, and I. R. Epstein, J. Phys. Chem. **100**, 19017 (1996).

[58] H. Mahara, T. Saito, Y. Amagishi, H. Nagashima, and T. Yamaguchi, J. Phys. Soc. Jpn. **69**, 3552 (2000).

[59] M. Hendrey, K. Nam, P. Guzdar, and E. Ott, Phys. Rev. E **62**, 7627 (2000).

[60] C. Vidal and A. Pagola, J. Phys. Chem. **93**, 2711 (1989).

[61] A. S. Mikhailov, Physica D **55**, 99 (1992).

[62] H. Sakaguchi, Prog. Theor. Phys. **87**, 241 (1992).

[63] A. B. Rovinsky, A. M. Zhabotinsky, and I. R. Epstein, Phys. Rev E **56**, 2412 (1997).

[64] S. Alonso, I. Sendiña-Nadal, V. Pérez-Muñuzuri, J. M. Sancho, and F. Sagués, Phys. Rev. Lett. **87**, 078302 (2001).

[65] P. Parmananda, H. Mahara, T. Amemiya, and T. Yamaguchi, Phys. Rev. Lett. **87**, 238302 (2001).

[66] P. Gray and S. K. Scott, Ber. Bunsenges. Phys. Chem. **90**, 985 (1986).

[67] S. K. Scott, *Chemical Chaos* (Oxford University Press, Oxford, 1991).

[68] A. v. Oertzen, Ph.D. thesis, Freie Universität Berlin, 1992.

[69] M. Ipsen, Ph.D. thesis, University of Copenhagen, 1997.

[70] J. J. Tyson and J. P. Keener, Physica D **32**, 327 (1988).

[71] A. C. Newell and J. A. Whitehead, J. Fluid. Mech **38**, 279 (1969).

[72] A. C. Newell and J. A. Whitehead, in *Instability of Continuous Systems*, Proc. of IUTAM Symposium, Herrenalb (1969), edited by H. Leipholz (Springer, Berlin, 1971), pp. 284–289.

[73] Y. Kuramoto and T. Tsuzuki, Prog. Theor. Phys. **52**, 1399 (1974).

[74] M. Ipsen, F. Hynne, and P. G. Sørensen, Chaos **8**, 834 (1998).

[75] L. Brusch, M. G. Zimmermann, M. van Hecke, M. Bär, and A. Torcini, Phys. Rev. Lett. **85**, 86 (2000).

[76] B. Janiaud, A. Pumir, D. Bensimon, V. Croquette, H. Richter, and L. Kramer, Physica D **55**, 269 (1992).

[77] S. M. Tobias and E. Knobloch, Phys. Rev. Lett. **80**, 4811 (1998).

[78] M. Bär and M. Or-Guil, Phys. Rev. Lett. **82**, 1160 (1999).

[79] B. Sandstede and A. Scheel, Phys. Rev. E **62**, 7708 (2000).

[80] M. Golubitsky, E. Knobloch, and I. Stewart, J. Nonlin. Sci. **10**, 333 (2000).

[81] I. S. Aranson, L. Aranson, L. Kramer, and A. Weber, Phys. Rev. A. **46**, R2992 (1992).

[82] A. L. Hodgkin and A. F. Huxley, J. Physiol. **117**, 500 (1952).

[83] R. FitzHugh, Biophys. J. **1**, 445 (1961).

[84] J. S. Nagumo, S. Arimoto, and S. Yoshizawa, Proc. IRE **50**, 2061 (1962).

[85] B. van der Pol, Phil. Mag. **27**, 978 (1926).

[86] B. van der Pol and J. van der Mark, Phil. Mag. Suppl. **6**, 763 (1928).

[87] K. F. Bonhoeffer, J. Gen. Physiol. **32**, 69 (1948).

[88] D. Armbruster, in *Nonlinear Dynamics*, edited by A. Guran (World Scientific, Singapore, 1997), pp. 89–102.

[89] R. J. Field, E. Körös, and R. M. Noyes, J. Amer. Chem. Soc. **94**, 8649 (1972).

[90] J. J. Tyson, J. Phys. Chem. **86**, 3006 (1982).

[91] K. Krischer, Ph.D. thesis, Freie Universität Berlin, 1990.

[92] M. Eiswirth, K. Krischer, and G. Ertl, Appl. Phys. A **51**, 79 (1990).

[93] K. Krischer, M. Eiswirth, and G. Ertl, Surf. Sci. **251/252**, 900 (1991).

[94] K. Krischer, M. Eiswirth, and G. Ertl, J. Chem. Phys. **96**, 9161 (1992).

[95] M. Bär, M. Falcke, and M. Eiswirth, Physica A **188**, 78 (1992).

[96] D. Barkley, Physica D **49**, 61 (1991).

[97] A. von Oertzen, A. S. Mikhailov, H.-H. Rotermund, and G. Ertl, Surf. Sci. **350**, 259 (1996).

[98] K. Krischer and A. S. Mikhailov, Phys. Rev. Lett. **73**, 3165 (1994).

[99] A. M. Zhabotinsky, M. Dolnik, and I. R. Epstein, J. Chem. Phys. **103**, 10306 (1995).

[100] E. M. Nicola, Ph.D. thesis, Technische Universität Dresden, 2001.

[101] P. E. Cladis, P. L. Finn, and H. R. Brand, Phys. Rev. Lett. **75**, 1518 (1995).

[102] M. Assenheimer and V. Steinberg, Nature **367**, 345 (1994).

[103] K. J. Lee, E. C. Cox, and R. E. Goldstein, Phys. Rev. Lett. **76**, 1174 (1996).

[104] K. J. Lee, Phys. Rev. Lett. **79**, 2907 (1997).

[105] K. J. Lee, R. E. Goldstein, and E. C. Cox, Phys. Rev. Lett. **87**, 068101 (2001).

[106] P. Grauel, H. Varela, and K. Krischer, Faraday Discuss. **120**, 165 (2001).

[107] S. K. Scott, J. Wang, and K. Showalter, J. Chem. Soc., Faraday Trans. **93**, 1733 (1997).

[108] S. K. Scott, http://www.chem.leeds.ac.uk/chaos/Osc.html.

[109] H. H. Rotermund, in *IMA Conference on Pattern Formation in Continous and Coupled Systems*, Vol. 115 of *The IMA Volumes in Mathematics and its Application*, edited by M. Golubitsky, D. Luss, and S. H. Strogatz (Springer, New York, 1999), pp. 231–249.

[110] J. Wolff, Ph.D. thesis, Freie Universität Berlin, 2002.

[111] F. Huneus, B. Schäpers, T. Ackemann, and W. Lange, Appl. Phys. B **76**, 191 (2003).

[112] P. B. Umbanhowar, F. Melo, and H. L. Swinney, Physica A **249**, 1 (1998).

[113] U. Middya and D. Luss, J. Chem. Phys. **102**, 5029 (1995).

[114] O. Nekhamkina and M. Sheintuch, Physica A **249**, 134 (1998).

[115] M. Motoyama, Y. Yamazaki, and T. Ohta, J. Phys. Soc. Jpn. **70**, 792 (2001).

[116] J. M. Greenberg, SIAM J. Appl. Math. **34**, 391 (1978).

[117] N. Kopell, Adv. Appl. Math. **2**, 389 (1981).

[118] P. S. Hagan, Adv. Appl. Math. **2**, 400 (1981).

[119] D. Walgraef, G. Dewel, and P. Borckmans, J. Chem. Phys. **78**, 3043 (1983).

[120] Y.-X. Zhang, P. Foerster, and J. Ross, J. Phys. Chem. **96**, 8898 (1992).

[121] H. Hastings, preprint.

[122] E. Mori and J. Ross, J. Phys. Chem. **96**, 8053 (1992).

[123] T. J. Lewis and J. Rinzel, Neurocomputing **38–40**, 763 (2001).

[124] T. J. Lewis and J. Rinzel, Network: Comput. Neural Syst. **11**, 299 (2000).

[125] K. I. Agladze, V. A. Davydov, V. S. Zykov, and A. S. Mikhailov, JETP Lett. **45**, 767 (1987).

[126] S. C. Müller, O. Steinbock, and J. Schütze, Physica A **188**, 47 (1992).

[127] G. Dewel and P. Borckmans, in *Solitons and Chaos*, edited by I. Antoniou and F. J. Lambert (Springer, Berlin, 1991), pp. 138–141.

[128] G. Dewel and P. Borckmans, Europhys. Lett. **17**, 523 (1992).

[129] R. J. Deissler and H. R. Brand, Phys. Rev. Lett. **72**, 478 (1994).

[130] N. Akhmediev, J. M. Soto-Crespo, and G. Town, Phys. Rev. E **63**, 056602 (2001).

[131] V. M. Eguiluz, E. Hernandez-Garcia, and O. Piro, Int. J. Bif. Chaos **9**, 2209 (1999).

[132] C. Vidal, A. Pagola, J. M. Bodet, P. Hanusse, and E. Bastardie, J. Phys. (France) **47**, 1999 (1986).

[133] K. I. Agladze and V. I. Krinsky, in *Self-Organization, Autowaves and Structures far from Equilibrium*, edited by V. I. Krinsky (Springer, Berlin, 1984), pp. 147 – 149.

[134] J. J. Tyson, J. Chim. Phys. (France) **84**, 1359 (1987).

[135] T. Ohta, Y. Hayase, and R. Kobayashi, Phys. Rev. E **54**, 6074 (1996).

[136] R. Kobayashi, T. Ohta, and Y. Hayase, Physica D **84**, 162 (1995).

[137] R. Kobayashi, T. Ohta, and Y. Hayase, Phys. Rev. E **50**, R3291 (1994).

[138] H. Kokubo, M. Sano, B. Janiaud, and Y. Sawada, J. Phys. Soc. Jpn. **63**, 895 (1994).

[139] V. A. Vasilev and M. S. Polyakova, Vestn. Mosk. U. Fiz. AS **16**, 99 (1975).

[140] V. A. Vasiliev, D. S. Chernavskii, Y. M. Romanovskii, and V. G. Yakhno, *Autowave Processes in Kinetic Systems* (Reidel, Dordrecht, 1987).

[141] A. N. Zaikin and A. L. Kawczynski, J. Non-Equilib. Thermodyn. **2**, 39 (1977).

[142] A. L. Kawczynski, Pol. J. Chem. **60**, 223 (1986).

[143] A. L. Kawczynski, in *Spatial Inhomogeneities and Transient Behaviour in Chemical Kinetics*, *Proceedings in Nonlinear Science*, edited by P. Gray, G. Nicolis, F. Baras, P. Borckmans, and S. K. Scott (Manchester University Press, Manchester, 1990), pp. 447–457.

[144] S. Bose, S. Bose, and P. Ortoleva, J. Chem. Phys. **72**, 4258 (1980).

[145] P. J. Ortoleva, *Nonlinear Chemical Waves* (John Wiley & Sons, New York, 1992).

[146] A. S. Mikhailov, Dokl. Akad. Nauk SSSR **270**, 590 (1983).

[147] M. Stich and A. S. Mikhailov, Z. Phys. Chem. **216**, 521 (2002).

[148] A. S. Mikhailov and A. Engel, Phys. Lett. A **117**, 257 (1986).

[149] W. van Saarloos and P. C. Hohenberg, Physica D **56**, 303 (1992).

[150] M. van Hecke, C. Storm, and W. van Saarloos, Physica D **134**, 1 (1999).

[151] J. A. Sepulchre, G. Dewel, and A. Babloyantz, Phys. Lett. A **147**, 380 (1990).

[152] A. Rabinovitch, M. Gutman, and I. Aviram, Phys. Rev. Lett. **87**, 084101 (2001).

[153] H. Sakaguchi, Prog. Theor. Phys. **80**, 743 (1988).

[154] V. Petrov, Q. Ouyang, G. Li, and H. L. Swinney, J. Phys. Chem. **100**, 18992 (1996).

[155] O. Decroly and A. Goldbeter, Proc. Natl. Acad. Sci. USA **79**, 6917 (1982).

[156] M. Alamgir and I. R. Epstein, J. Am. Chem. Soc. **105**, 2500 (1983).

[157] P. Lamba and J. L. Hudson, Chem. Eng. Commun. **32**, 369 (1985).

[158] C. Pérez-Iratxeta, J. Halloy, F. Morán, J. L. Martiel, and A. Goldbeter, Biophys. Chem. **74**, 197 (1998).

[159] T. Haberichter, M. Marhl, and R. Heinrich, Biophys. Chem. **90**, 17 (2001).

[160] H.-J. Krug, L. Pohlmann, and L. Kuhnert, J. Phys. Chem. **94**, 4862 (1990).

[161] M. Stich, M. Ipsen, and A. S. Mikhailov, Phys. Rev. Lett. **86**, 4406 (2001).

[162] M. Stich, M. Ipsen, and A. S. Mikhailov, Physica D **171**, 19 (2002).

[163] M. Ipsen, F. Hynne, and P. G. Sørensen, Physica D **136**, 66 (2000).

[164] M. Ipsen, L. Kramer, and P. G. Sørensen, Phys. Rep. **337**, 193 (2000).

[165] E. M. Izhikevich, Neural Networks **11**, 495 (1998).

[166] S. Koga and Y. Kuramoto, Prog. Theor. Phys. **63**, 106 (1980).

[167] D. Haim, G. Li, Q. Ouyang, W. D. McCormick, H. L. Swinney, A. Hagberg, and E. Meron, Phys. Rev. Lett. **77**, 190 (1996).

[168] M. Suzuki, T. Ohta, M. Mimura, and H. Sakaguchi, Phys. Rev. E **52**, 3645 (1995).

[169] R. Woesler, P. Schütz, M. Bode, M. Or-Guil, and H.-G. Purwins, Physica D **91**, 376 (1996).

[170] M. Stich, Diploma thesis, Freie Universität Berlin, 1999.

[171] Y. Kuramoto, preprint.

[172] I. Aranson, H. Levine, and L. Tsimring, Phys. Rev. Lett. **76**, 1170 (1996).

[173] U. Middya, D. Luss, and M. Sheintuch, J. Chem. Phys. **101**, 4688 (1994).

[174] M. Sheintuch and O. Nekhamkina, in *IMA Conference on Pattern Formation in Continous and Coupled Systems*, Vol. 115 of *The IMA Volumes in Mathematics and its Application*, edited by M. Golubitsky, D. Luss, and S. H. Strogatz (Springer, New York, 1999), pp. 265–282.

[175] A. T. Winfree, Phys. Lett. A **149**, 203 (1990).

[176] A. T. Winfree, Physica D **49**, 125 (1991).

[177] G. Bordiougov, personal communication.

[178] M. Ipsen, F. Hynne, and P. G. Sørensen, Int. J. Bifurcation and Chaos **7**, 1539 (1997).

[179] A. v. Oertzen, http://w3.rz-berlin.mpg.de/~mik/oertzen/vlg/virtlab.html.

Acknowledgments

In the first place I would like to thank Professor Dr. Gerhard Ertl for giving me the opportunity to prepare this work in a first-class environment in his department at the Fritz-Haber-Institut.

I would like to express my gratitude to Professor Dr. Alexander Mikhailov for his excellent advice and support during this thesis.

This work certainly would have been much more difficult without the excellent collaboration with Dr. Mads Ipsen, Professor Dr. Yoshiki Kuramoto, and Dr. Tsyoshi Mizuguchi. I also would like to thank Dr. Albrecht Preusser for his valuable software support and Dr. Lutz Brusch for helpful discussions.

I would like to thank all the present and former members of the Complex Systems Group who through many scientific discussions and practical help assisted me, and who made my stay at the Fritz-Haber-Institut to a very pleasant time, in particular Matthias Bertram, Vanessa Casagrande, Mads Ipsen, Carsten Beta, Sergio Alonso, and Alexander von Oertzen. Special thanks to Michael *Mex* Hildebrand, who introduced me to nonlinear dynamics and the Fritz-Haber-Institut.

My colleagues from other groups at the Fritz-Haber-Institut have also contributed to this work by providing a very pleasant atmosphere, especially Janpeter *JP* Wolff (Cappuccino connection), Stefano Cerasari (Cafeteria connection), *Butt* Rotermund (Mensa connection), Florian Plenge, Michael Pollmann, Athanasios Papathanasiou, and Dieter Bauer.

I am very grateful to my dear colleagues and friends, especially to Ben Liebelt, who have read the manuscript of this thesis and who have made very valuable suggestions.

Während des gesamten Studiums und der Doktorarbeit war mir meine Familie ein starker Rückhalt, insbesondere meine Mutter Evemarie. Vielen lieben Dank!

Nati, ¡muchas gracias por todo!

List of publications

[1] M. Stich, M. Ipsen, and A.S. Mikhailov, *Self-organized stable pacemakers near the onset of birhythmicity*, Phys. Rev. Lett. 86 (2001), 4406-4409.

[2] M. Stich and A.S. Mikhailov, *Complex pacemakers and wave sinks in heterogeneous oscillatory chemical systems*, Z. Phys. Chem. 216 (2002), 521-533.

[3] M. Stich, M. Ipsen, and A.S. Mikhailov, *Pattern formation in birhythmic media*, Physica D 171 (2002), 19-40.

Curriculum Vitae

Name	Michael Stich
Born	20/07/1972, Bayreuth, Federal Republic of Germany
Languages	English (fluent), Spanish (fluent), French (basic), Italian (basic)

09/1978 - 07/1991	Primary and secondary school in Bayreuth, finished with exams (*Abitur*) with overall grade 2.1.
07/1991 - 10/1992	Community service in Bayreuth at *Bund Naturschutz e.V.*.

Physics

10/1992 - 07/1994	Undergraduate studies at the Free University Berlin, finished with exams (*Vordiplom*) with overall grade 1.5.
10/1994 - 07/1995	Graduate studies at the Free University Berlin.
10/1995 - 07/1996	Graduate studies at the University of Granada, Spain, with an ERASMUS grant from the European Union.
10/1996 - 07/1999	Graduate studies at the Free University Berlin, obtained degree: *Diplom-Physiker* with overall grade 1.3.
05/1998 - 05/1999	Diploma thesis "Analytical and numerical investigations of pattern formation in a three-component reaction-diffusion system" at the Fritz Haber Institute (Advisors: Prof. Dr. G. Ertl and Prof. Dr. A.S. Mikhailov), grade: 1.0.
10/1999 - 02/2003	Doctoral student at the Fritz Haber Institute. (Advisor: Prof. Dr. A.S. Mikhailov).

Studium generale

10/1993 - 07/1999	Undergraduate studies in Cultural Anthropology of Latin America, Philosophy, and Psychology (Free University Berlin).
10/2001 - 07/2002	*Robocup*, project on autonomous, soccer-playing robots (Institute of Computer Science, Free University Berlin).

Hay una fuente niña
Que la llaman del amor
Donde bailan los luceros
Y la luna con el sol.

Jesús de la Rosa

Triana, *Abre la puerta*, 1975.

Why ask how I feel
Well how does it look to you
I feel kinda sick
Lost my cabin and my crew
I'm standing on the landing
There's no one there but me
That's where you'll find me
Looking out on the deep blue sea

Rory Gallagher

Rory Gallagher, *A million miles away,* 1973.